RIGA TECHNICAL
UNIVERSITY

Deniss Kolosovs

ADAPTIVE BLIND EQUALIZATION ALGORITHMS FOR QAM SYSTEMS

Doctoral Thesis

RIGA TECHNICAL UNIVERSITY

Faculty of Electronics and Telecommunications

Institute of Radioelectronics

Deniss Kolosovs

Doctoral Student of Study Programme "Electronics"

ADAPTIVE BLIND EQUALIZATION ALGORITHMS FOR QAM SYSTEMS

Doctoral Thesis

Scientific supervisors:

Associate Professor Dr. sc. ing.
ARTŪRS ĀBOLTIŅŠ

Associate Professor Dr. sc. ing.
ANNA LITVIŅENKO

RTU Press

RIGA 2022

I E G U L D Ī J U M S   T A V Ā   N Ā K O T N Ē

DOCTORAL THESIS PROPOSED TO RIGA TECHNICAL UNIVERSITY FOR THE PROMOTION TO THE SCIENTIFIC DEGREE OF DOCTOR OF SCIENCE

To be granted the scientific degree of Doctor of Science (Ph. D.), the present Doctoral Thesis has been submitted for the defence at the open meeting of RTU Promotion Council on 10 June 2022, 13:30, at the Faculty of Electronics and Telecommunications of Riga Technical University, 12 Āzenes Street, Room 201.

OFFICIAL REVIEWERS

Professor, Dr. sc. ing. Vjačeslavs Bobrovs
Riga Technical University

Professor, Dr.-Ing. habil. Andreas Ahrens
Hochschule Wismar, University of Applied Sciences Technology, Business and Design, Germany

Associate Professor, Dr. Rasa Brūzgienė
Kaunas University of Technology, Lithuania

DECLARATION OF ACADEMIC INTEGRITY

I hereby declare that the Doctoral Thesis submitted for the review to Riga Technical University for the promotion to the scientific degree of Doctor of Science (Ph. D.) is my own. I confirm that this Doctoral Thesis had not been submitted to any other university for the promotion to a scientific degree.

Deniss Kolosovs —————————————

Date: —————————————

The Doctoral Thesis has been written in English. It consists of Introduction, 5 chapters, Conclusions, 35 figures, 3 tables, 4 appendices; the total number of pages is 98, not including appendices. The Bibliography contains 80 titles.

ABSTRACT

The work "Adaptive Blind Equalization Algorithms for QAM Systems" summarizes the research conducted for the degree of Doctor of Science (Ph. D.). It is devoted to the issues of blind equalization in quadrature-amplitude-modulation-based (QAM) wireless data transmission systems. The thesis offers several equalization algorithms and approaches for synthesizing these algorithms.

The thesis proposes an optimization for the decision-adjusted modulus algorithm, which minimizes the probability of decision-making error during the adjustment of the equalizer coefficients. Empirical investigations have shown a significant increase in the convergence capability of an equalizer.

The work considers and gives a theoretical foundation for grouping QAM constellation points to synthesize blind equalization algorithms. This approach makes it possible to use the minimization of the intersymbol interference variance as a cost function for the equalizer adjustment. On the other hand, it reduces the deviation variance of the equalizer tap values.

The research suggests switching between algorithms synthesized by the above approach. Criteria, thresholds, and hysteresis values for these switchings are given, as well as a method for calculating them. The technique allows one to balance the speed of the equalizer adjustment and its ability to converge.

Within the research framework, the described algorithms were implemented as FPGA firmware and incorporated into the QAM receiver. The proposed solution has gone into manufacturing and found application in the commercial market. The thesis presents the results of field measurements of the convergence of the created device.

The Doctoral Thesis has been written in English. It consists of Introduction, 5 chapters, Conclusions, 35 figures, 3 tables, and 4 appendices; the total number of pages is 98, not including appendices. The Bibliography consists of 80 titles.

ANOTĀCIJA

Promocijas darbā "Adaptīvie aklās izlīdzināšanas algoritmi QAM sistēmās" apkopoti pētījumi, kas veikti zinātņu doktora grāda (*Ph. D.*) iegūšanas nolūkos. Tas ir veltīts aklās izlīdzināšanas jautājumiem uz kvadratūrās amplitūdas modulācijas (QAM) balstītās bezvadu pārraides sistēmās. Promocijas darbā piedāvāti vairāki izlīdzināšanas algoritmi, kā arī pieejas šo algoritmu sintēzei.

Promocijas darbā ir piedāvāta optimizācija ar lēmumu koriģētam moduļa algoritmam (DAMA), kas balstīta uz lēmuma pieņemšanas kļūdas varbūtības minimizācijas ekvalaizera koeficientu pieskaņošanas laikā. Empīriskie pētījumi ir parādījuši ievērojamu ekvalaizera konverģences spējas pieaugumu.

Darbā ir apskatīta aklās izlīdzināšanas algoritmu sintēzes pieeja, kas balstīta uz QAM zvaigznāja punktu grupēšanas, un sniegts tās teorētisks pamatojums. Šī pieeja ļauj izmantot starpsimbolu interferences dispersijas samazināšanu kā mērķa funkciju ekvalaizera pieskaņošanai. No otrās puses, tas samazina ekvalaizera izvadu vērtību dispersiju.

Pētījums piedāvā starp algoritmiem, kas sintezēti, izmantojot iepriekš minēto pieeju, pārslēgšanas tehniku. Ir norādīti šīs pārslēgšanas kritēriji, sliekšņi un histerēzes vērtības, kā arī to aprēķināšanas metodes. Šī metodika ļauj līdzsvarot ekvalaizera pieskaņošanas ātrumu un tā spēju konverģēt.

Pētījuma ietvaros aprakstītie algoritmi tika realizēti kā FPGA programmaparatūra un iekļauti QAM uztvērējā. Piedāvātais risinājums ir nonācis ražošanā un atradis pielietojumu komerciālajā tirgū. Darbā ir sniegti izveidotās iekārtas konverģences mērījumu rezultāti.

Promocijas darbs ir uzrakstīts angļu valodā, tajā ir ievads, piecas nodaļas, secinājumi, literatūras saraksts, 35 attēli, trīs tabulas, četri pielikumi; kopējais lappušu skaits 100, neieskaitot pielikumus. Literatūras sarakstā ir 80 nosaukumu.

CONTENTS

LIST OF FIGURES

LIST OF TABLES

ACRONYMS

ACF autocorrelation function

ACM adaptive coding and modulation

ADC analog-to-digital converter

AGC automatic gain control

AWGN additive white Gaussian noise

BPSK binary phase-shift keying

CMA constant modulus algorithm

DAC digital-to-analog converter

DAMA decision adjusted modulus algorithm

DD decision-directed

DSB-SC double-sideband suppressed-carrier

DSP digital signal processing

EDAMA enhanced decision-adjusted modulus algorithm

ETSI European Telecommunications Standards Institute

FCC Federal Communications Commission

FPGA field-programmable gate array

IP intellectual property

ISI inter-symbol interference

IT Information Technology

MIMO multiple-input and multiple-output

MMA multimodulus algorithm

OFDM orthogonal frequency-division multiplexing

PAPR peak-to-average power ratio

PDF probability density function

PDM polarization-division multiplexing

PSAM pilot symbol assisted modulation

QAM quadrature amplitude modulation

QPSK quadrature phase-shift keying

VHDL VHSIC hardware description language

VHSIC very high speed integrated circuit

WSSUS wide-sense stationary uncorrelated scattering

XPIC cross-polarization interference canceling

LIST OF SYMBOLS

Operations

.*   complex conjugation

| a | absolute value of variable a

$E[\cdot]$ mathematical expectation

$s_1(t) * s_2(t)$ continuous-time convolution of signals $s_1(t)$ and $s_2(t)$

Variables

$\delta(t)$ delta-function

$\delta[n]$ Kronecker pulse

$\mathbf{c}[n]$ vector of equalizer's coefficients on the clock cycle n

μ step-size coefficient

ω angular frequency $\omega = 2\pi f$

$\rho(R)$ probability density function for the variable R

σ standard deviation

a QAM constellation point, a complex cumber

f frequency, variable of the Fourier transform

f_0 carrier frequency

F_s sampling frequency

$H(\omega)$ frequency response of a system with impulse response $h(t)$

$h(t, \tau)$ time-varying impulse response of a linear system

j imaginary unit $j^2 = -1$

K number of taps of a discrete linear finite-impulse response system

k number of the coefficient of a filter

L number of iterations

N number samples

n discrete time moment, clock cycle number

$P(A)$ probability of the event A

$P(A \mid B)$ conditional probability of the event A if the event B has already happened

R radius of a constellation circle

R_{CMA}^2 dispersion constant for the algorithm CMA

$S(\omega)$ spectral density of a signal $s(t)$

$s_{\mathrm{in}}(t)$ analog input signal of a block

$s_{\mathrm{out}}[n]$ discrete output signal of a block

T_{sym} symbol duration

INTRODUCTION

Rationale

From the beginning of the XXI century, we have witnessed the rapid transition from the post-industrial to the information society. This phenomenon is accompanied by the ongoing growth of the share of Information Technology (IT) in the world economy. Thus, the communications industry tends to form the most significant part of IT market. This trend has been particularly reinforced by the COVID-19 pandemic, numerous lockdowns, and a massive transition to remote learning and work. On the other hand, the information society implies an increased demand for access to information for each member. Meeting this demand requires an increase in the capacity of communication services. Moreover, this task should be solved in limited time, bandwidth, and spatial resources.

Numerous solutions to the problem have appeared in recent years. Many of them use multiplexing techniques such as frequency division in orthogonal frequency-division multiplexing (OFDM), space division in case of multiple-input and multiple-output (MIMO), or polarization division in polarization-division multiplexing (PDM). However, all of these technologies typically use complex baseband signal forming and quadrature channel division and thus are based on quadrature amplitude modulation (QAM). The QAM is widely used, especially in backbone link establishment when high capacity is needed and data multiplexing is unnecessary. Therefore possible optimizations applicable to the QAM transmission model could be widely utilized for more complex communication technologies.

The signal acquisition stage is a blindside of each data transmission-receiving scheme. It is also true for QAM and its based technologies. Firstly, locking dynamical loops such as automatic gain control (AGC), equalizer, timing or frequency recovery systems takes noticeable time. Secondly, acquisition can be computationally capacious or impossible, especially in the case of disastrous initial conditions or high order modulations. Typically these problems are solved by the transmission of known or well distinguishable data:

- Training sequences can be transmitted at the stage of link establishment. The identical sequences are generated on the receiver side. The coincidence of the generated and recovered training sequences is a target function for adjusting dynamic loops. The described technology requires a service channel to request the start of user data transmission. The approach is not suited for cases of non-full-duplex links. The need for a service channel also results in lower throughput.
- The use of low order modulation, such as binary phase-shift keying (BPSK), quadrature phase-shift keying (QPSK), or 4-QAM, significantly simplifies target functions and decreases acquisition time. The drawback of this technique is a dramatic drop in link capacity.
- Adaptive coding and modulation (ACM) is an evolution of the previous idea. In this case, the transmission starts with low order modulation. After the receiver's dynamic loops have been

locked ACM engine increases an order of modulation. This technology requires a service channel for ACM engine operation, similar to the training sequences. The usage of ACM is possible only in full-duplex links. The presence of a service channel as well as air-framing decreases channel capacity.

- Predefined symbols can interleave user data traffic as implemented in the pilot symbol assisted modulation (PSAM). This approach does not require a service channel and full-duplex link. On the other hand, the channel capacity lowers due to the pilot symbols.

All the methods mentioned provide an opportunity to solve the acquisition problem. However, they also have noticeable drawbacks: a method either requires a service channel and full-duplex link or reduces capacity.

Blind adjustment is an alternative solution to the problem. In this case, dynamical loops engines estimate the statistical properties of the received signal. There is no need to know the precise value of the transmitted symbol. So, blind algorithms do not require predefined symbol transmission at all. If possible, the acquisition is performed using the standard operation mode signal. This approach does not have the drawbacks of the methods described above.

This work considers mitigation of multipath phenomena effects. Thus it is focused mainly on blind equalization. The idea of blind algorithm application for channel equalization is nearly half a century old. It was initially proposed in [1]. The generalization of this technique, known as a constant modulus algorithm (CMA), was subsequently made by Domenique N. Godard in [2]. The proposed algorithm was carrier phase invariant and showed good convergence properties. Thus, it became widespread among scientists and modem developers, an unspoken blind equalization standard.

The CMA also has serious drawbacks. The accordance of equalized signal statistical properties to the defined patterns is the essence of CMA operation. In other words, the algorithm does not ensure perfect equalization of each symbol. As a result, CMA has a non-zero steady-state error. Empirical evidence also shows limited CMA's ability to adjust the equalizer of many taps.

The popularity of CMA and its obvious drawbacks are a reason of interest to the field of blind equalization. Numerous researches have been published from the moment of CMA announcement, especially in recent years, when modern digital signal processing (DSP) chips and field-programmable gate arrays (FPGAs) allowed implementing complex computationally capacious algorithms. There are some distinct directions of the research in the variety of accessible publications:

- Plenty of authors attempted to fix the main drawback of CMA. The enhancement proposed in this group of papers is based mainly on the fact that CMA does not estimate a received symbol. While the CMA tries to pull all the constellation points to a single circle on the constellation plain, some authors suggest using circles of multiple radii [3], [4]. These algorithms keep the CMA's property of carrier-phase invariance.
- Another improvement direction is the modification of CMA for separate processing of the received symbol real and imaginary parts [5] (widely referred to as MCMA). This approach

requires carrier recovery before a signal is equalized. The signs of real and imaginary parts are also considered in [6], which proposes widespread multimodulus algorithm (MMA). The method is often used for more complex specific equalization algorithms. For example, a combination of CMA and MMA target functions is mentioned in [7].

- An application of CMA for initial adjustment of equalizer taps is a conventional way of its usage. Afterward, an algorithm with zero steady-state error takes control over equalizer taps. Usually, it is a decision-directed (DD) algorithm, which estimation of the received symbol value is needed. An idea to use a dual-mode type algorithm for the first time appeared in [8]. It suggested switching between the target functions of CMA and a DD algorithm. The combination of this idea with the "Stop-and-Go" operation mode (proposed in [9]) became fertile soil for numerous researches that have been being published in recent years [[10]–[15]].

- Many authors consider enhancements and optimizations on more than one of the previously described ideas. Thus the authors of [16], [17] propose dual-mode algorithms, where one of the combined target functions is the modification of CMA for operation with real and imaginary parts of a complex symbol.

- An additional group of publications interested in CMA-based blind equalization consists of non-standard applications. For example, a modification of CMA to perform joint equalization and timing recovery is proposed in [18]. Another variation of this algorithm is used in carrier phase recovery described in [19].

An application of CMA in QAM-based communication systems is also a topic of broad interest. Considering previously mentioned technologies, the usage of blind equalization methods is as follows:

- Though OFDM standard involves specific equalization approaches, commonly used blind equalization mechanisms often are in the focus of scientific and engineering discussions. The CMA technique is suggested to solve the peak-to-average power ratio (PAPR) minimization problem for the OFDM signal [20], [21]. An ability to recover the carrier phase of the CMA is used for carrier frequency offset estimation for coherent optical OFDM in [22].

- In the case of MIMO technology, equalization-like operations are utilized for the separation of multiplexed signals. A derivation from the CMA for suppressing inter-source interference and demultiplexing is proposed in [23]. Attention to this topic was recently paid in [24], [25].

- The cross-polarization interference canceling (XPIC) technology ensures the feasibility of PDM communication systems. A standard XPIC node can be treated as a complex equalization engine. Therefore the broad utilization of blind equalization methods in this field is not surprising. The authors of [26], for example, introduce CMA and DD algorithm into the XPIC mechanism. Different modifications of CMA are proposed to separate different polarization signals in [27], [28].

- Some publications suggest using CMA for beam separations in phased antenna arrays [29]–

[31]. This direction has become especially popular with the advent of massive MIMO technology and the introduction of the 5G standard. The authors of [32], [33] propose to use blind equalization algorithms to estimate channel state information and suppress inter-user interference.

Concluding the review of the publication, intense attention to the field of blind equalization must be ascertained. Authors propose new equalization algorithms and their optimizations and research their application to more complex multiplexing-based communication systems. Although there are many blind equalization algorithms, their limitations make them an optimal signal processing tool only in particular operating requirements. The field of blind alignment requires an approach to form an algorithm suitable for given working conditions. A generalized CMA-like algorithm might also be applied in the cases described above.

The Objective Statement and the Tasks

The **objective** of this Doctoral Thesis is the generalization of existing CMA-like algorithms and the development of a blind equalization technique that will ensure performance for the defined operating conditions. The requirement fulfillment criteria, in this case, are convergence ability, adjustment speed, and residual error.

The following **tasks** are stated to achieve the previously defined objectives:

- Explicit description of the utilized multipath channel and precise definition of the implemented model of QAM-based communication system.
- Analytical and empirical exploration of popular blind equalization algorithms with the fixation of their drawbacks.
- Suggestion of a new algorithm: the minimizing of misadjustment probability is a basis of CMA optimization.
- Generalization of the proposed algorithm to ensure its operation in dual and multiple modes.
- Establishment of the "Stop-and-Go" concept for switching between modes.
- FPGA implementation of the equalizer tuned by the proposed algorithm and its incorporation into QAM modem and field measurements.

The expected effectiveness of the developed algorithm will be shown by comparative measurements of the proposed approach and existing widely used blind alignment algorithms, such as CMA and decision adjusted modulus algorithm (DAMA).

The Subject and the Object of the Research

This Doctoral Thesis mainly focuses on the equalization of the signals in a QAM-based communication system. However, an equalization should be considered bound to a received signal, which is

affected by the multipath phenomenon. Therefore the **object** of this research is a baseband of a QAM communication system. Regarding our research, it consists of:

- A part of a communication system that is responsible for signal generation. It corresponds to the transmitter of the QAM modem.
- Baseband model of a multipath channel with additive white Gaussian noise (AWGN). It is also a part of the standard model of the QAM communication system.
- QAM receiver that contains:
  - A part of the QAM receiver that processes the signal prior to the equalizer. It consists of the matched filter, a gain control system, and timing recovery. Other sub-blocks that usually are presented in the receiver are out of the scope of this research.
  - An equalization system consists of a linear filter and a tap tuning mechanism.
  - The received symbol estimating block.

Whereas the equalizer is the device of primary interest in this Thesis, observation of other mentioned items is presented to derive appropriate signal models.

The **subject** of this research is the blind equalization algorithm. The purpose of this mechanism is an adjustment of the equalizer taps. Typically it is a structure that performs the following operations:

- Analysis of current equalizer output.
- Estimation of the algorithm cost function.
- Evaluation of current vector of increments for equalizer taps coefficients.

Research Methodology

The main goal of this Thesis is to develop an approach for synthesizing blind equalization algorithms best suited to the receiving conditions. Existing algorithms cannot always ensure the fulfillment of that requirement due to their natural drawbacks. Understanding blind equalization algorithms synthesis logic and identifying their shortcomings requires careful analysis of publications in the field of study. Within the framework of this Doctoral Thesis, a comprehensive literature review was made.

The correct model is a matter of absolute necessity in signal processing in general and in the case of the development of an algorithm in particular. Therefore, the first chapter of the Thesis describes used theoretical models and proves their consistency theoretically and numerically. In the research, the developed models for the signals in specific nodes of the communication system are utilized for the equalization engine numerical verification. Ultimate attention is also paid to the model of the multipath channel.

The Doctoral Thesis is an adaptation of several engineering projects. Therefore a set of technical tasks determined the strategic direction of the research. A development from the initial idea to the final algorithm has a pronounced incremental nature:

- Exploration of existing solutions limits and drawbacks.
- Specification of terms of reference for a developing method.
- Formulation of an idea whose implementation can fulfill the terms.
- Analytical exploration of the idea and confirmation of its productivity.
- Implementation in script programming language for rapid prototyping (Matlab or Python) and its simulation.
- Numerical Monte Carlo verification of the convergence properties and residual error levels.
- Implementation in a hardware description language (VHDL) and solution incorporation into the existing scheme.
- Field experiments and verification, whether the proposed method is consistent and meets the requirements.

Scientific Novelty and Main Results

Original ideas that form the overall scientific contribution provided by this research appeared in separate publications or are described for the first time in the body of this document. They are either entirely original ideas or applications of the concepts from the other fields of technical knowledge to blind equalization. The following list points out the most prominent of them:

- For the first time, the minimization of detection error probability was used to optimize the cost function of a blind equalization algorithm.

- For the first time, a cost function, which is dependent on the residual level of inter-symbol interference (ISI) at the output of the equalizer, is utilized in an algorithm of blind equalization.

- For the first time, the grouping of constellation points in the cost function of the blind equalization algorithm is used for the definition of initial limit values of ISI.

- For the first time, grouping constellation points in the cost function of a blind equalization algorithm is used to minimize misadjustment probability in the case of high order modulation and high interference level.

- For the first time, the stop-and-go algorithm is used to switch to a smoother equalization algorithm.

Several proposed solutions and methods not currently described in the literature are the result of an engineering approach to development. The list below outlines the main practical results of this research:

- A probability-based enhancement for DAMA that significantly increases its acquisition ability and convergence speed has been proposed.

- An algorithm for blind adjustment of the equalizer that guarantees the maximum limiting probability of detection error for a given initial ISI has been proposed.

- A multiple-mode blind equalization algorithm with a parametric constellation-based cost function is proposed.

- An approach to synthesizing blind alignment algorithms that satisfy the receiving conditions is proposed.

The Theses to be Defended

1. Applying of the enhanced decision-adjusted modulus algorithm instead of the constant modulus algorithm for the blind equalization of a QAM signal ensures zero-dispersion residual error in the case of equalizer impulse response adjusted so that its convolution with the channel impulse response produces delta-function.

2. The usage of optimal symbol detection thresholds in the enhanced decision adjusted modulus algorithm (DAMA) allows decreasing the number of the equalizer coefficients misadjustment events compared to the ordinary DAMA algorithm.

3. Grouping the QAM constellation points in the case of inter-symbol interference (ISI) induced signal dispersion equal to or higher than signal dispersion without ISI allows decreasing the number of the equalizer coefficients misadjustment events and thus increases equalizer convergence probability.

4. The gradual switching of the QAM constellation point grouping algorithms introduces the upper limit of the detection error probability in the blind decision-directed equalizer coefficients adjustment.

The Approbation and Practical Significance

Initially, the Thesis inherited main ideas from several engineering projects performed by the author. The goal of these works was an implementation of a blind equalization system for the QAM communication system. The development of the described system was started by performing practical tasks and was completed by this Doctoral Thesis. The equalizer as an intellectual property (IP) core has been implemented in VHSIC hardware description language (VHDL) and afterwards incorporated in a working QAM modem. Thus a prototype of the proposed blind equalizer has been implemented and successfully run on FPGA. Moreover, field measurements have been performed, as well as modem and equalizer compliance with European Telecommunications Standards Institute (ETSI) and Federal Communications Commission (FCC) standards has been tested with a positive result. The

modem with the proposed equalization system has been prepared for commercial use. In addition, the Latvian representative of the electronics industry JSC "SAF Tehnika" has experience in the serial production of this device. At this Thesis writing time, devices using the proposed blind equalization technique are deployed in the US, the EU, and some Asian countries and provide low latency microwave links.

The following list enumerates publications written while the author was working on the Thesis. The most important of them, reflecting the main ideas of the current work, are marked in bold:

[34] D. Kolosovs and E. Bekeris. "Chaos Code Division Multiplexing Communication System." In: *7th International Conference on Computational Intelligence, Communication Systems and Networks (CICSyN)*. Riga, Latvia: IEEE, June 2015, pp. 65–69. ISBN: 978-1-4673-7016-5. DOI: 10.1109/CICSyN.2015.22

[35] S. Šarkovskis et al. "Encoder Improvement for Simple Amplitude Fully Parallel Classifiers Based on Grey Codes." In: *Procedia Engineering* 178 (2017), pp. 604–614. ISSN: 18777058. DOI: 10.1016/j.proeng.2017.01.119

[36] D. Kolosovs, A. Zelenkov, and A. Jersovs. "Enhanced Decision Adjusted Modulus Algorithm for Blind Equalization." In: *Procedia Computer Science* 104 (2017), pp. 429–436. ISSN: 18770509. DOI: 10.1016/j.procs.2017.01.156

[37] D. Kolosovs. "A Generalization of the Enhanced Decision Adjusted Modulus Algorithm for Blind Equalization of Constellations with Closely Positioned Circles." In: *2020 IEEE Microwave Theory and Techniques in Wireless Communications (MTTW) (MTTW'20)*. Riga, Latvia: IEEE, Oct. 2020, pp. 195–200. ISBN: 978-1-72819-398-4. DOI: 10.1109/MTTW51045.2020.9244924

[38] F. Capligins et al. "FPGA Implementation and Study of Synchronization of Modified Chua's Circuit-Based Chaotic Oscillator for High-Speed Secure Communications." In: *2020 IEEE 8th Workshop on Advances in Information, Electronic and Electrical Engineering (AIEEE)*. Vilnius, Lithuania: IEEE, Apr. 2021, pp. 1–6. ISBN: 978-1-66542-538-4. DOI: 10.1109/AIEEE51419.2021.9435783

[39] D. Kolosovs. "A Multi-Mode Approach for the Enhanced Decision Adjusted Modulus Algorithm Usage in Blind Equalization of QAM Signals." In: *2021 IEEE Microwave Theory and Techniques in Wireless Communications (MTTW)*. Riga, Latvia: IEEE, Oct. 2021, pp. 40–45. ISBN: 978-1-66542-469-1. DOI: 10.1109/MTTW53539.2021.9607265

[40] F. Capligins, A. Litvinenko, and D. Kolosovs. "FPGA Implementation and Study of Antipodal Chaos Shift Keying Communication System." In: *2021 IEEE Microwave Theory and*

Techniques in Wireless Communications (MTTW). Riga, Latvia: IEEE, Oct. 2021, pp. 1–6. ISBN: 978-1-66542-469-1. DOI: 10.1109/MTTW53539.2021.9607226

The author presented the ideas reflected in this Doctoral Thesis at the following international scientific conferences:

1. D. Kolosovs. "Chaos Code Division Multiplexing Communication System." Riga Technical University 55th International Scientific Conference, Section Electronics. 14–17 October 2014, Riga.

2. D. Kolosovs. "Chaos Code Division Multiplexing Communication System." 7th International Conference on Computational Intelligence, Communication Systems and Networks, 3–5 June 2015, Riga.

3. D. Kolosovs. "Equalization Possibilities for Non-harmonic Multicarrier Communication Systems." Riga Technical University 56th International Scientific Conference, Section Electronics, 14–16 October 2015, Riga.

4. D. Kolosovs. "Constellation-Based Blind Equalization Cost Function Optimization." Riga Technical University 57th International Scientific Conference, Section Electronics, 14–18 October 2016, Riga.

5. Riga Technical University 58th International Scientific Conference, Section Electronics, 12–15 October 2017, Riga.

6. D. Kolosovs. "A Generalization of the Enhanced Decision-Adjusted Modulus Algorithm for Blind Equalization of Constellations with Closely Positioned Circles." 2020 IEEE Microwave Theory and Techniques in Wireless Communications (MTTW), 1–2 October 2020, Riga.

7. D. Kolosovs. "A Multi-Mode Approach for the Enhanced Decision Adjusted Modulus Algorithm Usage in Blind Equalization of QAM Signals." 2021 IEEE Microwave Theory and Techniques in Wireless Communications (MTTW), 7–8 October 2021, Riga.

During the writing of the Thesis, the author participated in the following projects. The list below enumerates projects where some of the ideas described in the paper were implemented or the study results were used.

1. Research No. 1.20. "Integra—New Generation Data Transmission Solutions" of the of the "Latvian Electrical and Optical Equipment Industry Competence Center."

2. Research No. 1.19. "Experimental Development for Data Transmission in Radio Frequency Bands above 60 GHz" of the "Latvian Electrical and Optical Equipment Industry Competence Center."

3. Research No. 1 "Wideband Dual Polarization Radio" of the "Latvian Electrical and Optical Equipment Industry Competence Center." Project 1.2.1.1./16/A/002.

4. SAM 8.2.2. "Rīgas Tehniskās universitātes akadēmiskā personāla stiprināšana stratēģiskās specializācijas jomās." in Riga Technical University. Project 8.2.2.0/18/A/017.

5. Research "Real-Time Spectrum Analyzer Structure and Material Research " of the "Latvian

Electrical and Optical Equipment Industry Competence Center." Project 1.2.1.1/18/A/006.

An essential result of the current Doctoral Thesis is a developed simulation workaround. It consists of Python and MathWorks MATLAB ® implementations of main blocks of QAM communication system (transmitter, various multipath baseband channels model, and sub-blocks of modem receiver: AGC, matched filters, and timing recovery system). There have also been performed multiple implementations of different structures of the equalizer. All blind equalization target factions that occurred in the bibliography have been implemented. All these workings can be used by engineers and scientists involved in digital signal processing to simulate processes in QAM-based communication systems. Students can also use them for learning principles of digital communications. Moreover, the author has already used these developments to form the program and prepare educational materials for the courses at Riga Technical University:

1. RRI705 "5G Wireless Technologies," 4.5 ECTS credits.
2. RRI706 "5G Wireless Technologies (course project)," 3.0 ECTS credits.
3. RTR532 "Simulation of Functional and Logical Circuits," 6.0 ECTS credits.
4. RRI324 "Digital Signal Processing," 3.0 ECTS credits.

This Doctoral Thesis's multiple modes parametric blind equalization algorithm generalizes constant modulus algorithm (CMA). It ensures the same or better convergence of equalizer and has zero steady-state and high tracking stability in case of successful convergence. The algorithm proved its properties in test stands and showed an end-user stable operation in the exploitation process. Therefore a replacement of CMA by this algorithm has no drawbacks, except a slight increase in implementation complexity, which is not a crucial problem for modern chips.

The Structure of the Thesis

Whereas the Thesis contains an appreciable amount of well-known concepts, especially in the description of QAM communication basics, it is oriented on the declarations, proofs, and development of original ideas. The author tried to avoid writing a textbook and described non-original subjects either to refer to them in the future or to proceed with writing in comparison with them.

The research evolved incrementally by generalizing the results obtained in the previous step. Therefore the structure of this Doctoral Thesis reflects this incremental approach to development. The following paragraphs outline the main topic of each chapter of the Thesis.

The first chapter is devoted to the basics of the QAM communication system. It designs models of the signals that are used in the research. Attention is also paid to the models of baseband multipath channels. An overview of the convenient structures of an equalizer and the principles of its operation are given. The chapter gives insight into the usage of blind equalization algorithms, introduces QAM, and emphasizes its advantages and drawbacks.

The second chapter is dedicated to the probabilistic approach to enhancing the target function

of DAMA. It shows a minimization process of the equalizer misadjustment probability and proposes DAMA. A short analysis of the main properties of the new algorithm is given. The simulation results and comparison withCMA and DAMA are supplemented.

The third chapter introduces an approach to the grouping of constellation points. The main applications and benefits of its usage are described.

The fourth chapter proposes a multiple mode parametric algorithm of blind equalization. It describes an idea of the generalization of CMA and proves the operating efficiency of the new algorithm. The chapter also focuses on proof of channel state tracking properties of the proposed algorithm.

The fifth chapter describes a VHDL implementation of the equalizer based on the proposed algorithm. It also contains the data on the equalizer connection to the QAM modem and the testing of the FPGA prototype. The results of field measurement and compliance with international communication standards have been also added.

1   RESEARCH FIELD GENERAL DESCRIPTION

As already noted, we tried to avoid writing a textbook. However, in this section, several reasons lead us to violate this intention. First, it is essential to keep the terminological minimum necessary for further presentation. Thus, we will give a rigorous definition of the research subject and show it as an aspect of the research object. As a result, at the end of this chapter, terms crucial for presenting the proposed ideas will be introduced and explained. Second, we understand that the reader may not be a blind equalization expert. Therefore, this chapter will give a brief theoretical background for the models used in this Thesis. Thirdly, such descriptions will enable us to emphasize the constraints for the models used and, consequently, for the proposed algorithms. Thus, the following chapter will be descriptive and not pretend to introduce scientifically novel ideas.

The first section is devoted to the theoretical basics of QAM. Schematic diagrams of the transmitter and receiver parts of the link are given, the necessity of each block is substantiated. This subsection introduces a mathematical description of the signal processing procedures used.

The second section focuses on the concept of the complex baseband for narrowband signal processing. Its application to the previously introduced QAM communication system is described. The limitations related to the use of the complex baseband approach are defined. This subsection also describes signal forming, dynamic processing, and detection nuances.

The third section discusses the approach to describing the transmission channel. The technique of the complex baseband for the channel model is applied; examples of the channels used in the Thesis are given.

The fourth section describes the effect of multipath propagation on a QAM signal. The subsection also discusses the concept of equalization and introduces an equalizer as one way to implement it. This subsection describes the static equalizer model and methods for adjusting it. The possibility of dynamic adjustment of the equalizer is considered.

The fifth section is devoted to the concept of blind equalization. The evolution of blind equalization algorithms is depicted, as well as the advantages and disadvantages of these algorithms. Several paragraphs discuss existing ways to compensate these drawbacks. The concept of the stochastic gradient is introduced. Particular attention is paid to the CMA algorithm. The subsection explains the need for research carried out in this Thesis.

1.1   Quadrature Amplitude Modulation Concept

The modulation process in data transmission systems ensures the transfer of the spectral density of a band-limited signal from zero to the carrier frequency region. In this way, it is possible to solve the following tasks:

- to provide frequency division of channels or users,

- to form a signal suitable for transmission and reception in wireless data transmission systems (to ensure that the resonance frequency of the antenna and the center frequency of the modulated signal correspond).

The simplest way to perform the modulation process and ensure that the specified conditions are met is to modulate the amplitude of the carrier and provide a double-sideband suppressed-carrier (DSB-SC) transmission. Assuming that the modulating signal is $s(t)$, the modulated signal can be expressed in this case as follows:

$$s_{\text{DSB-SC}}(t) = s(t) \cos 2\pi f_0 t, \tag{1.1}$$

where f_0 is the carrier frequency. According to one of the variations of the Euler's formula, the cosine can be decomposed into the sum of complex exponents $\cos x = (e^{jx} + e^{-jx})/2$. On the other hand, it follows from the frequency shift property of the Fourier transform that DSB-SC modulation produces two copies of the spectral density of a real signal $s(t)$ symmetrically at frequencies f_0 and $-f_0$. Thus, we obtain a real signal $s_{\text{DSB-SC}}(t)$ at a carrier frequency, corresponding to the requirements put forward above. Note that the bandwidth of the signal $s_{\text{DSB-SC}}(t)$ is twice the bandwidth of the real baseband signal $s(t)$.

The QAM approach can be considered a signal modulation method that eliminates the disadvantage of a twofold reduction in spectral efficiency. It uses the orthogonality property of sine and cosine functions of the same frequency f_0. In this case, two arbitrary signals $s_{\text{I}}(t)$ and $s_{\text{Q}}(t)$, which we will call the quadrature components, modulate carriers $\cos 2\pi f_0 t$ and $-\sin 2\pi f_0 t$, respectively. Thus, the signal obtained using this method can be expressed as

$$s_{\text{QAM}}(t) = s_{\text{I}}(t) \cos 2\pi f_0 t - s_{\text{Q}}(t) \sin 2\pi f_0 t. \tag{1.2}$$

The process of generating a QAM signal corresponds to the above-described approach of amplitude modulation with the suppressed carrier (DSB-SC). Thus we have two signals whose spectral densities are transferred to the same carrier frequency with a doubling of the bandwidth. Since both the occupied bandwidth and the amount of information transmitted have doubled, the spectral efficiency is as good as at baseband.

The forming of the quadrature components used for carriers modulation is generally limited only by the narrowband requirement, i.e., the frequency range occupied in the baseband Δf must be significantly less than the carrier frequency $\Delta f \ll f_0$. This requirement is necessary to ensure that the orthogonality property is locally fulfilled and signals $s_{\text{I}}(t)$ and $s_{\text{Q}}(t)$ are separable. However, an identical approach to information insertion and joint formation of both quadrature components gives several advantages:

- simplification of the signal forming and detecting parts of the transmitter and receiver,
- simplification of the operation of dynamic distortion compensation units,

- the possibility of forming a cost function for component separation in the case of incoherent receiving.

Joint and synchronous shaping of the quadrature components requires a clock signal and typically occurs in the digital domain. In this research, the transmitted signals are formed and processed discretely and then transferred to the analog domain. Thus, a QAM transmitter requires a digital-to-analog converter (DAC). In the analog signal at the output of this device, copies of the spectral density of the signal remain at frequencies that are multiples of the sampling frequency F_s. However, it must be noted that depending on the type of interpolation used in the DAC, these images may be partially suppressed. Nevertheless, the presence of a DAC implies the setting of a smoothing filter to suppress unnecessary spectral components in the analog signal. Thus, we have discussed the necessary elements of the QAM transmitter structure. Its block diagram is shown in Fig. 1.1.
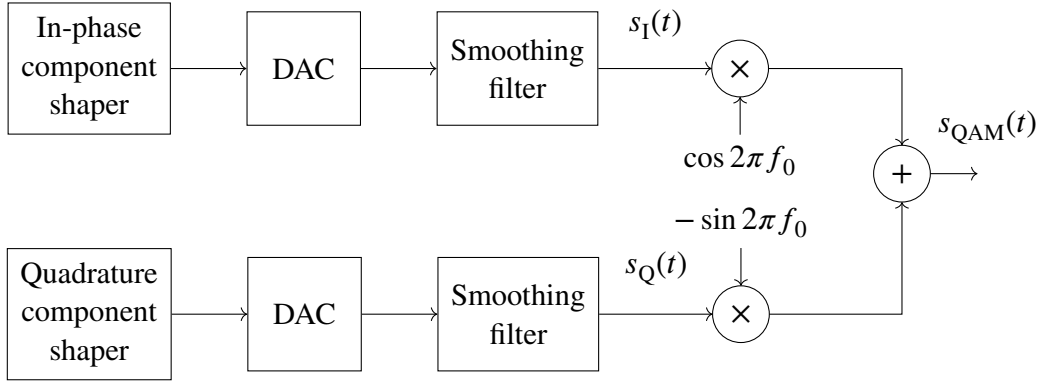
Fig. 1.1. QAM transmitter block diagram

The recovery of the transmitted data at the receiver requires demodulation of the signal $s_{\text{QAM}}(t)$. The spectral density of each quadrature component $s_{\text{I}}(t)$ and $s_{\text{Q}}(t)$ must be moved from the carrier f_0 to the baseband separately. As noted earlier, spectral density frequency shift involves multiplication by a complex exponent $e^{-j2\pi f_0 t}$. However, to preserve the signal's realness, the signal's spectral density must remain symmetrically distributed with respect to the zero frequency. Since the signal has spectral components at frequencies f_0 and $-f_0$, it must be multiplied by the weighted sum of the complex exponents $e^{-j2\pi f_0 t}$ and $e^{j2\pi f_0 t}$, corresponding to multiplying by the cosine or sine of these frequencies:

$$\hat{s}_{\text{I}}(t): \quad s_{\text{QAM}}(t)\frac{e^{j2\pi f_0 t} + e^{-j2\pi f_0 t}}{2} = s_{\text{QAM}}(t)\cos 2\pi f_0 t; \tag{1.3}$$

$$\hat{s}_{\text{Q}}(t): \quad s_{\text{QAM}}(t)\frac{e^{j2\pi f_0 t} - e^{-j2\pi f_0 t}}{2j} = s_{\text{QAM}}(t)\sin 2\pi f_0 t. \tag{1.4}$$

This approach is also consistent with the orthogonality of the two carriers used to form the signal. It is obviously necessary to find an analog of the correlation coefficient between the received signal $s_{\text{QAM}}(t)$ and the intended carrier to reconstruct the modulating signal. Given the narrowband re-

quirement for modulating signals $\Delta f \ll f_0$, it can be assumed constant for several carrier periods. Thus, according to its definition, it is necessary to multiply the received signal and the carrier and integrate the product over time to estimate the correlation in a certain period. The following result can be obtained by substituting 1.2 into the previous expressions:

$$\hat{s}_I(t): \quad s_{QAM}(t)\cos 2\pi f_0 t = \frac{s_I(t)}{2} + \frac{s_I(t)}{2}\cos 4\pi f_0 t - \frac{s_Q(t)}{2}\sin 4\pi f_0 t; \qquad (1.5)$$

$$\hat{s}_Q(t): \quad s_{QAM}(t)\cos 2\pi f_0 t = \frac{s_Q(t)}{2} - \frac{s_I(t)}{2}\cos 4\pi f_0 t - \frac{s_Q(t)}{2}\sin 4\pi f_0 t. \qquad (1.6)$$

Note that as a result of multiplication, terms with the corresponding double carrier frequency appear. Their presence also fits the approach with multiplication by the sum of two complex exponents. It is necessary to perform integration to estimate the local value of the correlation coefficient, which in practice is approximated by using a low-pass filter. The bandwidth of this filter is chosen to suppress components with double the carrier frequency and not distort the information signal. Thus the cut-off frequency f_c of the filter is conditioned be $\Delta f < f_c < f_0$. At the output of the filter the estimates of quadrature components $\hat{s}_I(t)$ and $\hat{s}_Q(t)$ are obtained. Fig. 1.2 shows the periodogram estimates of the modulated QAM signal and its changes in the QAM receiver. A QAM signal with symbol rate $R = 25$ Mbaud and the carrier frequency $f_0 = 150$ MHz is used for simulation.
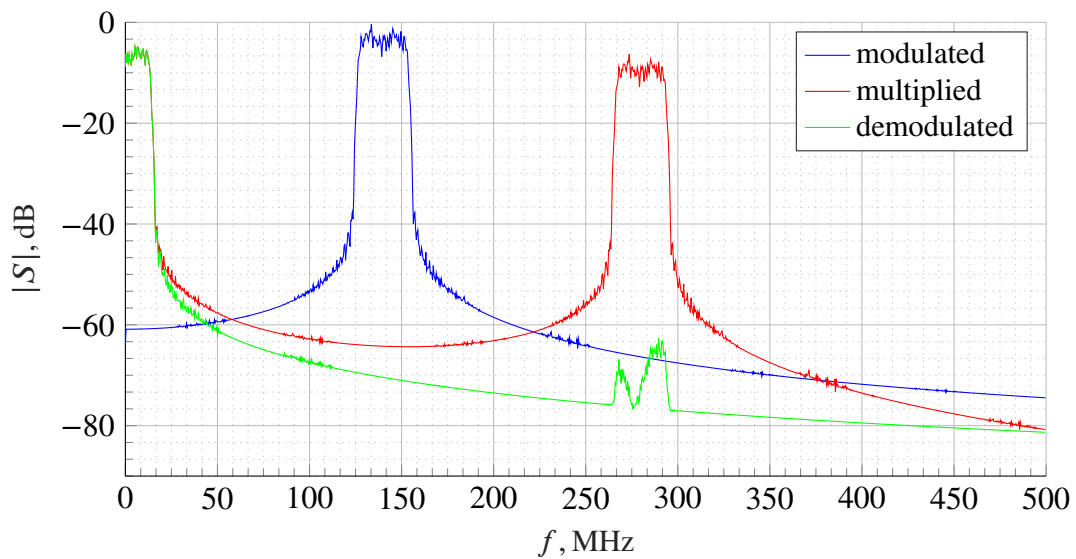
Fig. 1.2. Periodogram of the QAM signal changes in the receiver

Similarly, as in the case of the transmitter, the receiver requires joint processing of demodulated quadrature components. Within the framework of this research, the forming, processing, and detection take place on discrete signals. Therefore, a necessary part of the receiver is an analog-to-digital converter (ADC). Obviously, to fulfill the Sampling theorem and avoid overlapping the spectral densities of the signal after sampling, it is necessary to suppress the spectral components

28

above the Nyquist frequency $f_N = 0.5f_s$, where f_s is the ADC clock frequency. Thus, an anti-aliasing filter must be placed before the ADC. It is a low-pass filter with a cutoff frequency equal to the Nyquist frequency f_N. Since the anti-aliasing filter is more stringent than the aforementioned integrating filter (for narrowband signals), the two blocks are usually combined. The structure of the QAM receiver that performs the above actions is shown in Fig. 1.3.
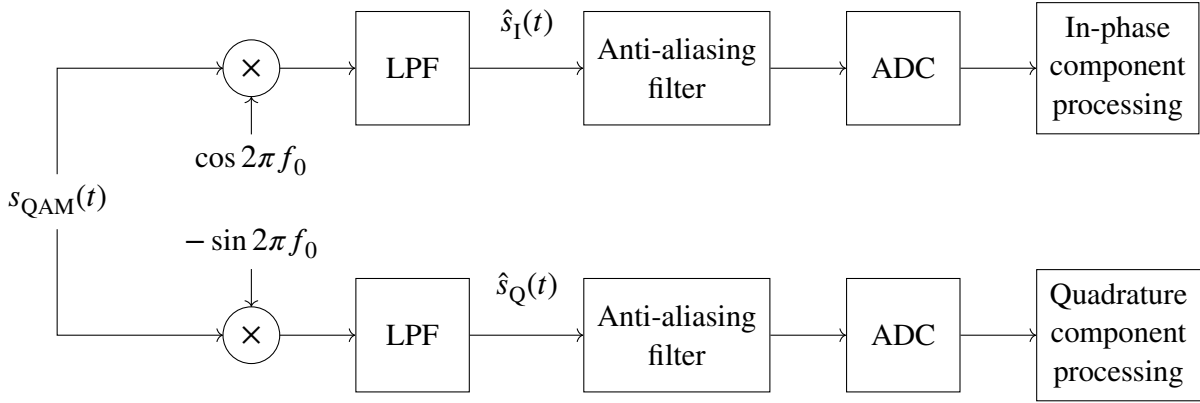
Fig. 1.3. QAM receiver block diagram

For further discussion, we introduce the following assumption. It is often impossible to generate sine and cosine waves of the same frequency and phase at the receiver as at the transmitter. Therefore, we consider the case of incoherent reception. Let us assume that the input signal at the receiver is multiplied by sine $\sin(2\pi f_0 t + \varphi(t))$ and cosine $\cos(2\pi f_0 t + \varphi(t))$, where $\varphi(t)$ is the time-varying instantaneous phase. Then, substituting these functions into the expressions (1.5) and (1.6), multiplying and discarding the terms of the double frequency, we obtain the following expressions

$$\hat{s}_I(t) = \frac{s_I(t)}{2}\cos\varphi(t) + \frac{s_Q(t)}{2}\sin\varphi(t); \tag{1.7}$$

$$\hat{s}_Q(t) = -\frac{s_I(t)}{2}\sin\varphi(t) + \frac{s_Q(t)}{2}\cos\varphi(t). \tag{1.8}$$

Analysis of expressions for demodulated quadrature components in the case of incoherent reception leads to the following conclusions. First, assume the phase linearly increases in time, i.e., there is a frequency difference between the transmitter and receiver oscillators. Then the spectral density of the modulated signal is shifted not to zero frequency but a frequency equal to the difference of the carriers frequencies. It is easy to see that the frequency range occupied by the signal in the baseband increases in this case. This can lead to distortion caused by passing through band-matched filters. Second, non-coherent receiving leads to the appearance of a time-varying correlation between the quadrature components. Imagine that the in-phase and quadrature components are vector projections in a Cartesian coordinate system. Then (1.7) and (1.8) coincide with the expressions for the Given rotation of this vector. In the case of a linearly growing phase difference, the angle of rotation of

this vector will also change with time.

The most straightforward data transmission system consists of three parts: a transmitter, which generates a signal intended for transmission, a propagation channel, which is a medium for signal transmission, and a receiver, which extracts information from the transmitted signal. A structural diagram of such a data transmission system is shown in Fig. 1.4.
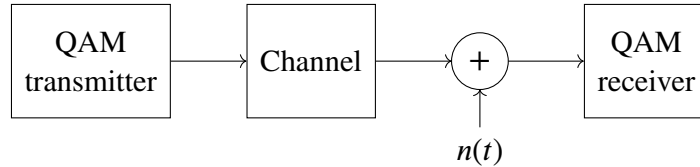
Fig. 1.4. QAM wireless data transmission system block diagram

In the figure, the block in which AWGN $n(t)$ is applied to the transmitted signal is shown separately from the channel. That approach is made for two reasons. First, in wireless data transmission systems, the primary source of such noise is the first stages of the radio path of the receiver, especially the low-noise radio frequency amplifier. Secondly, due to the specifics of this work, the channel is singled out separately as a model for effects added by the multipath propagation.

1.2 Complex Baseband Model of the QAM Communication System

Simulating a narrowband signal and explicitly using the data transmission system shown in Figure 1.4 is complicated for several reasons. On the one hand, the sampling frequency for the correct display of the carrier waveform must be several times higher than the frequency of the carrier itself. On the other hand, for signal processing (both baseband and bandpass), it is enough to take the sampling frequency that satisfies the Sampling theorem: twice the maximum frequency in the spectral density of the signal. In practice, it is taken slightly higher to perform pulse-shaping in the digital domain correctly. Considering that the $\Delta f \ll f_0$ requirement is fulfilled for bandpass signals, we observe the presence of a significant frequency overhead, which is not necessary for simulating an information signal. It should also be noted that in this work, not only signal transmission is simulated, but also its forming and subsequent processing. Since the study is orientated on the transmitter and receiver implementation, a frequency overhead in the transmitter and receiver is impossible. Therefore, these two blocks must be simulated using the complex baseband approach. For this reason, the same approach will be applied to simulation and signal transmission in a multipath channel.

Let us consider the extraction of a complex envelope from a QAM signal and the applicability of working with a complex envelope to simulate the described data transmission system. The so-called analytical signal $\dot{s}(t)$ is calculated for a real signal $s(t)$ and describes one that does not contain negative-frequency spectral components. The Fourier transform properties imply that such a signal

30

has a non-zero imaginary component. The Hilbert transform relates the real $s(t)$ and imaginary $\hat{s}(t)$ parts of such a signal:

$$\dot{s} = s(t) + j\mathscr{H}\{s(t)\}, \tag{1.9}$$

where $\mathscr{H}\{\cdot\}$ denotes Hilbert transform. In the case of narrowband signals, the analytical signal $\dot{s}$ can be expressed as the product of the complex envelope $\dot{S}(t)$ and the complex exponent corresponding to the carrier frequency $e^{j2\pi f_0 t}$.

The quadrature components $s_I(t)$ and $s_Q(t)$ in the QAM transmitter described above are frequency-limited baseband signals. The signal obtained at the output of the quadrature modulator $s_{QAM}(t)$ is narrowband and is described in (1.2). The analytical signal, in this case, can be represented as

$$\begin{aligned}
\dot{s}_{QAM}(t) &= s_I(t)\cos 2\pi f_0 t - s_Q(t)\sin 2\pi f_0 t + j\left[s_I(t)\sin 2\pi f_0 + s_Q(t)\cos 2\pi f_0 t\right] \\
&= s_I(t)\,e^{2\pi f_0 t} + j s_Q(t)\,e^{2\pi f_0 t} \\
&= \left[s_I(t) + j s_Q(t)\right]e^{2\pi f_0 t} = \dot{S}_{QAM}(t)\,e^{2\pi f_0 t}.
\end{aligned} \tag{1.10}$$

In this derivation, the narrowband property of the signal was used, in which the modulating signal can be considered constant over several periods of the carrier. In this case, the following equalities are valid (for positive frequencies $f_0 > 0$)

$$\mathscr{H}\left\{s(t)\cos 2\pi f_0 t\right\} = s(t)\sin 2\pi f_0 t \quad \text{and} \quad \mathscr{H}\left\{s(t)\sin 2\pi f_0 t\right\} = -s(t)\cos 2\pi f_0 t. \tag{1.11}$$

Thus, in the case of a QAM signal, the complex envelope is the sum of the in-phase (with a weight of one) quadrature (with a weight of imaginary unit j) components. For further derivations, we denote the signal generated at the transmitter as $s_{Tx}(t)$ and the signal that came to the receiver as $s_{Rx}(t)$. The complex envelopes of these signals will be $\dot{S}_{Tx}(t)$ and $\dot{S}_{Rx}(t)$, respectively. Assume the channel is a linear time-variant system with impulse response $h(\tau, t)$. However, we will consider the changes in the channel are slow enough to assume the channel time-invariant for a certain number of carrier periods. The channel frequency response $H(f, t) = \mathscr{F}\{h(\tau, t)\}$ is expressed as the Fourier transform of the impulse response with respect to the τ variable. In the system shown in Fig. 1.4, the signal at the receiver input can be obtained as a convolution of the transmitter signal with the channel impulse response:

$$s_{Rx}(t) = s_{Tx}(t) * h(\tau, t). \tag{1.12}$$

Let us take into account that the Hilbert transform is a convolution with the impulse response of the Hilbert filter $h(t) = 1/\pi t$. Passing a signal through such a filter is identical to the product of positive-frequency spectral components by $-j$ and negative-frequency spectral components by j.

Taking this into account, we can express the analytical signal from both parts of expression (1.12):

$$s_{\text{Rx}}(t) + j\mathcal{H}\left\{s_{\text{Rx}}(t)\right\} = s_{\text{Tx}}(t) * h(\tau,t) + j\mathcal{H}\left\{s_{\text{Tx}}(t) * h(\tau,t)\right\}$$
$$= s_{\text{Tx}}(t) * h(\tau,t) + j\mathcal{H}\left\{s_{\text{Tx}}(t)\right\} * h(\tau,t)$$
$$= \left[s_{\text{Tx}}(t) + j\mathcal{H}\left\{s_{\text{Tx}}(t)\right\}\right] * h(\tau,t), \qquad (1.13)$$

where the associative and commutative properties of convolution have been applied. For arbitrary signals $a(t)$, $b(t)$, and $c(t)$ expression $a(t) * [b(t) * c(t)] = [a(t) * b(t)] * c(t)$ is valid. Further, let us recall that the analytical signal has only positive frequency spectral components. Thus calculating an analytic signal from an analytic signal will give the same signal. In the previous equation, let us denote the expressions for analytical signals with $\dot{s}_{\text{Tx}}(t)$ and $\dot{s}_{\text{Rx}}(t)$. The calculation of the analytical signal from both parts will give

$$\dot{s}_{\text{Rx}}(t) + j\mathcal{H}\left\{\dot{s}_{\text{Rx}}(t)\right\} = \dot{s}_{\text{Tx}}(t) * h(\tau,t) + j\mathcal{H}\left\{\dot{s}_{\text{Tx}}(t) * h(\tau,t)\right\}$$
$$= \dot{s}_{\text{Tx}}(t) * h(\tau,t) + j\dot{s}_{\text{Tx}}(t) * \mathcal{H}\left\{h(\tau,t)\right\}$$
$$= \dot{s}_{\text{Tx}}(t) * \left[h(\tau,t) + j\mathcal{H}\left\{h(\tau,t)\right\}\right]$$
$$= \dot{s}_{\text{Tx}}(t) * \dot{h}(\tau,t), \qquad (1.14)$$

where $\dot{h}(\tau,t)$ is the analytic signal for the channel impulse response. According to the property of the Fourier transform (the Convolution Theorem), convolution in the time domain corresponds to the product of the spectral densities in the frequency domain. Then the previous expression can be rewritten into

$$\mathcal{F}\left\{\dot{s}_{\text{Rx}}(t)\right\} = \mathcal{F}\left\{\dot{s}_{\text{Tx}}(t)\right\}\mathcal{F}\left\{\dot{h}(\tau,t)\right\}. \qquad (1.15)$$

Given that the analytic signal can be expressed as the product of a complex envelope and a complex exponent, the expression becomes

$$\mathcal{F}\left\{\dot{S}_{\text{Rx}}(t)\,e^{j2\pi f_0 t}\right\} = \mathcal{F}\left\{\dot{S}_{\text{Tx}}(t)\,e^{j2\pi f_0 t}\right\}\mathcal{F}\left\{\dot{H}(\tau,t)\,e^{j2\pi f_0 t}\right\}$$
$$\mathcal{F}\left\{\dot{S}_{\text{Rx}}(t)\right\}(f - f_0) = \mathcal{F}\left\{\dot{S}_{\text{Tx}}(t)\right\}(f - f_0)\mathcal{F}\left\{\dot{H}(\tau,t)\right\}(f - f_0). \qquad (1.16)$$

We can shift the frequency axis for all presented Fourier images using substitution $f - f_0 \rightarrow f'$. Applying the Convolution theorem again, we find that convolving the complex envelope of the transmitter signal $\dot{S}_{\text{Tx}}(t)$ with the complex envelope of the channel impulse response $\dot{H}(\tau,t)$ gives the complex envelope of the received signal $\dot{S}_{\text{Rx}}(t)$:

$$\dot{S}_{\text{Rx}}(t) = \dot{S}_{\text{Tx}}(t) * \dot{H}(\tau,t) + \dot{N}(t), \qquad (1.17)$$

where $\dot{N}(t)$ is the complex envelope of the AWGN applied to the received signal at the first stages

of the radio path. We have omitted this term in the previous derivations for the sake of simplicity; however, it does not impact the generality of the results. It can be easily proved that (1.17) is valid for band-limited noise signals, which fits in the existing systems.

Consider the changes that occur to the signal in the receiver. In the case of in-phase generation of harmonic oscillations at the receiver and sufficient attenuation of the low-pass filter, the received signal will coincide with the transmitted one, as follows from (1.5) and (1.6). If we are dealing with incoherent receiving, then the signal at the receiver output is described by (1.7) and (1.8). These two real baseband signals are obtained by shifting the spectral density of the received bandpass signal from the carrier to zero frequency with a phase difference of $\varphi(t)$. Section 1.1 noted that such a shift in the frequency domain corresponds to multiplication by a complex exponent in the time domain. Suppose the received bandpass signal is represented as an analytical one. In that case, it is only necessary to carry out a shift from frequency f_0 since the signal lacks negative-frequency spectral components. We have added a term in the exponent argument $e^{-j2\pi f_0 t - j\varphi(t)}$ to take into account the phase difference. Let us represent the analytical received signal in the following form:

$$\dot{s}_{\text{Rx}}(t) = \left[s_{\text{RxI}}(t) + j s_{\text{RxQ}}(t) \right] e^{j2\pi f_0 t} \tag{1.18}$$

Then the result of the spectral density shift of the signal is expressed in the form

$$\dot{s}_{\text{Rx}}(t) \, e^{-j2\pi f_0 t - j\varphi(t)} = \left[s_{\text{RxI}}(t) + j s_{\text{RxQ}}(t) \right] e^{-j\varphi(t)} \tag{1.19}$$
$$= \left[s_{\text{RxI}}(t) \cos\varphi(t) + s_{\text{RxQ}}(t) \sin\varphi(t) \right] + j \left[s_{\text{RxQ}}(t) \cos\varphi(t) - s_{\text{RxI}}(t) \sin\varphi(t) \right].$$

Here, the Euler formula was used to expand the complex exponents. Analyzing the received demodulated signal, we see the following.

- The signal is a complex envelope, i.e., it lacks a carrier multiplier. It is in line with the essence because we should receive a signal in the baseband as a result of demodulation.
- We see their coincidence when comparing the real and imaginary parts of the expression (1.19) with (1.7) and (1.8).

Thus, we have shown that considering a complete model and using complex envelopes to simulate the data transmission system shown in Fig. 1.4 gives the same results if the following conditions are met:

1. The smoothing filter is present in the system, and its attenuation in the stopband is sufficient to ignore the suppressed spectral components corresponding to the harmonics of the sampling frequency F_s.
2. The modulating signal bandwidth to the carrier frequency ratio is such $\Delta f \ll f_0$ that the signal can be considered a narrowband.
3. The changes in the channel parameters over time are slow enough to be considered time-invariant for several carrier periods.

33

4. The difference in carrier frequencies at the transmitter and receiver (mean value of the $\varphi(t)$ time derivative) is that passing the demodulated signal through the low-pass filter and anti-aliasing filter does not introduce linear distortion into the signal.

5. The anti-aliasing filter is present in the system. Its stopband attenuation is sufficient to ignore the spectral components corresponding to frequencies above half the sample rate. The same requirement has been put forward to attenuate the spectral components of the sum of the transmitter and the receiver carrier frequencies.

A few clarifications need to be made regarding the choice of the sampling frequency. Both quadrature components are real signals, so the requirements for the feasibility of their sampling and recovery are determined by the Sampling theorem. It postulates that there should be no components corresponding to frequencies above half the sampling frequency in the spectral density of the signal. However, this means a step between passband and stopband for smoothing filters in practice.

Now consider the complex envelope $\dot{S}(t)$ of a signal $s(t)$. Assume that the choice of sampling frequency meets the requirements described in the previous paragraph. The Fourier transform of a signal describes its energy distribution in the frequency domain. We consider that this is a linear operation, and a complex signal is a weighted sum $\dot{S}(t) = s(t) + j\mathcal{H}\{s(t)\}$ of its real $s(t)$ and imaginary $\mathcal{H}\{s(t)\}$ parts. Thus, the Fourier transform of a complex envelope is the weighted sum of the Fourier transforms of its real and imaginary parts

$$\mathcal{F}\left\{\dot{S}(t)\right\} = \mathcal{F}\left\{s(t)\right\} + j\mathcal{F}\left\{\mathcal{H}\left\{s(t)\right\}\right\}. \tag{1.20}$$

Obviously, the appearance of spectral components not present in any of the signals is impossible. Therefore, identical requirements are put forward for choosing the sampling frequency of the complex envelope as for each of the quadrature components.

Consider an incoherent sampling of the received signal in the ADC. Assume that the signal sample $s[n]$ at the receiver was formed at time $t = nT_s$ ($T_s = 1/F_s$ is the sampling step) and converted into an analog signal $s(nT_s)$. At the receiver at the moment $t = nT_s + \tau(t)$, the instantaneous value of the signal $s(nT_s + \tau(t))$ is sampled and matched with the transmitter sample $s[n]$. We divide the variable $\tau(t)$ into the following components:

$$\tau(t) = \frac{t}{T_s}\frac{1}{\Delta F_s} + \tau_0 + \tau_N(t), \tag{1.21}$$

where ΔF_s is the transmitter and receiver sampling frequency difference, τ_0 is the constant transmission line delay, and $\tau_N(t)$ is a random time-variant delay component. Thus, if the transmitter and receiver sampling frequencies are different $\Delta F_s \neq 0$, each successive sample will be delayed by a linearly increasing amount of time $n/\Delta F_s$. As a result, the signal is stretched in time for $\Delta F_s > 0$ at the receiver and shrank for $\Delta F_s < 0$. According to the time scaling property of the Fourier transform, this implies spectral density shrinking and stretching, respectively. From (1.21) it follows

34

that the difference in sampling frequencies can be simulated by setting a time-varying delay at the receiver.

Thus, we can add two more requirements to the complex baseband model, which must comply with the existing data transmission system.

6. The sampling frequency must be chosen so that the Sampling theorem is fulfilled for each quadrature channel. Additionally, it must be possible to implement smoothing filters after the DAC.

7. Suppose the sampling rate at the receiver is greater than the sampling rate at the transmitter. In that case, the expansion of the spectral density of the signal should not lead to linear distortions in the digital filtering structures of the receiver.

In practice, both criteria are easily satisfied if baseband bandwidth to the sampling frequency ratio is $\Delta f / F_s < 0.4$. In this paper, simulations are made with an even smaller ratio of these variables.

We have described a complex baseband model of the data communication system shown in Fig. 1.4. Above, the requirements for system parameters have been given to ensure the relevance of the model. Fig. 1.5 shows a block diagram of a QAM-based wireless data transmission system model.
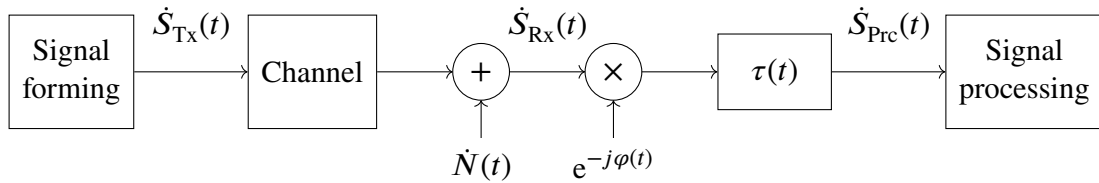
Fig. 1.5. Complex baseband model of the QAM-based wireless data transmission system

The figure indicates necessary signals for further discussion. So, $\dot{S}_{\mathrm{Tx}}(t)$ denotes the complex envelope of the signal generated at the transmitter. Expression (1.17) describes the complex envelope of the signal coming at the receiver $\dot{S}_{\mathrm{Rx}}(t)$. In turn, the signal prepared for further processing in the receiver in the form of a complex envelope is expressed through

$$\dot{S}_{\mathrm{Prc}}(t) = \dot{S}_{\mathrm{Rx}}(t - \tau(t)) \, e^{-j\varphi(t-\tau(t))} \,. \tag{1.22}$$

Consider the principles of signal shaping on the transmitter. In the complex baseband model of the QAM data transmission system shown in Fig. 1.5, the node that implements this function is designated as a "Signal forming" block. Its function is to convert the user data stream into a band-limited signal suitable for transmission. For simulation purposes, this block also generates user data, which is a sequence of integers

$$\{m_k | 0 \leqslant m_k < M\}, \tag{1.23}$$

where m_k is kth generated integer, an amount of user data, and $M \in \mathbb{N}$ is the cardinality of the set

from which these integers are taken. The elements of this sequence have the following properties.

- All elements of the set from which the generated elements of the sequence are taken are equally probable.

- The autocorrelation function of a given sequence is a delta-function, i.e., the value of the kth element of the sequence does not depend on any of the previous and subsequent generated elements.

It is not always necessary to match the user sequence to the listed properties in practical implementations. In this case, a scrambling device of sufficient length is installed on the transmitter to fulfill the above requirements for the transmitted sequence. The binding of a piece of user information corresponding to a sequence element m_k to the instantaneous values of the transmitted signal is performed through mapping. Each unique element of the sequence $\{m_k\}$ is associated with an element of the set of signal points $\{a_k\}$. The transmission of a signal point $s_k \in \{a_k\}$ means that an element m_k of the user sequence has been generated. Both sets have the same cardinality $|\{m_k\}| = M$ and $|\{a_k\}| = M$ and are related through bijection. Therefore the requirements of equiprobability and non-correlation fulfillment for the user data sequence will also be valid for signal points. Since the task of the block is to form a complex envelope $\dot{S}_{\mathrm{Tx}}(t)$, the elements belonging to the set of unique signal points are complex $a_k \in \mathbb{C}$. Further, the absolute value of a point will be denoted by $|a_k|$. In this work, we will refer to set $\{a_k\}$ as a constellation, and the sequence of transmitted or received signal points will be depicted on constellation diagrams. Fig. 1.6 shows the structure of the signal forming block representing the transmitter in the complex baseband model of the QAM communication system.
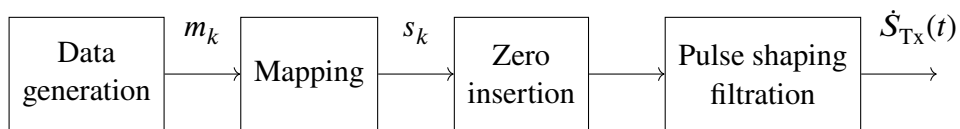
Fig. 1.6. Signal shaping block of the complex baseband QAM data transmission system

Consider the time parameters of the above-described blocks. All nodes shown in Fig. 1.6 operate on the edges of the transmitter clock signal, which corresponds to the sampling frequency. In the case of generating transmitted signal points on each clock cycle, the signal will be a sequence of Kronecker pulses. It is easy to prove that the spectral density of such a signal is uniformly distributed over the frequency range from zero to the Nyquist frequency f_{N}. Therefore, it is impossible to form a band-limited signal in the digital domain and apply smoothing filters in the analog domain using this approach. Thus, the conditions for the relevance of the complex baseband model are not met.

Let us regard the moments of time $t = kT_{\mathrm{sym}}$, where k is an integer, $T_{\mathrm{sym}} > T_{\mathrm{s}}$ is a certain time interval, so that $T_{\mathrm{sym}} = KT_{\mathrm{s}}$, $K \in \mathbb{N}$ (here T_{s} is the sampling step, and the variable T_{sym} will be referred to as symbol duration). If the user data sequence elements are generated at these time

moments, the generated signal $s_z[n]$ will consist of one signal point per K samples; the remaining samples are assumed to be represented by zeros. Such a signal can be considered a K times resampled sequence of Kronecker pulses. Recall that the spectral density of a resampled signal becomes periodic. Thus, in the $f \in [0, f_N]$ frequency range, the unique components of the signal spectral density populate the range $f \in [0, f_N/K)$. In this case, it is possible to suppress unnecessary spectral components, form a band-limited signal, and perform correct smoothing after the DAC.

The switching of the generated signal points and the non-information-carrying samples occurs in the "Zeros insertion" block. The signal at the output of the block will be denoted as $s_z[n]$. In the framework of this work, for practical implementation, the number of samples per symbol $K = 2$ was used; however, some simulations were also carried out with $K = 4$ for clarity of visualization. The spectral densities of signals with and without inserted zeros are shown in Fig. 1.7. $K = 4$ was used in this experiment; the high-frequency spectral components are slightly suppressed for visualization purposes.
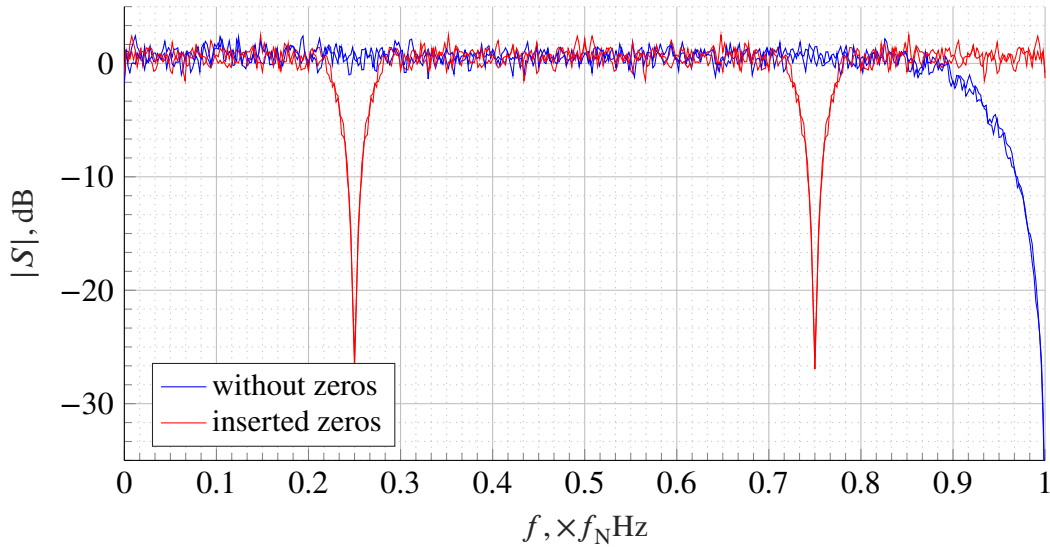
Fig. 1.7. Visualization of the effect of zero insertion on signal spectral density

We concluded that each signal point s_k, or symbol, can be transmitted during T_{sym}, including K samples. Let us represent this symbol as a rectangular pulse of duration $\Delta t = T_{\text{sym}} = KT_s$. The spectral density of such a signal is expressed as

$$\dot{S}(f) = s_k T_{\text{sym}} \operatorname{sinc}\left(\pi f T_{\text{sym}}\right). \tag{1.24}$$

The width of the main lobe of the spectral density is

$$\Delta f = \frac{1}{T_{\text{sym}}} = \frac{1}{KT_s} = \frac{F_s}{K} = \frac{2F_N}{K}, \tag{1.25}$$

which corresponds to a half-wave of the $\sin\left(\pi f T_{\text{sym}}\right)$. As noted earlier, the unique spectral compo-

nents in a zero-inserted signal are located within the frequency range $\Delta f = f_N/K$. Thus, this series of rectangular pulses must be passed through a low-pass filter with a $f_c = f_N/K$ cutoff frequency to limit the bandwidth of the transmitted signal. However, as a result of suppression of the side lobes, the duration of the rectangular pulse will increase $\Delta t > T_{sym}$, which will lead to symbol overlap and the appearance of inter-symbol interference. According to the Fourier transform properties, multiplication in the time domain corresponds to convolution in the frequency domain. Any time-limited pulse can be represented as the multiplication of a periodic signal by a rectangular pulse. It corresponds to the convolution of a function with a set of δ-functions in the frequency domain. Therefore, the pulse of any other shape will be of wider bandwidth.

The solution to this problem is to use a filter that satisfies the Nyquist ISI criterion. It is fulfilled if there are zeros in the filter impulse response $h(t)$ in places corresponding to the occurrence times of adjacent symbols $t = kT_s$. It should be noted that the criterion must be fulfilled for the sum of all filtering structures in the data transmission system. Usually, the shaping filter of the transmitter $h_{Tx}(t)$ and the matched filter of the receiver $h_{Rx}(t)$ are taken into account. The convolution of their impulse responses must fulfill the Nyquist ISI criterion. In the Thesis, root-raised cosine filter is used, the impulse response of which [41] describes as

$$
h[n] = \begin{cases} \dfrac{1}{T_{sym}}\left[1 + \alpha\left(\dfrac{4}{\pi} - 1\right)\right], & n = 0 \\[3mm] \dfrac{\alpha}{T_{sym}\sqrt{2}}\left[\left(1 + \dfrac{2}{\pi}\right)\sin\left(\dfrac{\pi}{4\alpha}\right) + \left(1 - \dfrac{2}{\pi}\right)\cos\left(\dfrac{\pi}{4\alpha}\right)\right], & n = \pm\dfrac{K}{4\alpha} \\[3mm] \dfrac{1}{T_{sym}}\dfrac{\sin\left[\pi\dfrac{n}{K}(1-\alpha)\right] + 4\alpha\dfrac{n}{K}\cos\left[\pi\dfrac{n}{K}(1+\alpha)\right]}{\pi\dfrac{n}{K}\left[1 - \left(4\alpha\dfrac{n}{K}\right)^2\right]}, & \text{otherwise} \end{cases}
\tag{1.26}
$$

In the expression, α is the roll-off factor. The following requirements are set to the selection of filters and their parameters.

- The filter must produce a signal whose spectral density fits into the spectral mask at the transmitter.
- At the receiver, the combined impulse response of the two filters must satisfy the Nyquist criterion.
- The receiver filter must have sufficient stopband attenuation to suppress the adjacent channel and additive noise.

In the Thesis, a filter with a length of $L = 64$ coefficients and a roll-off factor of $\alpha = 0.25$ is used for simulations. The filter coefficients are normalized to provide $G = 0\,\text{dB}$ DC gain.

In the complex baseband model, the output signal of the signal forming block is constructed by passing the signal with inserted zeros through the pulse-shaping filter. Thus, $\dot{S}_{Tx}[n]$ is expressed by

convolution

$$\dot{S}_{\text{Tx}}[n] = s_{\text{z}}[n] * h_{\text{Tx}}[n]. \tag{1.27}$$

In Fig. 1.8, red marks the real part (corresponds to the in-phase quadrature component) of the zero-insert block output signal $s_{\text{z}}[n]$. Blue line indicates the signal obtained passing the previous one through the pulse-shaping filter. Both the transmitter and the receiver filters were used to demonstrate the fulfillment of the Nyquist criterion. For the simulation, a 16-QAM constellation was used. It means the cardinality of the set of symbol points is $|\{a_k\}| = 16$; however, there are only four unique levels of the real part of the symbols. The number of samples per symbol, in this case, is $K = 4$.
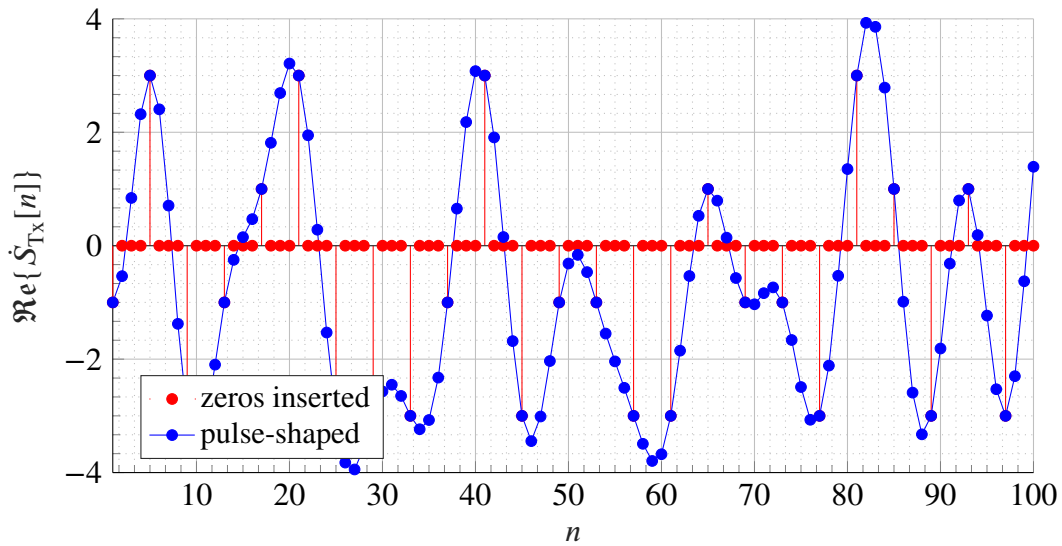
Fig. 1.8. The formation of the transmitter signal samples through the generation of symbols and pulse-shaping
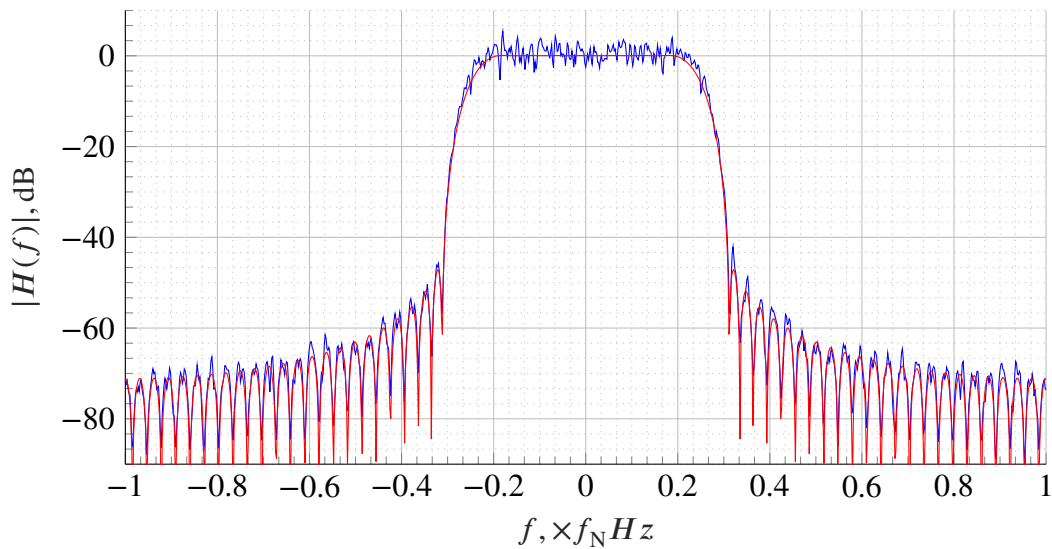
Fig. 1.9. The spectral density of the transmitter signal and the magnitude response of the pulse-shaping filter

In Fig. 1.9, the blue line estimates the two-sided spectral density of the signal generated at the

transmitter. The red line shows the frequency response of the filter used for the pulse-shaping. Because the transmitted signal is shaped as a complex envelope, its spectral density is not symmetrical around zero frequency (or carrier frequency in the case of a bandpass signal).

Consider the signal processing node from Fig. 1.5. It models the operation of the digital part of the QAM receiver. The simplest receiver performs the following functions.

- Estimate the correlation of the transmitted signal with a predefined a priori known pattern. In the system under consideration, this task is performed by a matched filter, which generates the maximum signal-to-noise ratio at the moments when the entire symbol generated at the transmitter is in the filter registers.

- Make a decision on the value of the transmitted signal. In our case, the distance to the nearest point of the QAM constellation is estimated.

However, in true-to-life systems, the signal during propagation and passage through the radio path of the receiver undergoes several distortions. In the case of non-compensation, this leads to degradation of the system performance. At the beginning of the section, we discussed a system model that considers:

- carrier frequency difference at the transmitter and receiver;
- difference of the modem clock frequencies at the transmitter and receiver;
- multipath signal propagation;
- the presence of thermal noise in the receiver.

Fig. 1.10 shows a system that takes into account the sequence of introducing distortions into the signal and the receiver unit in which these distortions are compensated.
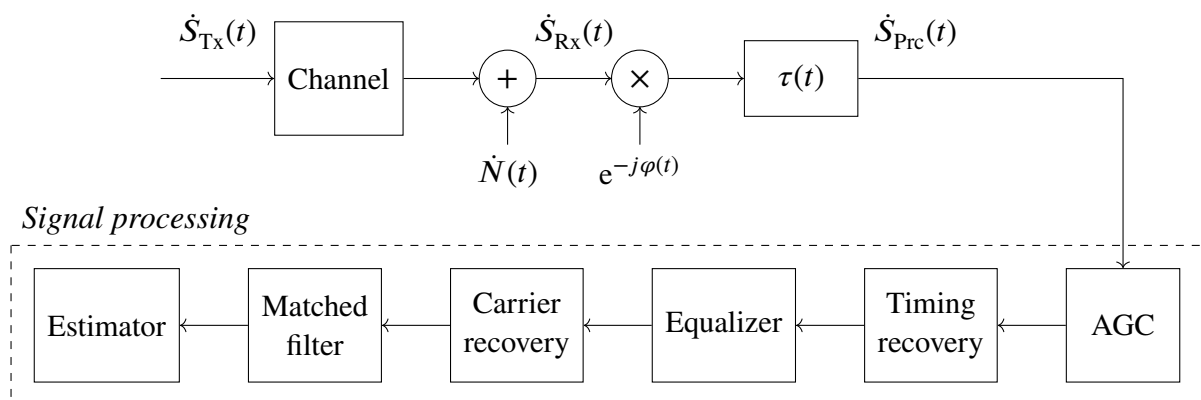
Fig. 1.10. Receiver signal processing block structure

To properly compensate for multiple signal distortions in the receiver, arranging the compensation blocks in a strictly defined order is necessary. The distortion introduced last into the signal must be compensated first in the receiver. The rule can be ignored for linear time-varying distortions. However, the above effects introduce time-varying distortions in practical data transmission systems. Therefore, the movement of blocks must be accompanied by an analysis of the rate of change of the effect. Let us analyze the blocks present in the " Signal processing" node in Fig. 1.10.

Adjustment of the power level of the received signal is often implemented in the radio part of the receiver. Duplication of the gain control functionality in the modem part is necessary to compensate for changes that:

- are faster than the analog block can correct;
- appeared after the filtration of unnecessary spectral components;
- occurred after analog AGC receiver.

These changes are usually associated with mechanical or thermal effects on the data transmission system. Therefore, changing the signal level and its dynamic compensation is slow enough to consider the signal level constant when regarding other effects. Applying correction in the AGC module is done through $s_{\mathrm{AGC}}[n] = \dot{S}_{\mathrm{Prc}}[n]a[n]$, where $a[n]$ is the current gain. The cost function for gain adjustment is signal power estimation $\mathbb{E}\left[|\dot{S}_{\mathrm{Prc}}[n]|^2\right]$ ($\mathbb{E}[\cdot]$ denotes mathematical expectation). It is important to note that changes in signal strength may occur due to a time-varying channel, e.g., in the case of flat fading. However, we will accept signal $s_{\mathrm{AGC}}[n]$ unchanged in power even in this case.

The last distorting effect on the analog signal, the time-varying sample time shift, occurs during the analog-to-digital conversion. Following the previously mentioned prescription, its compensation should be implemented at the first processing stage. The movement of the AGC block before the timing recovery is possible for two reasons:

- signal power level changes are much slower than time-shift effects;
- the effects do not affect the cost functions of these two blocks.

Compensation occurs by introducing an additional time-varying time shift into the received signal

$$s_{\mathrm{TR}}[n] = s_{\mathrm{TR}}\left[n - \tau[n] - \tau_{\mathrm{TR}}[n]\right], \tag{1.28}$$

where $\tau[n]$ is the system introduced time shift for the current clock cycle n, and $\tau_{\mathrm{TR}}[n]$ is the timing recovery block introduced additional time shift such that $\tau[n] + \tau_{\mathrm{TR}}[n] = \mathrm{const}$. With a difference in the clock frequencies of the transmitter and receiver, the time shift is constantly increasing. To prevent the accumulation of unprocessed samples, one must either stop processing for one clock cycle or process two samples simultaneously. Fractional time shift is performed using interpolating filters with a constant phase delay. The cost function of the adjustment used in the Thesis is the phase of the spectral component corresponding to the edge of the band. The implemented timing recovery algorithm in the Matlab environment is given in Appendix B.2. It should be noted that channel changes can also introduce a time shift into the signal. Considering the subsequent blocks of the signal processing node, we will assume that the timing has been restored.

The operation that distorts the signal and precedes the analog-to-digital conversion is quadrature demodulation, as seen in Fig. 1.3. Separately passing the quadrature components of the demodulated signal through anti-aliasing filters results in different powers of the quadrature components, different

time shifts, and the presence of DC components. All these effects cause quadrature components impairments. Dynamic compensation of these distortions is not particularly difficult. In the Thesis, these distortions' presence and dynamic compensation are not considered for theoretical studies and simulations. As part of the FPGA verification, the correction of these distortions is implemented. Note that the demodulation process also introduces an IQ impairment. The reason for this is the non-orthogonality of local oscillators, i.e., the phase difference between the sine and cosine generated at the receiver is not equal to $\pi/2$.

Non-coherent demodulation, as shown in Section 1.1, causes a channels energy redistribution. Consider the signal as a vector $s[n]$ on the complex plane, with projections on the real and imaginary axes equal to the quadrature components $\Re\{s[n]\}$ and $\Im\{s[n]\}$. A time-variable transmitter and receiver carriers phase $\varphi[n]$ difference results in a rotation of the vector relative to the origin, as follows from (1.19). The expression implies that the distortion can be compensated by multiplying the signal by a complex exponent of the opposite sign argument

$$s_{\text{CR}}[n] = s_{\text{EQ}}[n]\, e^{j\varphi[n]}, \tag{1.29}$$

where with $s_{\text{EQ}}[n]$ the carrier recovery block input signal. The following cost function $J_{\text{CR}}[n]$ is used to estimate the instantaneous value of the carrier phase difference:

$$J_{\text{CR}}[n] = \mathbb{E}\left[\arg s_{\text{CR}}[n] - \arg \hat{s}_{\text{CR}}[n]\right], \tag{1.30}$$

where $\hat{s}_{\text{CR}}[n]$ denotes the estimated value of the carrier recovery block output, while the arg operator denotes the argument of a complex value. Thus the phase difference value correction is adjusted by estimating the received symbol $s_{\text{CR}}[n]$ and finding these values phase difference. The phase adjustment is performed once per symbol; samples between symbols do not adjust phase difference.

It was noted that the cost function for adjusting the instantaneous value of the carrier phase contains an estimate of the received symbol. However, distortions in the signal significantly increase the probability of an erroneous estimate. A correct estimation process also requires maximizing the signal-to-noise ratio at the time of decision making. The maximization can be done by suppressing out-of-band noise with a matched filter. Therefore, it is necessary to perform signal equalization and matched filtering before carrier recovery.

Assume that the AGC and timing recovery blocks described above ideally reproduce signal $\dot{S}_\varphi[n]$. As shown from Fig. 1.10, this signal can be described as the receiver input multiplied by a complex exponent $\dot{S}_{\text{Rx}}[n]\, e^{j\varphi[n]}$. Let us pass this signal through an equalizer, whose task is to compensate for linear distortion in the channel. The following chapters will discuss its structure and customization options in detail. For now, it is a filter with the time-varying impulse response $h[k, n]$. The output of this device can be expressed by convolution of the input signal with an impulse

response

$$s_{\mathrm{EQ}}[n] = \sum_{l_{\mathrm{e}}=0}^{L_{\mathrm{e}}-1} s_{\mathrm{TR}}[n - l_{\mathrm{e}}]h[l_{\mathrm{e}}, n], \tag{1.31}$$

where L_{e} is the length of the impulse response of the equalizer. Substituting the above-mentioned expression for the equalizer input, one obtains

$$s_{\mathrm{EQ}}[n] = \sum_{l_{\mathrm{e}}=0}^{L_{\mathrm{e}}-1} \dot{S}_{\mathrm{Rx}}[n - l_{\mathrm{e}}] \, \mathrm{e}^{j\varphi[n-l_{\mathrm{e}}]} \, h[l_{\mathrm{e}}, n] \approx \mathrm{e}^{j\varphi[n]} \sum_{l_{\mathrm{e}}=0}^{L_{\mathrm{e}}-1} \dot{S}_{\mathrm{Rx}}[n - l_{\mathrm{e}}]h[l_{\mathrm{e}}, n]. \tag{1.32}$$

The previous expression is valid if $\varphi[n]$ changes are slow enough to be considered constant over L samples. Similarly, it can be shown that the output of a matched filter can be expressed in terms of

$$s_{\mathrm{MF}}[n] = \sum_{l_{\mathrm{mf}}=0}^{L_{\mathrm{mf}}-1} \dot{s}_{\mathrm{EQ}}[l_{\mathrm{mf}}]h_{\mathrm{mf}}[n - l_{\mathrm{mf}}] \approx \mathrm{e}^{j\varphi[n]} \sum_{l_{\mathrm{mf}}=0}^{L_{\mathrm{mf}}-1} \sum_{l_{\mathrm{e}}=0}^{L_{\mathrm{e}}-1} \dot{S}_{\mathrm{Rx}}[n - l_{\mathrm{e}} - l_{\mathrm{mf}}]h[l_{\mathrm{e}}, n]h_{\mathrm{mf}}[l_{\mathrm{mf}}], \tag{1.33}$$

where L_{mf} is the length of matched filter impulse response $h_{\mathrm{mf}}[n]$. As before, the expression will be valid at a constant $\varphi[n]$ for L_{mf} samples. The previous derivations make it possible to draw the following conclusions.

- The carrier recovery block can be moved after the equalizer and matched filter if the carrier phase changes are small enough to be considered constant over the length of the impulse responses of these two devices. Thus, we ensured equalization and suppression of out-of-band noise in the input signal of the carrier recovery unit and provided conditions for optimal signal estimation.

- Expressing a signal as a convolution of some two signals, one of which is multiplied by a time-varying coefficient $\mathrm{e}^{j\varphi[n]}$, the operations of convolution and multiplication are commutative and associative

$$s_1[n] * (s_2[n] \, \mathrm{e}^{j\varphi[n]}) = (s_1[n] * s_2[n]) \, \mathrm{e}^{j\varphi[n]} \tag{1.34}$$

if $\mathrm{e}^{j\varphi[n]}$ can be considered constant over the shortest of the convolved signals.

The following should be noted on the equalizer operation to discuss the receiver structure further. The output of this device is described in (1.31), where $h[k, n]$ stands for the equalizer's impulse response. The task is to adjust the impulse response to compensate for the signal passing through a multipath channel model. This Thesis is devoted to the equalizer cost functions and their use for adjusting the impulse response. All cost functions used in the Thesis are rotation-invariant, i.e., they are feasible for a signal without carrier recovery. However, some of them require an estimation of the received symbol. Therefore, as with the carrier recovery block, the equalizer must be moved after the matched filter. Note that the equalizer impulse response is time-varying. It changes during the acquisition and channel changes tracking. A convolution in (1.33) can be considered commutative if

the changes in the equalizer impulse response are slow enough to accept $h[k, n]$ to be constant over the length of the filter impulse response $h_{\mathrm{mf}}[n]$.

The operation nuances of the described dynamic circuits and the compensated distorting effects are summarized in Table 1.1.

The Summary of the Dynamical Circuits in QAM Receiver $\qquad$ Table 1.1

Distorting effect	Dynamic circuit	Compensation	Cost function
Power changes	AGC	$s_{\mathrm{in}}[n]a[n]$, where $a[n]$ is current gain	$\mathbb{E}\left[|\dot{s}_{\mathrm{ex}}[n]|^2\right]$
Modem clock difference	Timing recovery unit	$s_{\mathrm{in}}[n - \tau[n]]$, where $\tau[n]$ is current fractional time shift	$\mathbb{E}\left[s_{\mathrm{ex}} * h_{\mathrm{nb}}[n + 1] - s_{\mathrm{ex}} * h_{\mathrm{nb}}[n - 1]\right]$, where $h_{\mathrm{nb}}[n]$ is a narrow band filter impulse response
Multipath propagation	Equalizer	$s_{\mathrm{in}}[n] * h[k, n]$, where $h[k, n]$ is current impulse response	Discussed below
Carrier phase difference	Carrier recovery unit	$s_{\mathrm{in}}[n]\, e^{j\varphi[n]}$, where $\varphi[n]$ is current phase	$\mathbb{E}\left[\arg s_{\mathrm{ex}}[n] - \arg \hat{s}_{\mathrm{ex}}[n]\right]$

Thus, we have described the structure of the "Signal processing" unit in the QAM receiver. For clarity and reference in the future, we will reorganize the structure of the complex baseband model of the QAM wireless communication system, combining nodes that are not critical for further discussion. The resulting block diagram is shown in Fig. 1.11.
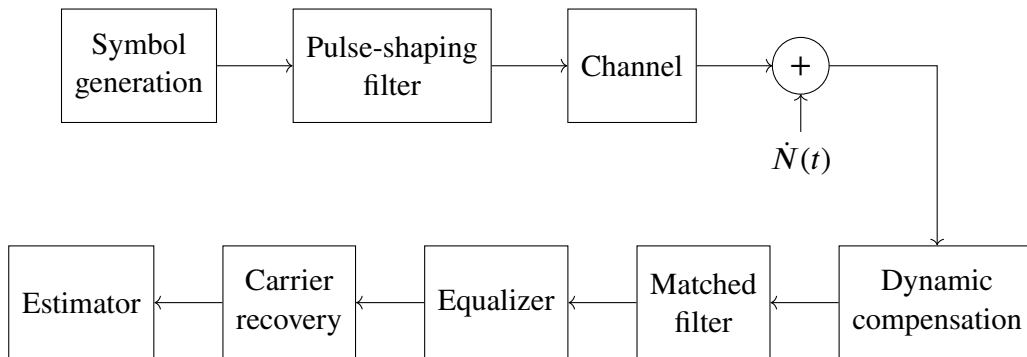
Fig. 1.11. Complex baseband model of QAM communication system for simulations

In the shown model, the symbol generation block performs:
- client data sequence generation,

- mapping, and

- zeros insertion.

In turn, the node designated as dynamic compensation performs the following actions:

- signal and time-varying $e^{j\varphi[n]}$ multiplication, which corresponds to the phase

- difference in the of the transmitter and receiver carriers,

- introduction of a time-varying time shift into the signal, emulating the difference in the clock frequencies of the transmitter and receiver modems,

- automatic gain control of the received signal, and

- dynamic timing recovery.

During the simulations produced within the framework of this Thesis, all operations inherent in this block were carried out. Note that the shown position of the matched filter, equalizer, and carrier recovery block is possible under the above-mentioned assumptions about the time-variability of the distorting processes. Thus, we complete the list of requirements for a complex baseband model of a QAM wireless communication system that must be fulfilled to ensure its relevance:

8. The time variation of the carrier phase difference must be such that it can be considered constant over the impulse responses of the matched filter and equalizer.

9. The rate of dynamic change in the equalizer impulse response must be such that it can be considered constant over the length of the matched filter impulse response.

10. The rate of change of the channel impulse response is less than the rate of the dynamic adjustment of the equalizer impulse response.

However, for theoretical analysis, the developed model is unnecessarily complex. Denoting the signal at the output of the generation module by $s_{\mathrm{z}}[n]$, the impulse response of the pulse-shaping filter by $h_{\mathrm{Tx}}[n]$, and the impulse response of the channel by $h_{\mathrm{c}}[k, n]$, we can express the signal at the input of the dynamic compensation module as

$$\dot{s}_{\mathrm{Rx}}[n] = s_{\mathrm{z}}[n] * h_{\mathrm{Tx}}[n] * h_{\mathrm{c}}[k, n] + \dot{N}[n]. \tag{1.35}$$

Let us assume the compensation of the distorting effects introduced into the signal in this module is complete. Thus, for further derivations, we can consider the signals at the input $\dot{s}_{\mathrm{Rx}}[n]$ and output $s_{\mathrm{DC}}[n]$ of the block to differ only in the introduced carriers' phase difference $e^{-j\varphi[n]}$. Denoting the impulse responses of the matched filter and the equalizer $h_{\mathrm{Rx}}[n]$ and $h_{\mathrm{EQ}}[k, n]$, respectively, we obtain the signal at the output of the equalizer

$$s_{\mathrm{EQ}}[n] = \dot{S}_{\mathrm{Rx}}[n] \, e^{-j\varphi[n]} * h_{\mathrm{Rx}}[n] * h_{\mathrm{EQ}}[k, n]. \tag{1.36}$$

The signal at the input of the received data evaluator is expressed through $s_{\mathrm{EQ}}[n] \, e^{j\hat{\varphi}[n]}$, where $\hat{\varphi}[n]$ is an estimate of the instantaneous value of the carriers' phase difference. Thus, the signal to be

estimated is expressed substituting (1.36) into (1.35)

$$s_{\mathrm{CR}}[n] = \left(s_z[n] * h_{\mathrm{Tx}}[n] * h_c[k,n] + \dot{N}[n]\right) \mathrm{e}^{-j\varphi[n]} * h_{\mathrm{Rx}}[n] * h_{\mathrm{EQ}}[k,n]\, \mathrm{e}^{j\hat{\varphi}[n]}. \tag{1.37}$$

We take into account that one of the requirements for the relevance of the model was a slow change in time-varying variables: the impulse response of the channel $h_c[k,n]$, the impulse response of the equalizer $h_{\mathrm{EQ}}[k,n]$, and the phase difference of the carrier $\varphi[n]$. Each of them assumed constant for the length of the impulse response of any linear circuit of the model. In this case, we can employ the commutativity and associativity properties of convolution and multiplication in (1.34). Then expression (1.37) can be rewritten as follows

$$s_{\mathrm{CR}}[n] = \Big[s_z[n] * \left(h_{\mathrm{Tx}}[n] * h_{\mathrm{Rx}}[n]\right) * h_c[k,n]\, \mathrm{e}^{-j\varphi[n]} \tag{1.38}$$
$$+ \dot{N}[n] * h_{\mathrm{Rx}}[n]\, \mathrm{e}^{-j\varphi[n]} \Big] * h_{\mathrm{EQ}}[k,n]\, \mathrm{e}^{j\hat{\varphi}[n]}.$$

The changes made correspond to moving the matched filter before the multipath model. By convolving the impulse responses of the pulse-shaping filter and the matched filter, we obtain the filter's impulse response

$$h_{\mathrm{FF}}[n] = h_{\mathrm{Tx}}[n] * h_{\mathrm{Rx}}[n] \tag{1.39}$$

that meets the Nyquist ISI criterion. In our case, it corresponds to the full raised-cosine filter. We will consider these two filters as a single for theoretical research in the future. Let us note the passing of the AWGN through the matched filter and multiplication by the complex exponent $\mathrm{e}^{-j\varphi[n]}$. The real and imaginary parts of the noise signal have a normal probability density distribution with equal standard deviations and zero means. Then the instantaneous phase of the signal is uniformly distributed over interval $\arg \dot{N}[n] \in [0, 2\pi)$. Since multiplication by the complex exponent only causes a change in the phase of the signal, this operation does not change the statist (1.38) can be replaced by band-limited Gaussian noise $N'[n]$.

Consider the complex baseband model of the QAM wireless communication system shown in Fig. 1.12, which we will use for theoretical derivations.
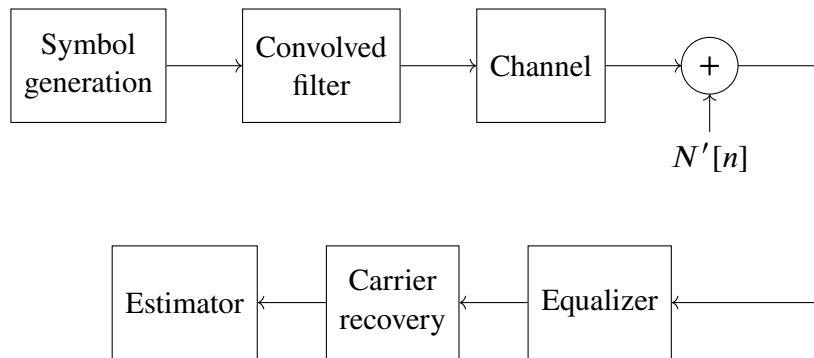
Fig. 1.12. Complex baseband model of QAM communication system for theoretical analysis

Here, the assumptions described earlier are taken into account:

- the pulse-shaping of the transmitter filter and the matched filter of the receiver are combined;
- the dynamic compensation block is omitted;
- the AWGN source is replaced by a band-limited noise generator.

In addition, the diagram does not include a block for introducing a phase difference into the carriers of the transmitter and receiver. The simplification is admissible because of rotation-invariant cost functions used for the equalizer adjustment. The mathematical description of the output signal of this system is given by expression

$$s_{\text{CR}}[n] = \left[s_{\text{z}}[n] * h_{\text{FF}}[n] * h_{\text{c}}[k, n] + N'[n] \right] * h_{\text{EQ}}[k, n] \, \text{e}^{j\hat{\varphi}[n]} \,. \tag{1.40}$$

1.3 Complex Baseband Multipath Channel Model

The multipath phenomenon in a wireless data transmission system is a characteristic of propagating an electromagnetic wave in a specific medium from a transmitter to a receiver. Under ideal conditions, an electromagnetic wave can be considered a plane wave, and its propagation between the transmitting and receiving antennas can be approximated as a line-of-sight ray. However, the exact propagation model is described as the sum of the primary and aberrant waves, and the beam corresponds to a set of confocal Fresnel ellipsoids. The presence of partial obstructions causes reflections and scattering. Moreover, antenna radiation patterns are not infinitely narrow. Therefore, the wave is not plane. As a result, the signal received by the secondary antenna is a weighted sum of the time-shifted transmitted signals. Moreover, mechanical changes in the propagation medium lead to time-variability of the weights of time shifts. As the number of scatterers in the first Fresnel zones and the number of reflectors increases, the mentioned parameters become random.

We use the multipath channel model to describe the multipath propagation of a signal from a transmitter to a receiver. Multipath propagation results in either constructive or destructive interference at the receiver, depending on the wave's frequency. In the case of a bandpass signal, some of its spectral components are amplified, and some are attenuated, i.e., the time-varying magnitude-frequency response of the channel is not constant. This Doctoral Thesis is devoted to the equalization of the channel frequency response. We use two models of different channels to evaluate equalization performance. Verification of the equalizer's ability to capture the signal will be tested on a stationary two-ray channel model. In turn, the equalizer's ability to track channel changes will be determined using a diffuse time-varying channel. Below are descriptions of these channels.

Consider a real bandpass channel model. We denote the transmitted modulated narrowband signal $s_{\text{Tx}}(t)$. As we mentioned, the signal can be described at the receiver by a weighted sum of time-shifted copies of the transmitted signal; moreover, each copy weight and time shift is time-varying. Let us denote these parameters $a(\tau, t)$ and $\tau(t)$, respectively. We will consider a diffuse channel, that is, one in which the time delay between two received copies of the transmitted signal

is infinitely small. Then the received signal can be expressed as follows:

$$s_{\text{Rx}}(t) = \int_{-\infty}^{\infty} a(\tau, t) s_{\text{Tx}}(t - \tau)\, d\tau. \tag{1.41}$$

The above expression is a convolution of signal $s_{\text{Tx}}(t)$ with a time-varying impulse response $h_{\text{c}}(\tau, t) = a(\tau, t)$ of a channel. Section 1.2 gave several reasons why it is worthwhile to use complex baseband models for simulating communication systems. It follows from (1.13) that by convolving the transmitter analytical signal with the real channel impulse response, one obtains an analytical signal at the receiver. Substituting these signals into (1.41), we get

$$\dot{S}_{\text{Rx}}(t)\, e^{j2\pi f_0 t} = \int_{-\infty}^{\infty} a(\tau, t) \dot{S}_{\text{Tx}}(t - \tau)\, e^{j2\pi f_0(t-\tau)}\, d\tau, \tag{1.42}$$

where f_0 is the carrier frequency. (1.14) says that equality will stay valid if the analytic signal $\dot{a}(\tau, t) = a(\tau, t) + j\mathscr{H}\{a(\tau, t)\}$ replaces $a(\tau, t)$:

$$\dot{S}_{\text{Rx}}(t)\, e^{j2\pi f_0 t} = e^{j2\pi f_0 t} \int_{-\infty}^{\infty} \dot{a}(\tau, t)\, e^{-j2\pi f_0 \tau}\, \dot{S}_{\text{Tx}}(t - \tau)\, d\tau, \tag{1.43}$$

where $\mathscr{H}\{a(\tau, t)\}$ is calculated with respect to τ. Dividing both parts of the expression by $e^{j2\pi f_0 t}$, we conclude that the complex envelope of the received signal $\dot{S}_{\text{Rx}}(t)$ is the convolution of the complex envelope of the transmitted $\dot{S}_{\text{Tx}}(t)$ signal with the channel complex baseband impulse response $\dot{H}_{\text{c}}(\tau, t)$, which is equal to

$$\dot{H}_{\text{c}}(\tau, t) = \dot{a}(\tau, t)\, e^{-j2\pi f_0 \tau}. \tag{1.44}$$

Thus, we can conclude that at each time instant t, a copy of the transmitted signal $\dot{S}_{\text{Tx}}(t)$ has delay τ and complex amplitude $\dot{a}(\tau, t)\, e^{-j2\pi f_0 \tau}$.

At time shift τ, $\dot{H}_{\text{c}}(\tau, t)$ is a sum of an infinite number of reflections. Therefore, by virtue of the central limit theorem, it is random and has complex Gaussian probability density function (PDF). To describe the statistical properties of the channel's impulse response, we use a wide-sense stationary uncorrelated scattering (WSSUS) model from [42], [43]. To describe the channel, one should specify multidimensional PDFs for the system functions. However, the autocorrelation function (ACF) makes it possible to simplify further channel simulation. In general, the ACF for a time-varying stochastic impulse response can be given as

$$R_H(\tau_1, \tau_2, t_1, t_2) = \mathbb{E}\left[\dot{H}_{\text{c}}(\tau_1, t_1)\dot{H}_{\text{c}}^*(\tau_2, t_2)\right], \tag{1.45}$$

where $[\cdot]^*$ denotes complex conjugation. Application of the criterion of wide-sense stationarity

gives the ACF invariance to the time moment t; $R_H(\tau_1\tau_2, t_1, t_2)$ becomes dependent only on the difference between the time instants $\Delta t = t_2 - t_1$, i.e.,

$$R_H(\tau_1, \tau_2, t, t + \Delta t) = R_H(\tau_1\tau_2, \Delta t) = \mathbb{E}\left[\dot{H}_c(\tau_1, t)\dot{H}_c^*(\tau_2, t + \Delta t)\right]. \tag{1.46}$$

The WSSUS model also assumes that the impulse response values between time shifts τ_1 and τ_2 are uncorrelated since they are two different weighted sums of copies of the transmitted signal. Then (1.46) can be rewritten as

$$R_H(\tau_1, \tau_2, \Delta t) = \mathbb{E}\left[\dot{H}_c(\tau_1, t)\dot{H}_c^*(\tau_1, t + \Delta t)\right]\delta(\tau_1 - \tau_2). \tag{1.47}$$

Thus, one can define the ACF of the complex baseband impulse response of the channel corresponding to the WSSUS model, as follows

$$R_H(\tau, \Delta t) = \mathbb{E}\left[\dot{H}_c(\tau, t)\dot{H}_c^*(\tau, t + \Delta t)\right]. \tag{1.48}$$

Section 1.2 introduces a discrete complex baseband model of the communication system, so the simulation is supposed to be digital. Therefore, it is also necessary to implement a discrete channel model. The methods used to convert analog linear systems to discrete ones are not applicable in this case. Generally speaking, the frequency characteristics of the channel outside the analyzed signal bandwidth are not known. Therefore, we convert the channel into a low-pass filter by suppressing all spectral components outside the $f \in [-F_s/2, F_s/2)$ band, where F_s is the sampling frequency. It can be done by passing the impulse response through a brick wall filter, which corresponds to the convolution of the channel impulse response with an unnormalized sinc-function:

$$\dot{C}(\tau, t) = \int_{-\infty}^{\infty} \dot{H}_c(\theta, t)\,\text{sinc}\left(\pi F_s(\tau - \theta)\right)\,\mathrm{d}\theta, \tag{1.49}$$

where $\dot{C}(\tau, t)$ is the same channel impulse response, though it can be safely sampled by substituting $\tau \leftarrow nT_s$. In this way, one obtains $\dot{C}(nT_s, t)$. Since we need to ensure the random character of the taps of the time-varying filter emulating the channel, the task is to generate mutually dependent random processes. Let us find the covariance matrix for the filter taps. Substituting the low-pass filtered channel impulse response into (1.47), we obtain

$$R_C(nT_s, kT_s, \Delta t) = \mathbb{E}\left[\dot{C}_c(nT_s, t)\dot{C}_c^*(nT_s, t + \Delta t)\right]\delta\left[(n - k)T_s\right]. \tag{1.50}$$

Substituting (1.49) into this expression and taking into account the properties of the integration of

δ-functions, we find the ACF of the impulse response of the discrete channel

$$R_C(nT_s, kT_s, \Delta t) = \int_{-\infty}^{\infty} R_H(\tau, \Delta t) \operatorname{sinc}\left(\pi(n - \tau F_s)\right) \operatorname{sinc}\left(\pi(k - \tau F_s)\right) d\tau. \tag{1.51}$$

The three-dimensional ACF can be viewed as a two-dimensional function that varies with time shift Δt. Since we are interested in synthesizing a discrete channel model, this time-varying function will be discrete with variables n and k. Generally speaking, it follows from (1.51) that for each time shift Δt, $R_C[n, k](\Delta t)$ represents the covariance matrix of the channel filter taps. Let us denote it as $\mathbf{R}_C(\Delta t) = \left(R_{nk}(\Delta t)\right)$, where $R_{nk}(\Delta t) = R_C[n, k](\Delta t)$. Thus, the problem is reduced to generating a certain number of random processes to satisfy the covariance matrix for each time shift Δt. For a simplified solution to this problem, we use the approximation proposed in [44]. It is based on the assumption that the ACF can be separated into two parts in such a way that

$$R_H(\tau, t) = p(\tau)\rho(\Delta t), \tag{1.52}$$

where $p(\tau)$ is the delay-power profile, and $\rho(\Delta t)$ is referred to as spaced-time correlation function, which are defined as

$$p(\tau) = \int_{-\infty}^{\infty} R_H(\tau, t) \, d\Delta t, \quad \text{and} \quad \rho(\Delta t) = \int_{-\infty}^{\infty} R_H(\tau, t) \, d\tau. \tag{1.53}$$

Substituting (1.51) into this approximation the channel impulse response ACF gives

$$R_C(nT_s, kT_s, \Delta t) = \rho(\Delta t) \int_{-\infty}^{\infty} p(\tau) \operatorname{sinc}\left(\pi(n - \tau F_s)\right) \operatorname{sinc}\left(\pi(k - \tau F_s)\right) d\tau. \tag{1.54}$$

Thus, the covariance matrix can be expressed as a product $\mathbf{R}_C(\Delta t) = \left(R_{nk}\right)\rho(\Delta t)$, where each element is $R_{nk} = R_C[n, k](\Delta t)/\rho(\Delta t)$. Hence, we can conclude that the samples of the impulse response of the band-limited channel, for this approximation, have identical one-dimensional ACF. Moreover, the covariance of the channel filter taps R_{nk}, in this case, remains proportional at different time shifts Δt. Thus, the generation of channel filter tap $\dot{C}[l](t)$ values satisfying (1.54) is as follows.

- Generate of L random processes $\xi_l(t)$ with a complex Gaussian PDF. The one-dimensional ACF of each of the processes corresponds to

$$\rho(\Delta t) = \mathbb{E}\left[\xi_l(t)\xi_l^*(t + \Delta t)\right]. \tag{1.55}$$

In this case, L is the length of the channel impulse response in samples. The synthesis of

non-δ-correlated processes within the framework of this Thesis will be performed using a low-pass filter with an impulse response $h_D[n]$ and a cutoff frequency $f_c = f_D$, where f_D stands for the maximum Doppler frequency.

- Introduce cross-correlation into random processes so that the generated L samples correspond to the covariance matrix (R_{nk}) at each time moment t. This problem is solved by multiplying the vector of samples $\Xi(t)$ by a matrix $\mathbf{L}$ for each time moment t.

$$\dot{\mathbf{C}}(t) = \Xi(t)\mathbf{L} = \begin{bmatrix} \xi_1(t) & \xi_2(t) & \cdots & \xi_L(t) \end{bmatrix} \begin{bmatrix} l_{11} & l_{12} & \cdots & l_{1L} \\ 0 & l_{22} & \cdots & l_{2L} \\ \vdots & \vdots & \ddots & \vdots \\ 0 & 0 & \cdots & l_{LL} \end{bmatrix}, \qquad (1.56)$$

where $\dot{\mathbf{C}}(t)$ is a $1 \times L$ big vector of band-limited channel impulse response. Matrix $\mathbf{L}$ is calculated by decomposing the covariance matrix using Cholesky factorization $(R_{nk}) = \mathbf{L}\mathbf{L}^\mathsf{T}$. The decomposition is possible because, due to the properties of the covariance matrix, it is symmetric, real, and positive semi-definite.

Indeed, the time shift dependent covariance matrix can be calculated as a mathematical expectation of the outer product of the impulse response taps vector

$$\begin{aligned} \mathbf{R}_C(\Delta t) &= \mathbb{E}\left[\dot{\mathbf{C}}(t) \otimes \dot{\mathbf{C}}^*(t)\right] = \mathbb{E}\left[(\Xi(t)\mathbf{L})^\mathsf{T} \Xi^*(t)\mathbf{L}\right] \\ &= \mathbf{L}^\mathsf{T}\mathbb{E}\left[\Xi^\mathsf{T}(t)\Xi^*(t)\right]\mathbf{L} = \mathbf{L}^\mathsf{T}\rho(t)\mathbf{I}\mathbf{L} = \rho(t)(R_{nk})^\mathsf{T} = \rho(t)(R_{nk}), \qquad (1.57) \end{aligned}$$

where $\mathbf{I}$ denotes the unity matrix, and $\otimes$ is the outer product sign. The validity of equality is based on the absence of cross-correlation of variables $\xi_l(t)$ and the identity of their ACFs.

Since the channel model will be implemented in the digital domain, channel time changes need to be sampled. A linear time-varying circuit can have a single sampling rate. Rigorously speaking, the presence of time variability imposes additional conditions on the choice of the sampling frequency. It is due to the possibility of expanding the spectrum of the signal transmitted through the channel. However, in this Thesis, we consider the effects of multipath, which can be mitigated through dynamic adjustment, i.e., we focus on slow fading. Thus, the maximum Doppler frequency f_D for the channel is much smaller than the coherence band Δf_T (frequency band in which most of the energy $\mathfrak{F}\{p(\tau)\}$ is concentrated), i.e., $f_D \ll \Delta f_T$. We also take into account that the signal transmitted through the channel is band-limited. Therefore, we assume that in the channel filter, the taps are T_s-spaced, where $T_s = 1/F_s$ is the sampling step of the signal formed in the complex baseband model of a wireless communication system from Section 1.2. The sampling rate of random process $\xi_l(t)$ is equal to F_s.

Thus, we can consider a system in which discrete random processes $\xi_l[n]$ are generated with a complex Gaussian PDF and ACF $\rho[n]$. The frequency characteristics of these signals were formed by

a filter with an impulse response $h_D[n]$. By introducing a correlation to these processes, the impulse response of channel $\dot{C}[k, n]$ is formed. The time-varying covariance matrix of the tap values of the impulse response is equal to $\mathbf{R}_C[n]$, and its two-dimensional ACF is equal to $R[k, n]$. The block diagram of the channel is shown in Fig. 1.13.
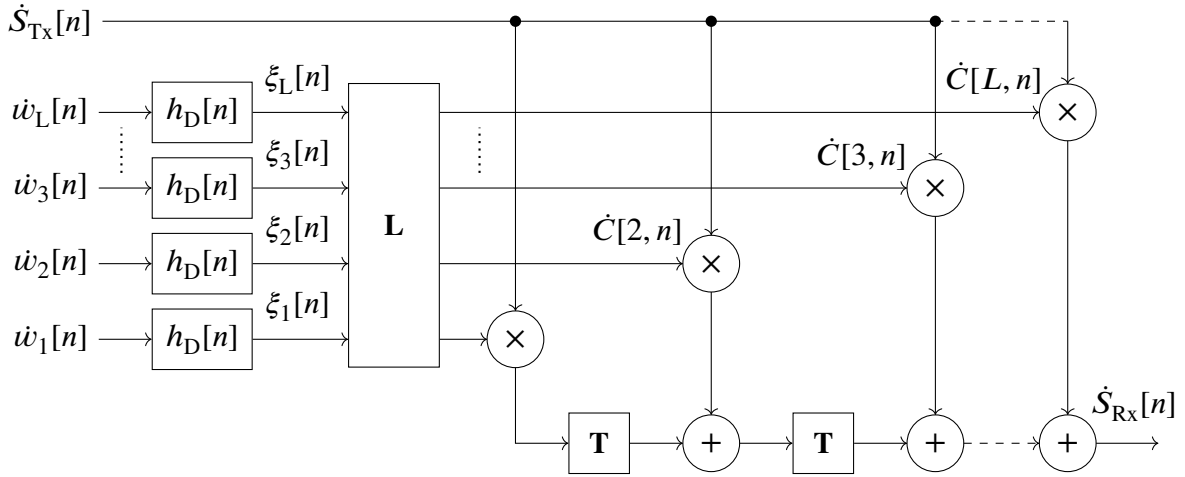
Fig. 1.13. Block diagram of the diffuse multipath chanel

In the figure, $\dot{w}_l[n]$ denotes a discrete complex Gaussian process with zero mean and uniform spectral density. We use a diffuse channel with a delay-power profile expressed as a Gaussian pulse $p(\tau) = \mathrm{e}^{-(\Delta f_T \tau)^2}$. Fig. 1.14 shows a set of impulse responses $\dot{C}[k, n]$ for different time moment n. In order to improve visualization, the coherence bandwidth is taken equal to $\Delta f_T = 2.5 \cdot 10^{-2} F_N$, and the maximum Doppler frequency is $f_D = 2.5 \cdot 10^{-3} F_N$. Matlab code implementing the complex baseband diffuse multipath channel model is available in Appendix C.1.
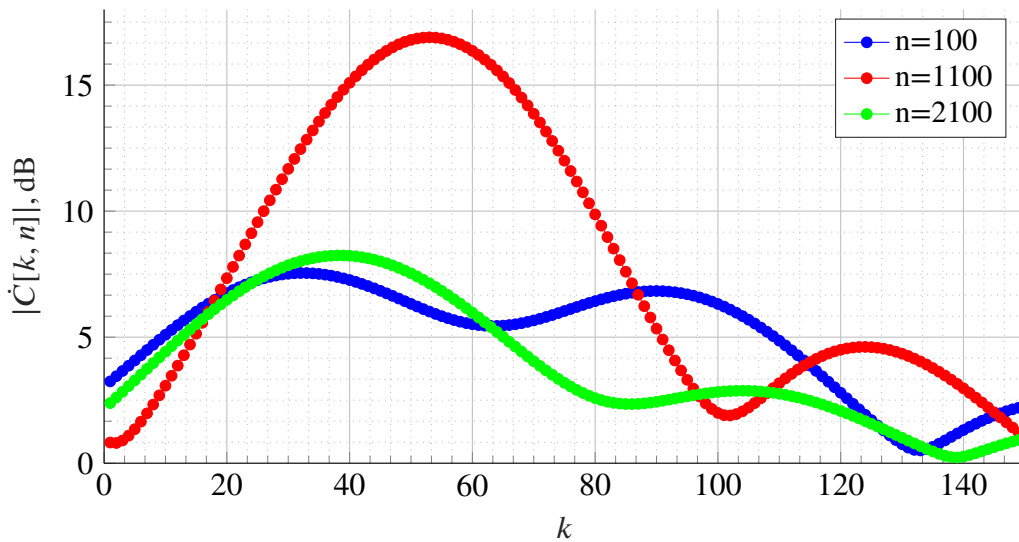
Fig. 1.14. Impulse response of a diffuse multipath channel

Fig. 1.15 shows the diffuse channel scattering function $S(\tau, f) = \mathscr{F}\{R(\tau, \Delta t)\}$, in which the

Fourier transform with respect to Δt is used.
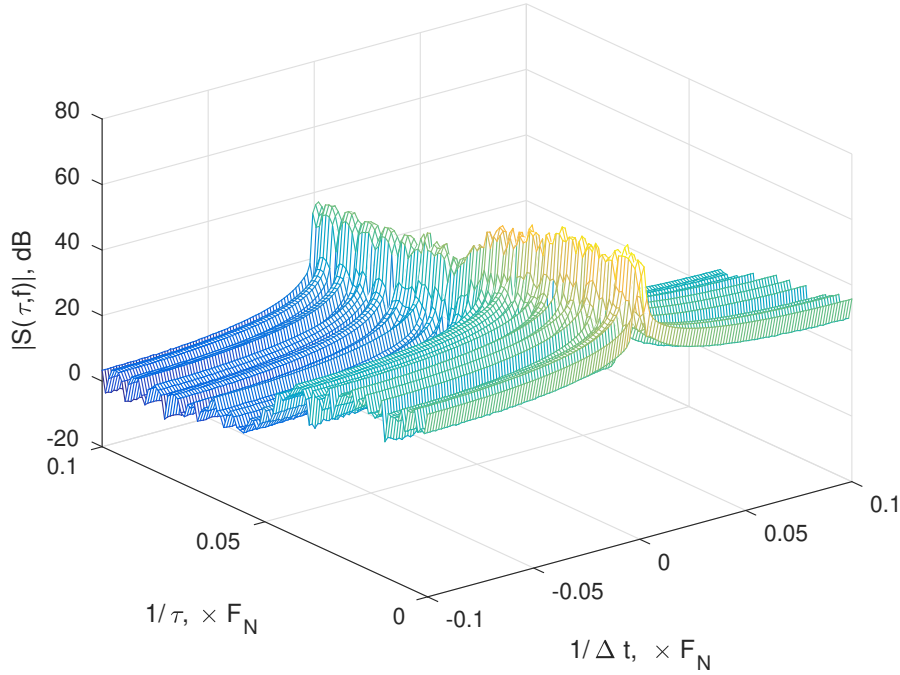
Fig. 1.15. Scattering function of a diffuse multipath channel

Verification of the algorithms developed in this Thesis will be based on radio-relay data transmission systems. Channel models describing the propagation of radio waves in such data transmission systems assume the presence of a line-of-sight beam. In such channels, atmospheric phenomena significantly contribute to the formation of a distorted multipath signal. It should be noted that fixed antennas with narrow radiation patterns are used in radio relay lines, which makes it possible to approximate the Fresnel ellipsoid with a beam. Moreover, at frequencies typically used in such channels, the reflection of the beam from the earth's surface can be described by the laws of geometric optics. Therefore, channel models describing multipath propagation in microwave links are usually considered to be slowly changing compared to the bandwidth of the transmitted signal. In addition, the number of time-delayed signal replicas arriving at the antenna is usually small.

The Rummler model is widely used to describe multipath propagation under conditions of slowly varying channel parameters. These channel characteristics correspond to communications in radio relay lines. The carrier frequencies of tens of gigahertz are required to use the model correctly.

According to the model, the received signal is formed as the sum of the primary and two delayed copies of the received signal:

$$s_{Rx}(t) = s_{Tx}(t) + \alpha s_{Tx}(t - \tau_1) + \beta s_{Tx}(t - \tau_2) \tag{1.58}$$

Let us consider the bandwidth limitation of the transmitted signal, i.e., the signal can be represented as a modulated harmonic oscillation. Taking the Hilbert transform and forming the complex enve-

lope of the received signal, we obtain

$$\dot{S}_{Rx}(t) = \dot{s}_{Tx}(t) + \alpha \dot{s}_{Tx}(t - \tau_1) e^{-j2\pi f_0 \tau_1} + \beta \dot{s}_{Tx}(t - \tau_2) e^{-j2\pi f_0 \tau_2} \tag{1.59}$$

where f_0 is the carrier frequency.

Rummler proposed to separate the two secondary beams in such a way that the frequency-selective and frequency-non-selective effects. The idea presented in the model is a division into beams, describing the frequency-selective and frequency-non-selective behavior that can be specified by the delay of each of the beams.

By limiting the bandwidth of the transmitted signal through Δf, we obtain $\Delta f \tau_1 \ll 1$ which causes flat fading. Therefore, $e^{-j2\pi f \tau_1} \approx 1$. Thus, we can express the received signal as:

$$\dot{S}_{Rx}(t) = (1 + \alpha) \dot{s}_{Tx}(t) + \beta \dot{s}_{Tx}(t - \tau_2) e^{-j2\pi f_0 \tau_2}, \tag{1.60}$$

where $\tau_1 \ll 1/\Delta f$ is much lower than the correlation time of the signal.

In practice, assuming the channel is locally stationary, i.e., for a certain number of symbols unchanged in time, we can state that Rummler's model reduces to a two-ray channel. The low-frequency equivalent of the impulse response of such a channel can be expressed as follows:

$$h(t) = a[\delta(t) + b e^{-j2\pi f_0 \tau_2} \delta(t - \tau_2)], \tag{1.61}$$

where we have used substitutions $a = 1 + \alpha$ and $b = \beta/(1 + \alpha)$. The transfer function of a linear system described by this expression can be obtained using the Fourier transform:

$$H(f) = a[1 + b e^{-j2\pi f_0 \tau_2}]. \tag{1.62}$$

To estimate the distortion of the spectrum of the signal passed through the channel described by this model, we construct its magnitude response, which can be expressed as:

$$|H(f)|^2 = a^2[1 + b^2 - 2b \cos[2\pi f_0 \tau_2]]. \tag{1.63}$$

This expression shows that the channel generates periodic "notches" in the signal spectrum. The position of this notch depends on the delay of the reflected signal τ_2, and the gain b determines its depth.

Fig. 1.16 shows the discrete impulse response of a two-ray channel. In this case, "notch" frequency $f_n = 0.1 F_N$, where F_N is the Nyquist frequency.
The multiple non-zero samples in the impulse response are due to band limitation of the channel frequency response during the sampling process. The absolute value of the frequency response of a two-ray channel is shown in Fig. 1.17. Note that in this case, it is more convenient to describe the
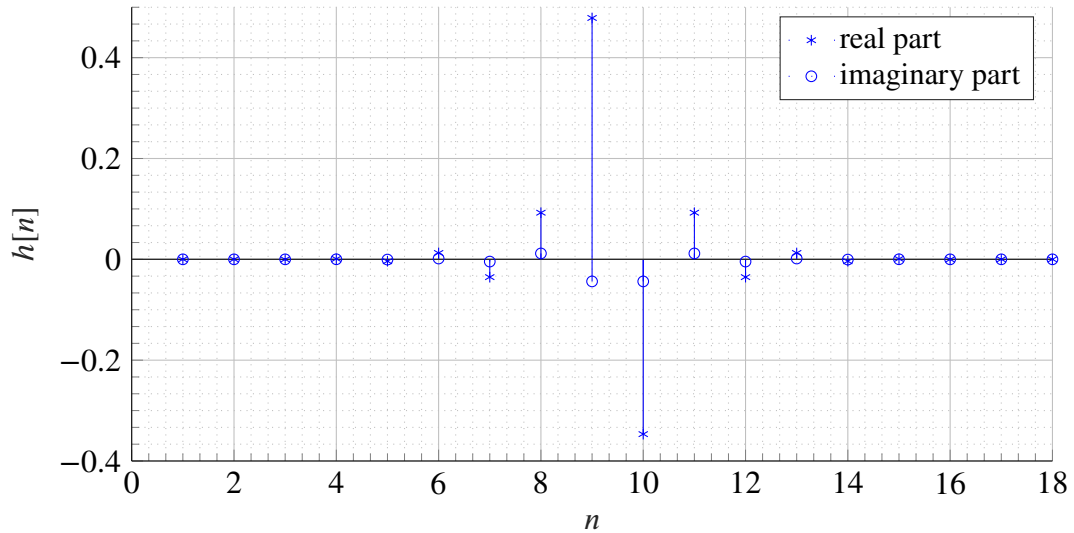
Fig. 1.16. Impulse response of a two-ray multipath channel

channel by the depth and frequency of the notch, which we will use later.
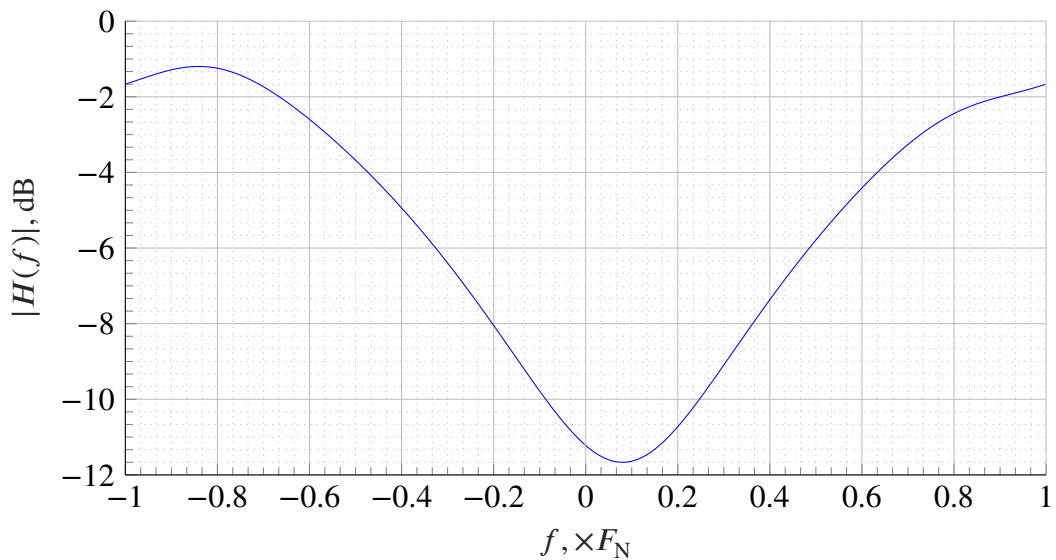
Fig. 1.17. Magnitude response of a two-ray multipath channel

Matlab code describing the calculation of a set of samples of the impulse response of a two-ray channel is given in Appendix C.2.

Consider the effect of multipath propagation of a radio wave on the transmitted signal. (1.17) shows that the signal at the receiving antenna is expressed as a convolution of the channel impulse response and the transmitter signal. Fig. 1.18 shows the received signal constellation diagram. The blue color shows the signal at the time points corresponding to the transmitted symbols $\{a_m\}$; the red color marks a set of available symbols. 5 dB deep notch at the position $f_n = 0.1\, F_N$ is used to obtain the signal.

Fig. 1.19 shows an estimate of the signal spectrum that has passed through the channel described above.
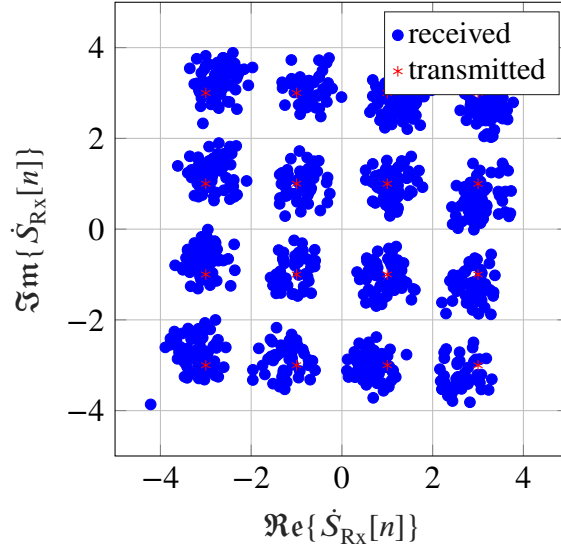
Fig. 1.18. Constellation diagram of the signal passed through a two-ray multipath channel
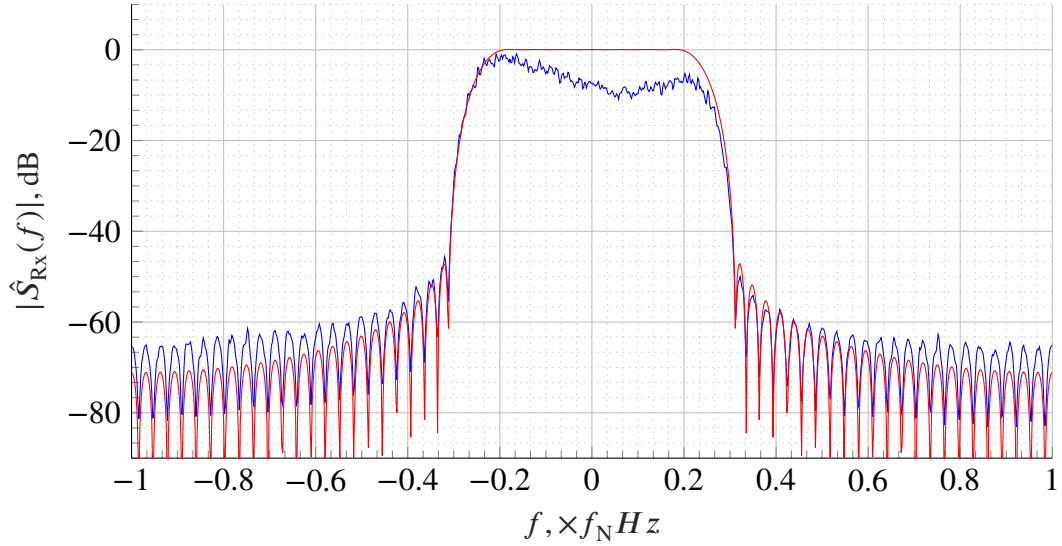
Fig. 1.19. Periodogram of the signal passed through a two-ray multipath channel

1.4   Equalization of QAM Signals

Consider ways to mitigate the distorting effects of multipath propagation. The complex baseband model used for theoretical research is shown in Fig. 1.12. The signal $s_{\text{Tx}}[k]$ generated by the transmitter is a random and uncorrelated sequence of constellation points $\{a_m\}$. Note that the total number of constellation points is $|\{a_m\}| = M$. Let us denote the impulse response of the multipath channel through $h[k]$, and the sample of the additive white noise through $n[k]$. Then one can express the input signal of the equalizer as

$$s_{\text{Rx}}[k] \equiv s_{\text{in}}[k] = \sum_{l_h=0}^{L_h-1} s_{\text{Tx}}[k - l_h]h[l_h] + n[k], \tag{1.64}$$

56

where L_h is the length of the channel impulse response. The equalizer in the system is represented by an FFF. Its time-varying impulse respone $c[l_c, k]$ is of length L_c. Thus, the output of the equalizer is expressed by

$$s_{\text{ex}}[k] = \sum_{l_c=0}^{L_c-1} s_{in}[k - l_c]c[l_c, k]. \tag{1.65}$$

By substituting (1.64) into (1.65), we can express the equalizer output $s_{\text{ex}}[k]$ as a function of the transmitted signal $s_{\text{Tx}}[k]$

$$s_{ex}[k] = \sum_{\substack{0 \leqslant l_h < L_h \\ 0 \leqslant l_c < L_c}} s_{tx}[k - l_h - l_c]h[l_h]c[l_c, k] + n'[k] \tag{1.66}$$

$$= s_{tx}[k - l_\delta] + \sum_{\substack{0 \leqslant l < L_h + L_c \\ l \neq l_\delta}} s_{tx}[k - l] \sum_{0 \leqslant l_c < l} h[l - l_c]c[l_c, k] + n'[k].$$

Thus, the output signal of the equalizer $s_{\text{ex}}[k]$ is composed of the transmitted signal $s_{\text{Tx}}[k]$ delayed by l_δ, the residual ISI represented by convolution in (1.66), and the noise that has passed through the equalizer $n'[k]$.

Consequently, the equalization problem is the adjustment of the tap weights $c[l, k]$ to minimize the effect of the sum in (1.66). To estimate it, the equalizer output dependent cost function $J[k]$ is defined. It is the essence of any blind equalization algorithm.

1.5 Blind Equalization Concept

The algorithm was introduced in [2], where the author proposes dispersion to represent the amount of ISI in a signal. The paper states that the variance of the squared output radius $|s_{\text{ex}}[k]|$ has a global minimum at zero ISI. Thus, the cost function for adjusting the equalizer is expressed as follows

$$J[k] = \text{E}\left[\left(\left|s_{ex}[k]\right|^2 - R_{\text{CMA}}^2\right)^2\right], \tag{1.67}$$

where $\text{E}[\cdot]$ denotes mathematical expectation and R_{CMA}^2 is the so-called dispersion constant, which is defined in [2] as

$$R_{\text{CMA}}^2 = \frac{\text{E}\left[|a_i|^4\right]}{\text{E}\left[|a_i|^2\right]}. \tag{1.68}$$

The equalizer coefficients $c[l, k]$ are adapted using the steepest descent along with $J[k]$, which is approximated by the stochastic gradient $\hat{\nabla}J[k]$. An increment of the equalizer coefficient is expressed

by the partial derivative

$$\left.\frac{\partial J[k]}{\partial c}\right|_{c=c[l,k]} = 2\left(\left|s_{\text{ex}}[k]\right|^2 - R_{\text{CMA}}^2\right)s_{\text{ex}}[k]s_{in}^*[k-l], \qquad (1.69)$$

where * denotes complex conjugation. Adding it to the current value of $c[l,k]$ gives the next weight of the equalizer tap

$$c[l,k+1] = c[l,k] - \mu\left(\left|s_{\text{ex}}[k]\right|^2 - R_{\text{CMA}}^2\right)s_{\text{ex}}[k]s_{in}^*[k-l], \qquad (1.70)$$

where μ is a step-size parameter to regulate the speed of adaptation. Computer simulations in [2] showed good convergence properties of CMA.

Note that for the mitigated ISI and zero noise, the output signal coincides with the time-delayed copy of the generated one by the transmitter $s_{\text{ex}}[k] = s_{tx}[k-l_\delta] \in \{a_m\}$. The inequality $\left|s_{\text{Tx}}[k]\right|^2 \neq R_{\text{CMA}}^2 \; \forall \, s_{\text{Tx}}[k] \in \{a_m\}$ from (1.70) implies that with an ideal equalizer adjustment, the tap weights will have nonzero increments. Their fluctuation around the transmitted values results in a high residual error in the output signal $s_{\text{ex}}[k]$. Reference [7] shows it mathematically strictly.

1.6 Conclusions

In this chapter, we have provided the necessary theoretical minimum for discussing blind equalization of QAM signals.

- The band model of a communication system based on QAM is introduced and described.
- The model of the complex baseband of the QAM communication system is described. The criteria necessary for its compliance with the band model are given.
- The sampling criteria for the model of a complex QAM baseband of a communication system are described.
- The blocks for generating the transmitted signal and processing the received signal are considered. The reasons for distorting effects and the possibilities of their compensation are described. The used dynamic loops, the methods of correction application, and the cost functions of these loops are mentioned.
- The models used in this study for simulations and analytical studies are described and constrained.
- The implemented models of multipath channels are described.
- The task of blind equalization is defined, and the equalization process is described. The CMA used for blind equalization of QAM signals is considered, its advantages and disadvantages are emphasized.

2 ENHANCED DECISION-ADJUSTED MODULUS ALGORITHM

In the previous chapter, we defined the problem of blind equalization in communication systems based on QAM. The widely used notorious CMA for adjusting equalizer weights has also been described. The main disadvantage of this approach is the high residual error level at the output of the equalizer when it is ideally tuned. This level depends on the step-size coefficient μ and grows with its increase.

This chapter proposes an approach to reduce residual error based on diminishing the variance of the signal used to adjust the equalizer weights. A decrease in the variance is performed by dividing the set of constellation points into circles with the same radius. The relation of the signal point at the output of the equalizer to the transmitted symbol is made by estimation, i.e., the algorithm requires decision making. The chapter describes the DAMA presented in [4] that uses this approach. Particular attention is paid to the calculation of threshold values for decision-making. Next, we consider an approach for estimating the PDF of the deviation of the signal point at the equalizer output from the radius of the corresponding constellation circle and, using simulation and statistical processing, show its compliance with the biased Rice distribution. Using knowledge of the PDF, we derive several approaches to calculate the optimal threshold values used to estimate the received symbol. The use of these thresholds leads us to the definition of the enhanced decision-adjusted modulus algorithm (EDAMA) proposed in this chapter for blind equalization of a QAM signal. At the end of the chapter, the results of simulations of this algorithm in the data transmission system model shown in Fig. 1.12 are presented.

2.1 Decision-Adjusted Multimodulus Algorithm

As it comes from (1.70), the goal of the CMA algorithm is positioning all symbols at the output of the equalizer $s_{ex}[k]$ to a single circle, radius R_{CMA} of which is called dispersion constant. The main disadvantage of that approach is the high residual error level. [4] proposes to divide the set of constellation points $\{a_m\}$ into subsets with the same radius R_i:

$$\{a_m\} = \bigcup_i \left\{ a_m \Big| |a_m| = R_i \; \forall \; m \right\}_i. \tag{2.1}$$

As a result, the proposed algorithm, DAMA, implements a CMA for each constellation circle. Equalizer coefficients updates are expressed as:

$$c[l, k+1] = c[l, k] - \mu \left(\left| s_{ex}[k] \right|^2 - R_i^2 \right) s_{ex}[k] s_{in}^*[k-l], \tag{2.2}$$

where the dispersion constant for each output radius $s_{ex}[k]$ value is such that its deviation from R_i is minimal $\min_i \left| \left| s_{ex}[k] \right|^2 - R_i^2 \right|$.

Unlike CMA, when the equalizer is converged, the increments of its coefficients are equal to zero $\forall s_{tx}[k] \in \{a_n\} \; \exists! \; R_i : \left| s_{tx}[k] \right|^2 = R_i^2$. Thus, DAMA is proposed to provide residual error significantly lower than CMA.

On the other hand, according to [11], DAMA converges only with minor initial misadjustment. The reason is a symbol estimation by the algorithm. Distortions can cause the signal $s_{ex}[k]$ to deviate from its original radius so much that it can be considered as a symbol of another circle. An incorrect estimate will be made, and the equalizer coefficients will move in the wrong direction.

2.2 Error Statistical Properties

Theoretical Considerations

Before optimizing probability, let us first define the statistical properties of the DAMA radial error. The error is highly dependent on the transmitted signal and the channel on which this signal is used. As the user determines the properties of the signal generated on the transmitter side, they can be considered *a-priori* known. On the other hand, the characteristics of the transmission channel are, in principle, unpredictable. The only way to analyze and model the behavior of a channel is to develop a model that is appropriate for a specific transmission case.

In the field of blind equalization, the channel impulse response, first introduced in [9], is usually used. For comparison, in this Thesis, the mentioned impulse response is used to test the statistical properties of the signal after it has passed the channel.

The transmitted signal is reflected from a countable number of buildings or terrain features for radio relay lines. Therefore, the received signal as interference of a finite number of transmitted signal copies is delayed and amplified. As discussed previously, *discrete multipath* channels are suitable for line-of-sight microwave links. Therefore, for the statistical properties estimation *two-ray model* also will be used. The following expression can be used to describe such a channel impulse response:

$$h(t) = A\delta(t) + (1 - A)\delta(t - \tau_0)e^{-j2\pi f_0 \tau_0}, \tag{2.3}$$

where $1 - A$ is the second path gain, τ_0—its relative delay and f_0 is a carrier frequency. Thus, it corresponds to the particular case of the Rummler model.

Let us consider the received bandlimited signal as pseudo-random and observe the many cross-sections at the symbol locations. These samples are transmitted symbols with some residual error. Our goal now is to study these properties of the error. The central limit theorem states that a signal with an arbitrary probability density function passing through a linear system will have a normal probability distribution. It is convenient to assume that the impulse response of a real linear system is

long enough to satisfy the infinite summation theorem conditions. In this case, the real and imaginary errors are normally distributed. It can be shown that the probability density function of the analyzed samples has a Rice distribution with a mean value equal to the absolute value of the complex symbol. In addition, the radial error probability density function is expressed by subtracting the mean from the Rice distribution. It is worth noting that the distribution will be close to normal for minor error deviations compared to the symbol values.

The linear system is represented by a pulse-shaping filter, channel, and receiving filter. However, for a two-ray channel, it is not obvious whether the convolution of the impulse responses of all three blocks is long enough to provide a normal distribution of the error following the central limit theorem. Therefore, it is useful to test the hypothesis about the normal distribution of the real and imaginary parts of the residual error in the case of a two-channel channel.

Radial Error Distribution Analysis Setup

The following section describes the setup to form a signal for numerical verification of the stated hypothesis. The setup block diagram is shown in Fig. 2.1.
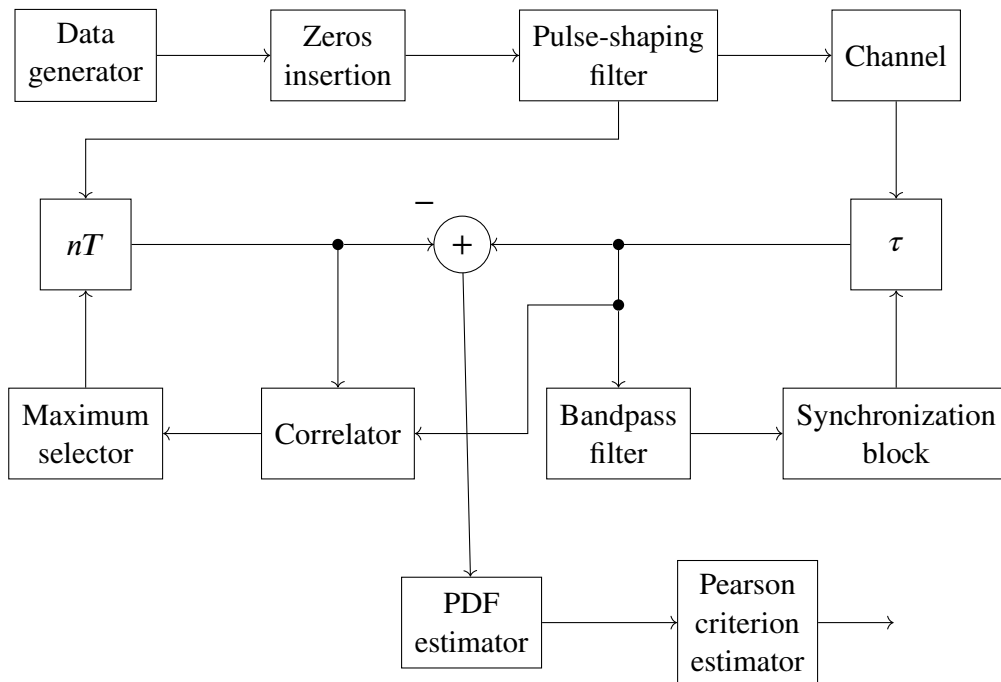
Fig. 2.1. Distribution analysis setup

It consists of three main parts: a received undistorted signal generator, a synchronization algorithm, and an error distribution analyzer. Let us take a closer look at each of them. The data generator, converter, and low-pass filter synthesize the received signal into a model. The first one provides a vector of m random bits at the output once every four clocks cycles. $m = \log_2 M$ depends on the modulation order of N-QAM. The complex symbol of the mapper block is formed according to the bit pattern from the previous block. In addition, zeros are inserted on three clock cycles

when the data generator is not enabled. In a convenient communication system, the pulse-shaping filter follows the mapper block. However, due to the property of linearity, the order in which linear systems are applied to a signal does not affect the resulting waveform. Therefore, the combination of pulse shaping filter, receiver filter, and the channel is implemented instead of pulse shaping filter, channel, and receiver filter in the model. Moreover, two filters are combined, forming a single low-pass filter.

The test channel is the next block that the signal must pass. Being a linear system, it introduces both integer and fractional delay. A synchronization system has been implemented to compensate for the time shift between the original data and those transmitted through the channel. It consists of two parts. The fractional delay canceler follows the channel. Its central part is a variable fractional delay line controlled by the fractional delay timing mechanism. Given that consecutive symbols interspersed with zeros correspond to the cutoff frequency, it becomes evident that all the necessary information to perform synchronization is concentrated in this region of the spectrum. Thus, the delay line output is passed through a narrow bandpass filter and returned to the clock engine. This block performs simple logical switching and loop filtering.

The integer part of the delay shift is compensated in by applying lowpass filter output to the shift register. Synchronization accuracy is controlled by estimating the correlation between the output of the fractional delay compensator and the delayed filtered signal. The number of clock cycles the signal spends in the shift register is determined by the maximum selector block observing correlator output for different shift register lengths.

After synchronization chains have grabbed delay values and switched to the tracking mode, a difference between the signal with recovered fractional delay and the one generated is immediately applied to the PDF estimation block.

PDF Verification Results

As mentioned above, the difference between ideally synchronized input and output of the channel is an error that behavior corresponds to a complex Gaussian process. In this Thesis, the Pearson's chi-squared test is used to determine whether the error distribution for actual data is sufficiently close to normal or not.

The PDF estimation block (shown in Fig. 2.1) accumulates data and builds a histogram. The operation starts after synchronization is established and continues until a necessary number of symbols is analyzed. The number of histogram bins for simulation is chosen equal to $K_1 = 100$ whereas the number of processed symbols, i.e., the sample size, is $K_2 = 100\,000$. After the simulation is finished Pearson criterion estimation block computes χ^2_{ev}-level to compare it to the critical value. Let us remind that the signal's mean value is known and equal to the symbol's real or imaginary part. Therefore, the only evaluated parameter is standard deviation, and for the given number of histogram bins, $K_1 = 100$, the number of degrees of freedom is $K_3 = K_1 - 2 = 98$. Assuming the

confidence level $\gamma = 0.95$, to accept the hypothesis that distribution is normal evaluated parameter χ^2_{ev} should be less than the critical level $\chi^2_{\text{cr}} = 122.1077$. If the error's both real and imaginary parts met the criterion, the system forms *passed* test marker.

Simulation was performed repeatedly $K_4 = 100$ times for different depth and frequency notches. The simulation results are summarized in Table 2.1.

Table 2.1

Distribution Verification Results

$f_n T$	Passed test percentage					
	1 dB	5 dB	10 dB	15 dB	20 dB	25 dB
-0.25	97	95	98	97	100	96
-0.20	97	96	96	100	97	99
-0.15	98	96	97	96	96	96
-0.10	99	97	100	96	99	99
-0.05	97	97	98	98	99	100
0.00	99	96	99	98	96	99
0.05	99	99	98	99	96	95
0.10	97	97	96	96	95	97
0.15	97	99	96	98	98	99
0.20	98	99	96	100	96	98
0.25	96	100	100	96	99	98

As shown in the table for all analyzed notched for more than 95 % cases distributions of error's both real and imaginary parts are considered normal. It is worth noting that, in general, standard deviations of these distributions are not equal. However, the difference between these two variables in all the analyzed cases was negligible. So, in the further description, the error's real and imaginary distributions are assumed normal with equal standard deviation. In case of channel mentioned in [9] percent of *passed test* results was 97 %.

2.3   Enhanced DAMA

Earlier, we have mentioned that in the DAMA algorithm current symbol radius detection method does not ensure minimal decision error probability. An approach to resolve this disadvantage is performed in the enhanced DAMA algorithm described in the current section.

Let one determine the threshold value to optimize detection according to this criterion. Recall distribution of complex error is assumed normal. Therefore PDF of radial error is shifted Ricean distributed $\varphi_n(R_n, \sigma) = \varphi(R_n, \sigma) - R_n$, where $\varphi(R_n, \sigma)$ is Ricean distribution with deviation σ and R_n is the n-th radius of the constellation. We also denote a number of constellation points of radius equal to R_n by m_n.

Two Radius Approach

First let us discuss a simplified case. Assume sample of radius R_x to be detected. Two nearest radii of the constellation are R_{n-1} and R_n such as $R_{n-1} \leq R_x < R_n$ are observed. The number of constellation points that correspond to these radii are m_{n-1} and m_n. An important assumption, in this case, is that there is zero impact of other radius points. It means that the original symbol that caused a sample of radius R_x was either from radius R_{n-1} or from R_n. Therefore, the probabilities that symbol was from radii R_{n-1} and R_n are, correspondingly,

$$P_{n-1} = \frac{m_{n-1}}{m_{n-1} + m_n} \quad \text{and} \quad P_n = \frac{m_n}{m_{n-1} + m_n}. \tag{2.4}$$

Our goal is to determine the sample of radius R_x affiliation minimizing error probability. Typically problems of this kind are solved using Bayesian decision theory. Thus, a risk coefficient r is appended to each error type. There are two possible errors in the observed case. Symbol of radius R_{n-1} is detected as of radius R_n and otherwise. Obviously, the probabilities of these actions are:

$$P_{n,n-1} = \int_{R_{\text{th }n-1}}^{\infty} \varphi(R_{n-1}, \sigma)\mathrm{d}R \quad \text{and} \quad P_{n-1,n} = \int_{-\infty}^{R_{\text{th }n-1}} \varphi(R_n, \sigma)\mathrm{d}R. \tag{2.5}$$

Introducing a risk coefficients $r_{n,n-1}$ and $r_{n-1,n}$ and expressing overall risk yields to

$$r = r_{n,n-1}P_{n,n-1}P_{n-1} + r_{n-1,n}P_{n-1,n}P_n. \tag{2.6}$$

Considering that $P_{n,n-1} = 1 - P_{n,n}$ and that the $P_{n,n}$ can be calculated integrating $\varphi(R_n, \sigma)$ from $R_{\text{th }n-1}$ to the infinity, (2.6) can be rewritten the following way:

$$r = P_n - \int_{R_{\text{th }n-1}}^{\infty} \left[P_n\varphi(R_n, \sigma) - P_{n-1}\varphi(R_{n-1}, \sigma) \right] \mathrm{d}R. \tag{2.7}$$

Here, for the sake of simplicity, risk coefficients are assumed equal to $r_{n,n-1} = r_{n-1,n} = 1$. To minimize overall risk r an integral value should be maximized. Conventionally it is ensured by choosing integration limits so that integrand in this interval would be positive. Therefore, the threshold level can be obtained by finding a radius value where inequality

$$\frac{\varphi(R_n, \sigma)}{\varphi(R_{n-1}, \sigma)} \geq \frac{P_{n-1}}{P_n} \tag{2.8}$$

becomes valid. Computing threshold in such a way, it is possible to minimize radius detection error probability. Constellation for 32-QAM and calculated thresholds are shown in Fig. 2.2.

(a) CMA   (b) DAMA

(c) EDAMA 2-level   (d) EDAMA multilevel
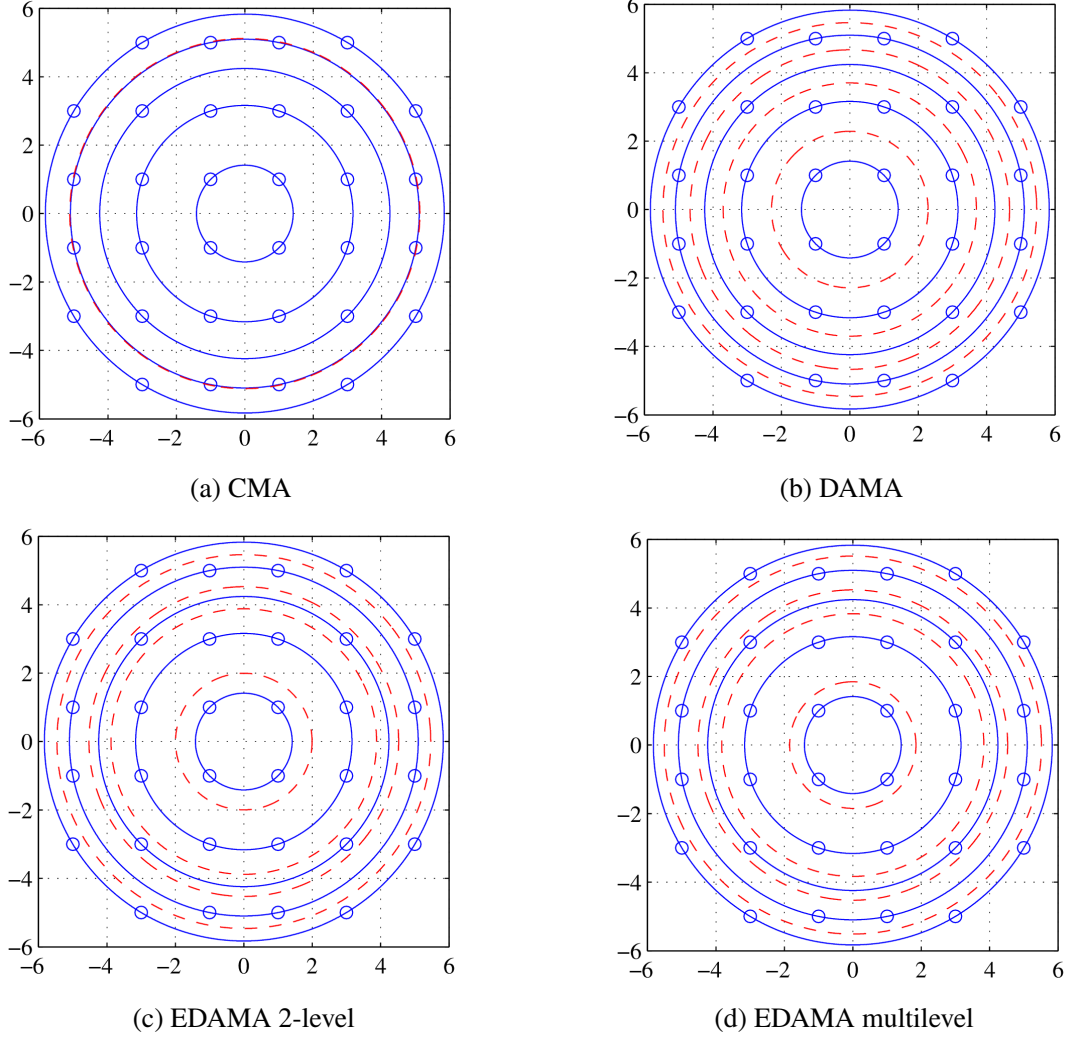
Fig. 2.2. Constellations and thresholds for (a) CMA, (b) DAMA, (c) EDAMA 2-level, and (d) EDAMA multilevel equalization algorithms

Multiple Radius Approach

Previously it was shown how to find threshold level under the assumption of zero possibility that sample of radius R_x has caused symbol of original radius $R < R_{n-1}$ or $R > R_n$. Unfortunately, a blind equalization mode is introduced to ensure reliable acquisition in cases of strong fading, which causes high error deviations. Therefore, the possibility of higher or lower radius point influence can not be assumed to be zero. Now let us generalize in the previous section given notorious derivation so that it would be suitable for our case.

Assume all constellation points can be divided to N groups of constant radii R_n, $n = 1 \dots N$. The number of points in each group is given by m_n. The possibility that an arbitrary point belongs to n-th group is expressed by

$$P_n = \frac{m_n}{M},$$ (2.9)

where M is overall number of constellation points.

65

Assume, as it was previously, that it is the sample of radius R_x and two nearest radii R_{n-1} and R_{n-1} satisfy inequality $R_{n-1} \leq R_x < R_n$. Obviously, the possibility that the sample of radius R_x is caused be the symbol of radius other than R_{n-1} or R_n is smaller of these two. If it was the symbol of radius $R > R_n$, detection of R_n ensures correct equalizer adjustment. And otherwise, if the symbol in the detector is assumed of radius R_{n-1}, it will cause misadjustment. Among a number of all possible error types we will observe only

$$\{P_{n-1,k}|k = n \ldots N\} \quad \text{and} \quad \{P_{n,k}|k = 1 \ldots n - 1\}. \tag{2.10}$$

Obviously, the first group of errors in the previous equation causes positive adjustment error and the second one—negative error. Therefore, possibilities of these errors can be expressed as

$$P_{n-1,k} = \int_{-\infty}^{R_{\text{th } n-1}} \varphi(R_n, \sigma) \mathrm{d}R, \quad k = n \ldots N \tag{2.11}$$

for positive and

$$P_{n,k} = \int_{R_{\text{th } n-1}}^{\infty} \varphi(R_{n-1}, \sigma) \mathrm{d}R, \quad k = 1 \ldots n - 1 \tag{2.12}$$

for negative ones. Assuming risk coefficients for all error types equal to $r_{n-1,k} = r_{n,k} = 1$ yields to the following overall risk expression

$$r = \sum_{k=1}^{n-1} P_{n,k} P_k + \sum_{k=n}^{N} P_{n-1,k} P_k. \tag{2.13}$$

Acting like previously, let us express $P_{n-1,k} = 1 - P_{k,k}$, where $k = n \ldots N$. Note also that $P_{k,k}$ can be calculated integrating $\varphi(R_k, \sigma)$ from $R_{\text{th } n-1}$ to the infinity. Thus, overall risk expression can be rewritten:

$$r = \sum_{k=n}^{N} P_k - \int_{R_{\text{th } n-1}}^{\infty} \left[\sum_{k=n}^{N} \varphi(R_k, \sigma) P_k - \sum_{k=1}^{n-1} \varphi(R_k, \sigma) P_k \right] \mathrm{d}R. \tag{2.14}$$

Integral value maximization is performed in the same manner as in the case of two radii, i.e., defining the integration interval so that the integrand is positive. Therefore, the threshold level is obtainable by the computation R location where inequality

$$\sum_{k=n}^{N} \varphi(R_k, \sigma) P_k \geq \sum_{k=1}^{n-1} \varphi(R_k, \sigma) P_k \tag{2.15}$$

becomes true. Calculating threshold level in this manner we decrease the wrong detection possibility

and therefore the equalizer misadjustment possibility. In Fig. 2.2, the 32-QAM constellation is shown as well as calculated thresholds.

2.4 Simulation Results

The performance of the proposed algorithm was tested through simulations in the Matlab environment. The signal forming at the equalizer input corresponds to the communication system model described in Section 1.2. The user signal is generated based on 32-QAM modulation. The equalizer is a 33-tap half-baud finite impulse response filter with dynamically adjustable gains. In the experiments, CMA, DAMA, and EDAMA objective functions were used to adjust the weights of the equalizer taps.

The first experiment was intended to show EDAMA's ability to converge for channels in which acquisition is impossible if DAMA is used to tune the equalizer. DAMA and EDAMA were tested by observing whether, after $K_5 = 200\,000$ samples, an equalizer has converged or not. The step-size parameter $\mu = 10^{-10}$ was chosen the same for both algorithms. Simulation results are summarized in Table 2.2. The first column corresponds to DAMA, the second—to EDAMA. **P** letter indicates that equalizer has converged, **F**—acquisition fail.

Table 2.2

Equalizer Convergence Results

	Passed test percentage										
f_nT	1 dB		5 dB		10 dB		15 dB		20 dB		25 dB	
-0.25	P	P	P	P	P	P	P	P	P	P	F	P
-0.20	P	P	P	P	P	P	P	P	P	P	F	P
-0.15	P	P	P	P	P	P	F	P	F	P	F	P
-0.10	P	P	P	P	P	P	F	P	F	P	F	P
-0.05	P	P	P	P	F	P	F	P	F	P	F	P
0.00	P	P	P	P	F	P	F	P	F	P	F	F
0.05	P	P	P	P	F	P	F	P	F	P	F	P
0.10	P	P	P	P	P	P	F	P	F	P	F	P
0.15	P	P	P	P	P	P	P	P	F	P	F	P
0.20	P	P	P	P	P	P	P	P	F	P	F	P
0.25	P	P	P	P	P	P	P	P	P	P	P	P

The table shows that EDAMA has ensured equalizer convergence for all the observed notches excluding 25 dB deep and positioned on carrier frequency. On the other hand, DAMA appeared unable to converge for notches of this length. Also indicative is the inability of the DAMA algorithm to converge for notches of lesser depth when they are shifted from the carrier frequency.

Obtaining convergence curves allows one to clearly demonstrate the convergence rate of the proposed algorithm and the level of residual error. It was noted above that in the case of EDAMA, the level of residual error is significantly lower compared to CMA. On the other hand, EDAMA should

show faster convergence than DAMA. 10 dB and 15 dB notch channels were applied to emulate multipath propagation. Simulation results for the case of 10 dB notch channel are shown in Fig. 2.3.
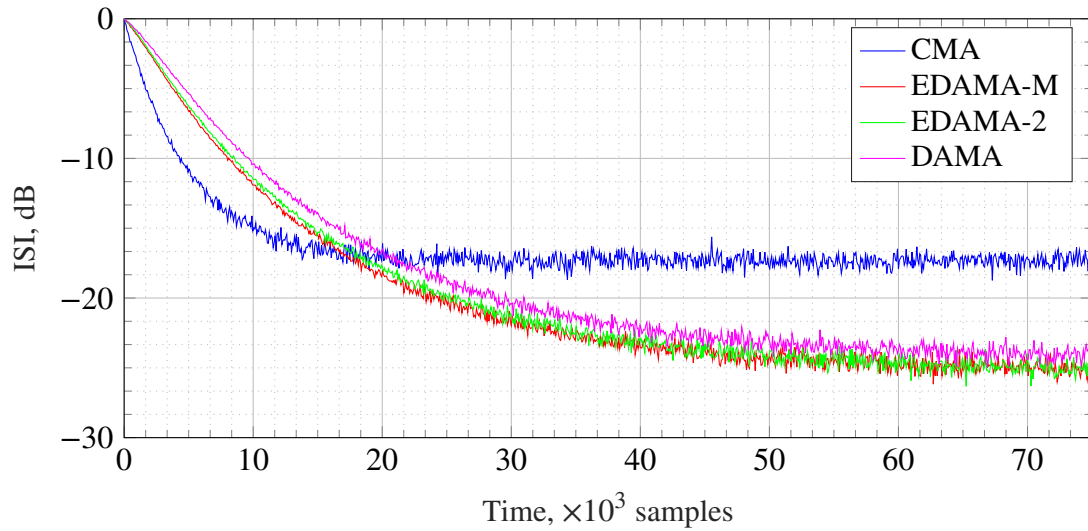
Fig. 2.3. Convergence curve for EDAMA in the case of 10 dB notch channel
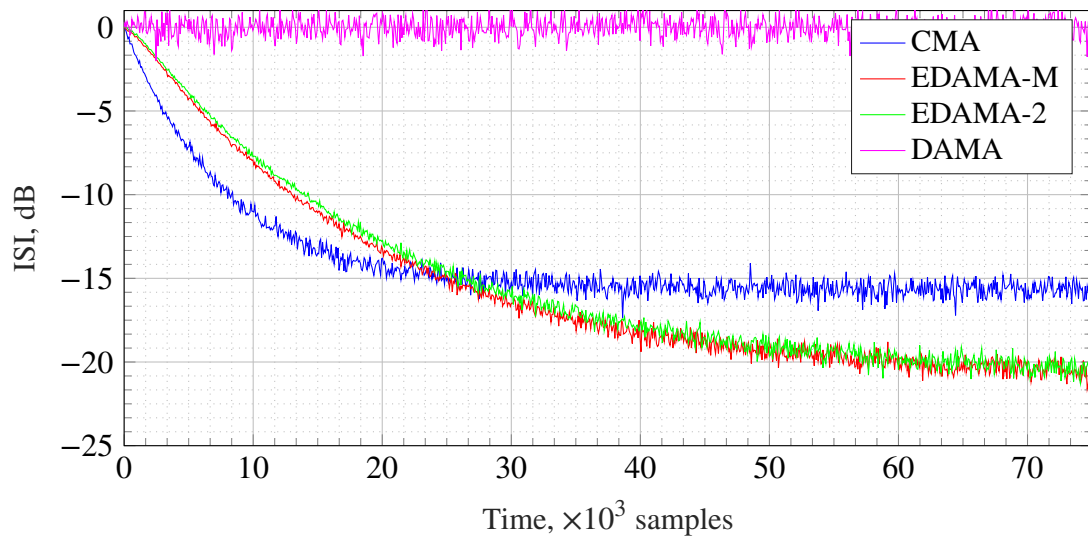
Fig. 2.4. Convergence curve for EDAMA in the case of 15 dB notch channel

According to the simulation results, CMA is the fastest equalization algorithm, showing the highest residual error level. EDAMA for the implemented channels showed the lowest steady-state intersymbol interference level. As postulated, this algorithm ensures faster convergence compared to DAMA. Worth noting that EDAMA with thresholds computed by the multiple radii approach (EDAMA-M) appeared faster than when the two radii approach performed computation. In the case of 15 dB deep notch channel, the DAMA algorithm was not able to converge. Concluding, EDAMA showed better performance than the classically used CMA method without losing the ability of deep notch acquisition.

2.5 Conclusions

The goal of this chapter was to propose a blind equalization algorithm for QAM signals that provides a reduced level of residual error at the output of the equalizer. The following milestones were passed in the course of this task.

- The DAMA for blind equalization of QAM signals was described. The cost function of the algorithm was considered in terms of the decision threshold values.

- The PDF of the deviation of the signal point at the output of the equalizer from the value of the radius of the transmitted symbol was considered. The correspondence between the PDF of this variable and the shifted Rice distribution was shown.

- Two-radius and multi-radius approaches were proposed for calculating the optimal thresholds for deciding on the received symbol. Optimal thresholds improve the cost function for adjusting the equalizer in EDAMA.

- An increase in the equalizer's ability to converge was demonstrated, associated with a decrease in the error probability in decision making.

- A decrease in residual error level was demonstrated, compared to CMA, in the case of limited equalizer length and a non-zero noise level.

- Zero residual error was shown for an infinite equalizer filter length and if its impulse response matched the channel.

3 GROUPED RADII APPROACH

In Chapter 2, we proposed an improvement to the multi-module algorithm based on optimal thresholds for deciding on the received symbol. This approach has been shown to reduce residual error at the equalizer output compared to CMA. On the other hand, the simulation showed the equalizer's inability to converge with notes deeper than 20 dB. A reduced ability to converge is also observed at high noise levels. This is due to an increase in the variance of the deviation of the signal point at the equalizer output from the radius of the transmitted point.

In this chapter, we consider approaches to improve the ability of an equalizer to converge when the signal point deviation at the equalizer output is comparable to the distance between nearby radii. The chapter shows the influence of the detection error probability on the convergence capability of an equalizer. We also consider the conditional probability of correct detection and correct adjustment of the equalizer weights. Based on these parameters, the concept of conditional PDF is introduced, which shows the dependence of the probability of an event receiving a signal with a particular absolute value. An approach to merging several nearby constellation circles is proposed evaluating the obtained functions for the used QAM orders. Thus, when receiving a signal from an area with merged circles, the cost function tries to reduce the variance in this area, resulting in a decrease in the probability of erroneous adjustment of the equalizer.

3.1 An Impact of Detection Error Probability on the Convergence of Equalizer

Note that an increase in the probability of erroneous detection reduces the convergence abilities of the algorithm for the given ISI and the noise level. Updates to the weights of the equalizer taps for EDAMA are expressed as

$$c[l, k+1] = c[l, k] - \qquad (3.1)$$
$$- \mu \left(\left| s_{ex}[k] \right|^2 - R^2 \right) \Big|_{R:\ |\hat{s}_{tx}[k]| = R} s_{ex}[k] s_{in}^*[k-l].$$

Consider the case of the symbol misestimation. It happens when the output radius has deviated beyond the detection threshold $|s_{ex}[k]| > T_i$. If $|s_{ex}[k]|$ has not reached the radius of the next circle R_{i+1}, the expression $\left(\left| s_{ex}[k] \right|^2 - R^2 \right) \Big|_{R=R_{i+1}}$ becomes of the opposite sign. Therefore, all equalizer taps move in the direction opposite to the true one. If the deviation has exceeded the distance between the radii, erroneous detection does not necessarily cause weights misadjustment. The lower deviation is more likely to happen, so the number of misadjustments in the case of erroneous symbol estimation is greater.

Convergence remains possible as long as the number of misadjustments allows to omit averaging in the steepest descent of the cost function (1.67) and approximate it with a stochastic gradient $\hat{\nabla} J[k]$. Thus, the variance of the radius deviation determines the limit of the algorithm's performance at

given positions of the constellation circles.

3.2   Detection Error Probability as a Function of Output Radius Variance

In this section, the effect of the output radius variance on the misadjustment probability is analyzed. In [36], it is shown that the deviation $s_{ex}[k]-s_{tx}[k-l_\delta]$ caused by ISI has a normal distribution for the channels used. Therefore, the output radius $R = |s_{ex}[k]|$ has a Ricean distribution $\varphi\left(R|R_i,\sigma_R\right)$, where R_i is the original symbol radius, and σ_R is the standard deviation.

Let us assume that $M_i = \left|\{a_m\}_i\right|$ is the number of points on the ith circle, and M is the total number of constellation points. Then, their ratio is equal to the probability of transmitting a symbol from this circle $P(R_i) = M_i/M$. The probability that the radius R_i at the output of the equalizer becomes R is equal to

$$P(R|R_i) = \lim_{\Delta R \to 0} \int_{R-\Delta R/2}^{R+\Delta R/2} \varphi\left(R|R_i,\sigma_R\right) dR. \tag{3.2}$$

Assume that the output radius R belongs to the detection area of the ith constellation circle $R \in [T_i, T_{i+1})$. An estimation will be correct if a point from $\{a_m\}_i$ has been transmitted. If a point from any other constellation circle has caused the output radius R, an estimation block will make an error. Thus, according to the law of total probability, the probability of misestimation $P_{er}(R)$ can be expressed as

$$P_{er}(R) = \sum_{k \neq i} P(R_k)P(R|R_k). \tag{3.3}$$

The substitution of (3.2) in (3.3) and changing summation and integration order allows expressing error probability

$$P_{er}(R) = \lim_{\Delta R \to 0} \int_{R-\Delta R/2}^{R+\Delta R/2} \sum_{k \neq i} P(R_k)\varphi\left(R|R_k,\sigma_R\right) dR. \tag{3.4}$$

Let us call the integrand the probability density function (PDF) of the estimation error

$$\varphi_{er}(R|\sigma_R) = \sum_{k \neq i} P(R_k)\varphi\left(R|R_k,\sigma_R\right). \tag{3.5}$$

Note that the integral of it over positive R is not equal to 1. Fig. 3.1 shows the misestimation PDF $\varphi_{er}(R|\sigma_R)$ for different values of standard deviation σ_R. Detection areas are marked with alternating gray and white stripes. The blue lines represent the radii R_i of the circles. One can conclude that $\varphi_{er}(R|\sigma_R)$ rises near the closely positioned constellation circles, especially for higher σ_R.

In Section 3.1, it was mentioned that an estimation error does not necessarily lead to the weights misadjustment. Let us now express the probability of such an event. Consider the following cases:
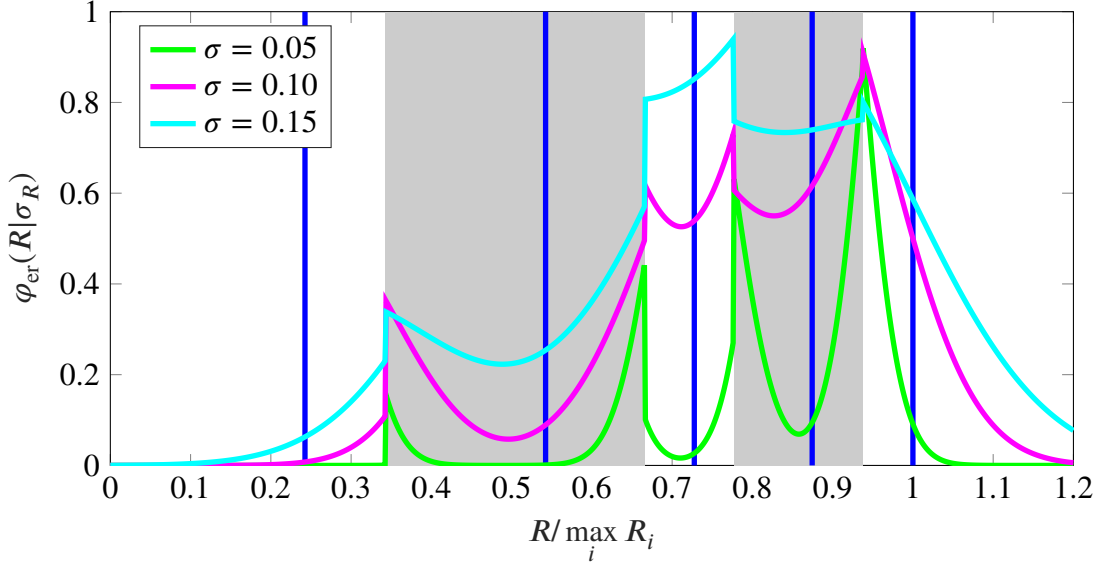
Fig. 3.1. The misestimation PDF $\varphi_{\text{er}}(R|\sigma_R)$

1. A point from the ith constellation circle has been transmitted, and the output radius falls into the detection zone $R \in [T_i, T_{i+1})$. The estimation then will be correct and will not cause a misadjustment of the weights.

2. A point from the subsets $\cup_{k>i}\{a_m\}_k$ or $\cup_{k<i}\{a_m\}_k$ has been transmitted; the output radius belongs to the detection areas $R \in [T_i, R_i)$ or $R \in [R_i, T_{i+1})$, respectively. The estimation will be incorrect; however, an expression $\left(\left|s_{ex}[k]\right|^2 - R_i^2\right)$ preserves the sign and will not cause a misadjustment of the weights.

3. A point from the subsets $\cup_{k>i}\{a_m\}_k$ or $\cup_{k<i}\{a_m\}_k$ has been transmitted; the output radius belongs to the detection areas $R \in [R_i, T_{i+1})$ or $R \in [T_i, R_i)$, respectively. The incorrect symbol estimation then will yield to a misadjustment of the weights.

The probabilities of misestimation and misadjustment in different detection zones are graphically shown in Fig. 3.2. The red areas show a misadjustment probability, while the green areas—a probability of misestimation. The red and black lines indicate the detection thresholds T_i and the radii R_i of the circles, respectively.

Considering the case 3, let us define the probability density function of the tap weights misadjustment

$$\varphi_{\text{mis}}(R|\sigma_R) = \begin{cases} \sum_{k<i} P(R_k)\varphi\left(R|R_k, \sigma_R\right) & \text{if } R \in [T_i, R_i) \\ \sum_{k>i} P(R_k)\varphi\left(R|R_k, \sigma_R\right) & \text{if } R \in [R_i, T_{i+1}). \end{cases} \tag{3.6}$$

Fig. 3.3 shows the dependence of $\varphi_{\text{mis}}(R|\sigma_R)$ on the deviation R for different values of standard deviation σ_R. Detection areas are marked with alternating gray and white stripes. The blue lines represent the radii R_i of the circles. Like the PDF of misestimation $\varphi_{\text{er}}(R|\sigma_R)$, the PDF of misadjustment $\varphi_{\text{mis}}(R|\sigma_R)$ rapidly grows up near the closely positioned circles of the constellation.
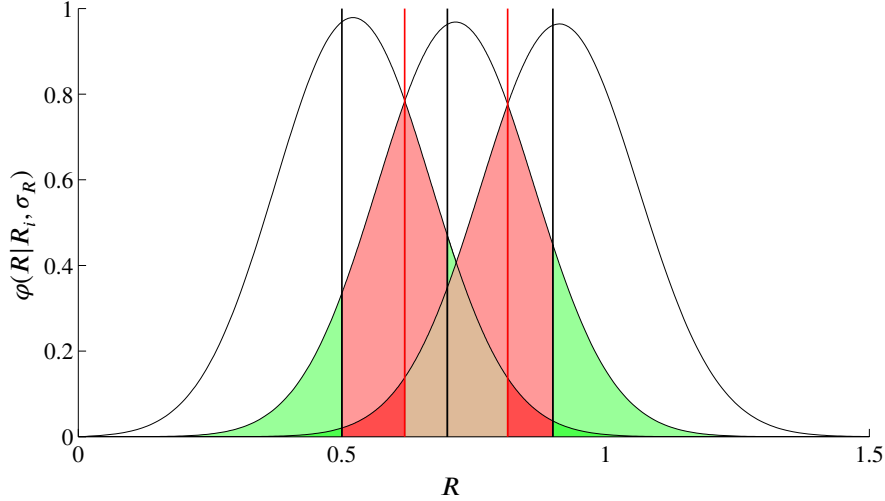
Fig. 3.2. The PDFs of the output radii
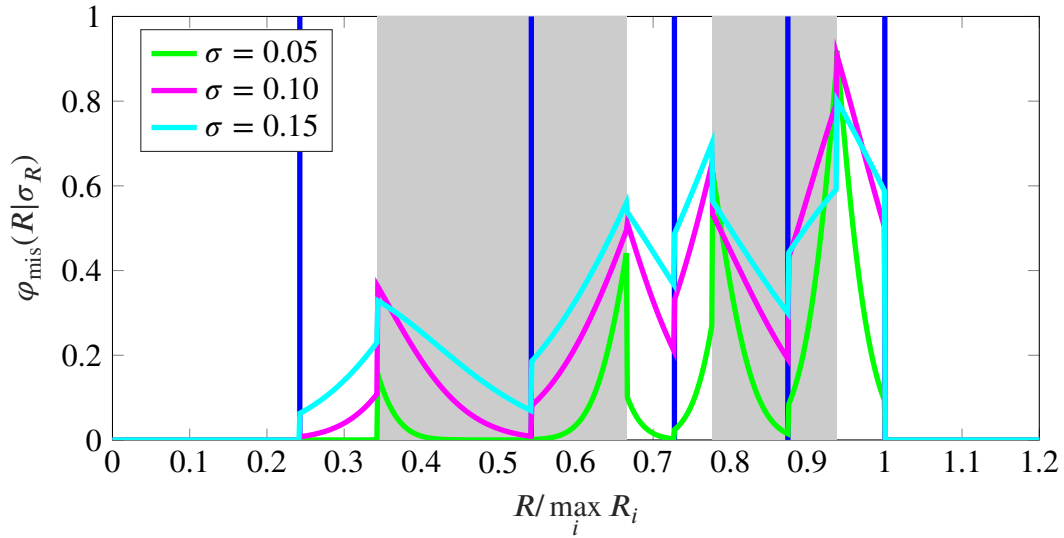
Fig. 3.3. The equalizer misadjustment PDF $\varphi_{\mathrm{mis}}(R|\sigma_R)$

3.3 Proposed Optimization Procedure

The proposed approach aims to reduce the probability of the dispersion (1.67) growth in case of misestimation. The procedure also allows customizing the algorithm to ensure optimal performance for a fixed σ_R.

Assume the circles $\{a_m\}_i$ and $\{a_m\}_{i+1}$ of the constellation $\{a_m\}$ are the most closely positioned to each other, i.e., the radii R_i and R_{i+1} of these circles are such that $\min_k \left(R_{k+1} - R_k\right) = R_{i+1} - R_i$. The idea of the proposed procedure is to combine the points of these two circles into a single subset $\{a_m\}_j = \{a_m\}_i \cup \{a_m\}_{i+1} \subset \{a_m\}$ (note the change in the subset indexing).

Like in the DAMA and EDAMA algorithms, each subset of the constellation points has its detection area. If the output radius R falls within the $\{a_m\}_j$ detection zone, the adaptation mechanism works like CMA, i.e., tries to minimize dispersion for points in this zone. Recall, (1.70) says that the CMA tries to pull the squares of the radii $|s_{ex}[k]|^2$ of all constellation points to one single value

73

R_{CMA}^2. It ensures a minimum of dispersion. Similarly, the proposed algorithm tries to pull the squares of the radii of points $\{a_m\}_j$ to the corresponding R_j^2. According to the method we have used to calculate (1.68), one can express the dispersion constant for subset $\{a_m\}_j$:

$$R_j^2 = \frac{\mathrm{E}\left[|a|^4\right]}{\mathrm{E}\left[|a|^2\right]} \quad \forall a \in \{a_m\}_j. \tag{3.7}$$

The dispersion constants R_j^2 must be calculated for all subsets $\{a_m\}_j$ formed by the union of the circles $\{a_m\}_i$:

$$\{a_m\}_j = \bigcup_{k=i}^{i+K-1} \{a_m\}_k, \tag{3.8}$$

where $K \geqslant 1$ is the number of united circles. For the subsets coinciding with the circles $\{a_m\}_j = \{a_m\}_i$, the dispersion constant R_j^2 is equal to the squared radius R_i^2 of the points on this circle. The subsets can also be formed by combining points of more than two adjacent circles ($K > 2$).

Section 2.3 specified the calculation principles of the detection zone thresholds for the EDAMA algorithm. There we have assumed that the output radius deviation can not exceed the distance between radii, which is generally not valid. Reference [36] describes the so-called EDAMA-M calculation method that takes into account the PDF values for higher radius deviations, which we apply to the proposed algorithm.

Consider the range of the output radii to which the detection threshold belongs $T_i \in [R_i, R_{i+1})$. Assume one has transmitted a point from the subsets $\bigcup_{k>i}\{a_m\}_k$ or $\bigcup_{k\leqslant i}\{a_m\}_k$. If the output radius falls below the threshold $R \in [R_i, T_i)$ or rises above the threshold $R \in [T_i, R_{i+1})$, respectively, a misadjustment will occur. Taking into account the probability of transmission a point from the ith constellation circle $P(R_i) = |\{a_m\}_i|/|\{a_m\}|$, the misadjustment probability is

$$P_{\text{mis}} = \sum_{k>i} P(R_i|R_k)P(R_k) + \sum_{k\leqslant i} P(R_{i+1}|R_k)P(R_k), \tag{3.9}$$

where $P(R_i|R_k)$ and $P(R_{i+1}|R_k)$ are the probabilities that the output radius R caused by a point from the kth circle will belong to the ranges $R \in [R_i, T_i)$ and $R \in [T_i, R_{i+1})$, respectively, i.e., will be interpreted as a symbol from the ith or the $(i+1)$th circle.

Since the PDF of the output radius caused by a point from the kth circle is $\varphi\left(R|R_k, \sigma_R\right)$, probability $P(R_i|R_k)$ can be calculated as follows:

$$P(R_i|R_k) = \int_{R_i}^{T_i} \varphi\left(R|R_k, \sigma_R\right)\, \mathrm{d}R \tag{3.10}$$

$$= Q_1\left(\frac{R_k}{\sigma_R}, \frac{R_i}{\sigma_R}\right) - Q_1\left(\frac{R_k}{\sigma_R}, \frac{T_i}{\sigma_R}\right),$$

74

where Q_1 is the Marcum Q-function. The second group of probabilities $P(R_{i+1}|R_k)$ is calculated similarly:

$$P(R_{i+1}|R_k) = Q_1\left(\frac{R_k}{\sigma_R}, \frac{T_i}{\sigma_R}\right) - Q_1\left(\frac{R_k}{\sigma_R}, \frac{R_{i+1}}{\sigma_R}\right). \tag{3.11}$$

The substitution of (3.10) and (3.11) into (3.9) gives

$$\begin{aligned}P_{\text{mis}}(T_i) &= \sum_{k\leqslant i} Q_1\left(\frac{R_k}{\sigma_R}, \frac{T_i}{\sigma_R}\right) P(R_k) \\ &\quad - \sum_{k>i} Q_1\left(\frac{R_k}{\sigma_R}, \frac{T_i}{\sigma_R}\right) P(R_k) + P'_{\text{const}},\end{aligned} \tag{3.12}$$

where P'_{const} is independent from T_i. An optimization criterion for the detection thresholds T_i is a minimum of the misadjustment probability. Thus, the problem is reduced to finding the extremum $\min\left[P_{\text{mis}}(T_i)\right]$, varying T_i in the range of $[R_i, R_{i+1})$.

Consider an example of the described approach. Fig. 3.4 exposes the misadjustment PDF $\varphi_{\text{mis}}\left(R|\sigma_R\right)$ for different standard deviation σ_R values. As in the case shown in Fig. 3.3, the algorithm used 32-QAM modulation. Notice a union of points of the 3rd, 4th, and 5th circles into one subset. Detection areas are marked with alternating gray and white stripes. The solid blue lines represent the dispersion constants R_j, and the dashed lines denote the radii, R_i, of the circles.
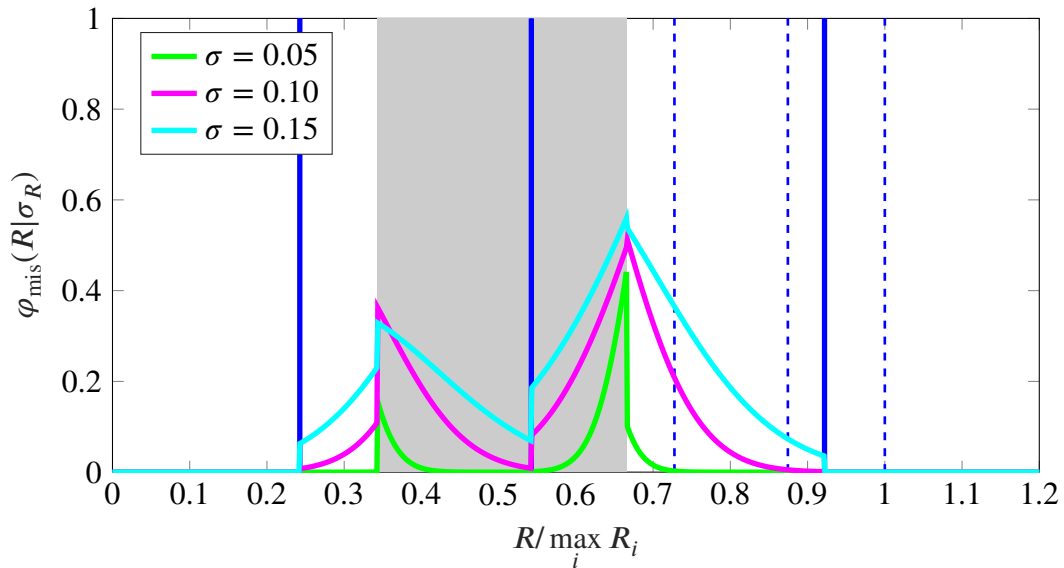
Fig. 3.4. The misadjustment PDF $\varphi_{\text{mis}}(R|\sigma_R)$ for the united 3rd, 4th, and 5th circles of the 32-QAM constellation

Comparing the misadjustment PDFs $\varphi_{\text{mis}}(R|\sigma_R)$ near the closely positioned constellation circles, it becomes apparent that the proposed algorithm significantly reduces the risk of dispersion growth at the equalizer output.

3.4 Simulation results

Simulations verified the performance and convergence properties of the proposed algorithm. The signal forming at the equalizer input corresponds to the communication system model described in Section 1.2. The transmitting signal was generated using standard 32-QAM and 64-QAM constellations. According to the previously described communication system model, the signal forming block incorporated the transmitter's pulse-shaping and the receiver's matched filters. The multipath phenomenon emulation was performed using a two-ray propagation model described in Section 1.3. The depth of the notch utilized as the channel was equal to 10 dB and 15 dB. White Gaussian noise has been added to the signal to provide a signal-to-noise ratio of 35 dB at the equalizer input.

Convergence curves show the dependence of residual error on the iteration number. The error is expressed as the difference between the equalizer output signal radius and the radius of the estimated symbol $\left| |s_{ex}[k]| - |\hat{s}_{tx}[k]| \right|$. For each set of system parameters and each algorithm, 200 Monte Carlo simulations were performed. The resulting curves were obtained by averaging them.

Fig. 3.5 shows the simulation result for a 32-QAM signal with the 10 dB deep notch channel for multipath propagation emulation. It shows convergence curves for CMA, EDAMA, and the constellation points grouping algorithm. The presented algorithm combines $i \in \{3; 4; 5\}$ circles of the 32-QAM constellation. In the figure, it is designated as TEST.
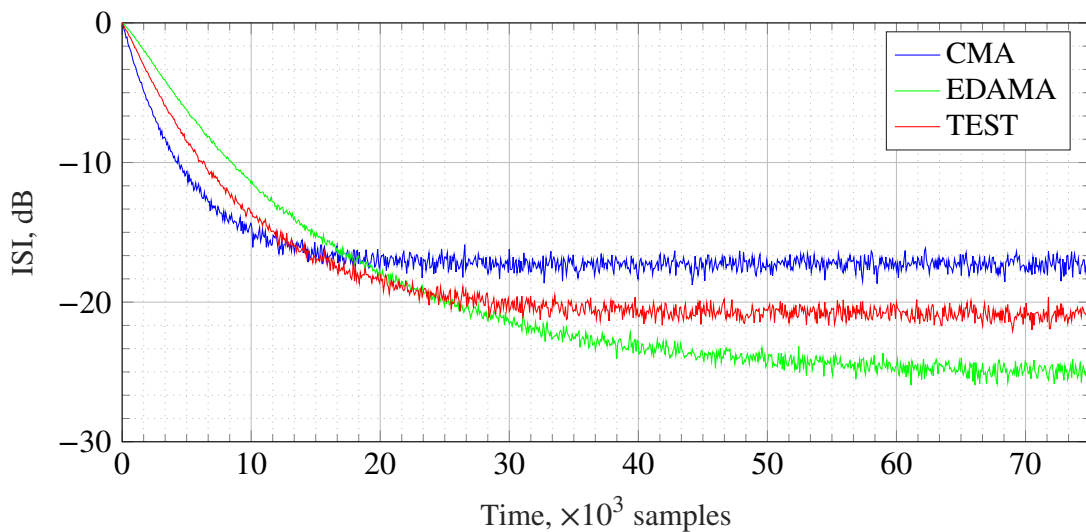
Fig. 3.5. Convergence curves for CMA, EDAMA, and the proposed algorithm in the case of the 10 dB notch channel

The convergence curves confirm that the constellation points grouping algorithm converges faster than EDAMA because of fewer detection errors at the initial adaptation stage. On the other hand, its intersymbol interference is lower than CMA due to the split dispersion constants.

Further, Fig. 3.6 shows the convergence curves for 64-QAM modulation and 15 dB deep notch. It also compares CMA, EDAMA and the proposed algorithm. The last one unifies $i \in \{3; 4; 5\}$ circles and $i \in \{6; 7; 8\}$ circles of the constellation. In the figure, it is designated as TEST.
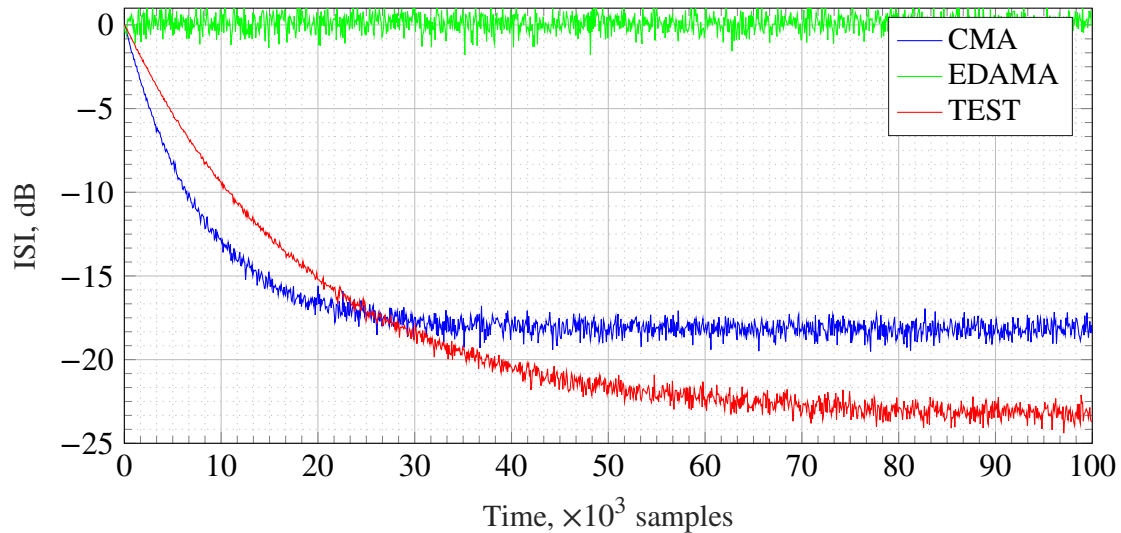
Fig. 3.6. Convergence curves for CMA, EDAMA and the proposed algorithm in the case of 15 dB noth channel

The proposed algorithm converged more slowly than the CMA but ensured much lower residual ISI. Due to the high number of misadjustments, EDAMA did not converge at all.

3.5 Conclusions

This chapter was devoted to cracking the equalizer convergence complexity problem due to the high level of variance of the signal at the output of the equalizer. A solution has been proposed using conditional probability distributions and grouping constellation circles. The following points should be noted summarizing the results obtained.

- A relationship has been shown between the probability of erroneous detection and the ability of an equalizer to converge.
- The concept of conditional probability density was introduced, and its application to optimization of the cost function was shown.
- It has been demonstrated that the probability of misestimation and the probability of misadjusting equalizer weights are not equivalent. The adjustment may be correct in case of an incorrectly detected symbol.
- An increased probability of equalizer misadjustment in intervals with closely spaced constellation circles has been demonstrated.
- An approach to group points from nearby circles of the constellation has been proposed. It allowed adjusting the cost function to reduce the variance of the equalizer output signal if the signal point belonged to the interval between these circles.
- Simulations using the proposed approach have shown that the equalizer gains the ability to converge under conditions in which it is not possible in the case of EDAMA.

4   ADAPTIVE SWITCHED GR-DAMA APPROACH

In Chapter 3, we have developed a decision-directed equalization algorithm that ensures optimal symbol detection and thus minimizes equalizer misadjustment probability. The algorithm, imposing lowest possible residual error, kept a high level of misadjustment probability. As a result, in the previous section, an approach for the balancing between the misadjustment probability and the residual error level minimization was described.

The optimal balance may be established for the given variance of the output equalizer signal. However, this parameter is dependent on a variety of factors, such as time-varying channel changes, the additive noise level in the signal to equalize, current equalizer adjustment degree, etc. Thus, the variance of the equalizer output signal is not constant, and immutable single algorithm usage during different link establishment stages means unbalanced suboptimal operation equalizer operation.

The chapter below introduces an approach to adapt the equalization algorithm to the instant channel conditions and coefficients state. Chapter 3 showed that the misestimation and misadjustment probability is unequivocally dependent on the variance of the output signal. Thus, considering this parameter a metric of the conditions mentioned above, one can conclude that the coefficients adjustment algorithm should be dependent on the variance of the output signal. The current section gives a mathematical foundation for the declared maxima and researches the concept of the adaptation of an equalization algorithm. Attention is paid to convergence speed and probability. The section describes the proposed approach implementation features and gives the results of the conducted simulations.

4.1   Error Measurement Methods

It was mentioned that the received signal is a weighted sum of the delayed replicas of a transmitted signal. Indeed, (1.66) shows that the output signal of the equalizer $s_{ex}[k]$ is a convolution of the transmitted signals $s_{tx}[k]$ with the convoluted impulse responses of channel $h[k]$ and equalizer $c[l, k]$. Thus, from the essence of the convolution process, each output sample can be expressed as a linear combination of the neighboring symbols in the transmitted signal $\{\dots, s_{tx}[k - 1], s_{tx}[k], s_{tx}[k + 1], \dots\}$

$$s_{ex}[k] = \sum_{l=0}^{L_c+L_h-1} (h * c[k])[l]s_{tx}[k - l], \qquad (4.1)$$

where L_c and L_h are lengths of the channel and equalizer impulse responses, respectively.

As changes in the channel and adaptation of the equalizer are relatively slow, signal $s_{ex}[k]$ can be assumed locally ergodic. Thus, the variance of the signal can be calculated, taking into account

that the symbols are uncorrelated:

$$E\left[|s_{ex}[k]|^2\right] = E\left[|s_{tx}[k]|^2\right] \sum_{l=0}^{L_c+L_h-1} |(h*c[k])[l]|^2. \tag{4.2}$$

For the ideal compensation, $E\left[|s_{ex}[k]|^2\right] = E\left[|s_{tx}[k]|^2\right]$. If the ISI is presented in the signal, the central coefficient of the $(h*c[k])[l]$ is still unweighted $\delta[k]$. Thus, the output radius variance $E\left[|s_{ex}[k]|^2\right]$ is minimal for the mitigated ISI. The variance of noise $E\left[|n'[k]|^2\right]$, as it is not correlated with the transmitted symbols, is appended to the variance of the data signal. Thus, variance indicates the amount of the ISI and noise in the signal. To construct probability densities of the received signal, one has to assess its parameters. In the case of the Ricean distribution, mean values correspond to the radii of the constellation circles. The standard deviation can be estimated from the received signal variance

$$\hat{\sigma}_R = \sqrt{E\left[|s_{ex}[k]|^2\right] - E\left[|s_{tx}[k]|^2\right]}, \tag{4.3}$$

where $E\left[|s_{ex}[k]|^2\right]$ can be calculated from the equalizer output signal and $E\left[|s_{tx}[k]|^2\right]$ is a predefined constant.

Section 3.2 described the dependence of the misadjustment probability density on the standard deviation of the noisy process in the signal. The calculation of the misadjustment probability $P_{\mathrm{mis}}(\sigma_R)$ is possible through the integration of (3.6):

$$
\begin{aligned}
P_{\mathrm{mis}}(\sigma_R) &= \int_0^\infty \varphi_{\mathrm{mis}}(R|\sigma_R)\,\mathrm{d}R = \\[2mm]
&= \sum_j \sum_{k\,:\,R_k<R_j} P(R_k)\left[Q_1\left(\frac{R_k}{\sigma_R},\frac{R_j}{\sigma_R}\right) - Q_1\left(\frac{R_k}{\sigma_R},\frac{T_j}{\sigma_R}\right)\right] + \\[2mm]
&+ \sum_j \sum_{k\,:\,R_k>R_j} P(R_k)\left[Q_1\left(\frac{R_k}{\sigma_R},\frac{T_{j+1}}{\sigma_R}\right) - Q_1\left(\frac{R_k}{\sigma_R},\frac{R_j}{\sigma_R}\right)\right],
\end{aligned}
\tag{4.4}
$$

where Q_1 is the Marcum Q-function; summation by j is performed among all subsets $\{a_m\}_j$, and summation by k—among all constellation circles $\{a_m\}_i$.

Fig. 4.1 shows the misadjustment probability $P_{\mathrm{mis}}(\sigma_R)$ dependence on the standard deviation in the Ricean probability density σ_R. Blue, red, green, and magenta lines denote curves for the generalized EDAMA of two, three, and four subsets of points and standard EDAMA algorithms, respectively. Dotted black lines indicate standard deviation σ_R values in which $P_{\mathrm{mis}}(\sigma_R) = 2\%$. For high variance values, only CMA algorithm is capable of equalizer adaptation with zero misadjustment probability. After equalizer sets have been partially adjusted, the output radius variance decreases, and two subset generalized EDAMA algorithm can now operate with $P_{\mathrm{mis}}(\sigma_R) \leqslant 2\%$. Further adjustment of the tap weights leads to the ability of the two subset generalized EDAMA

algorithm to converge equalizer. Thus, the adaptation process evolves from the CMA algorithm to the EDAMA algorithm. As throughout the adaptation $P_{\text{mis}}(\sigma_R)$ is kept low, the proposed approach demonstrates convergence abilities comparable to ones of the CMA; on the other hand, in the steady state, residual error is the same as for the EDAMA algorithm.
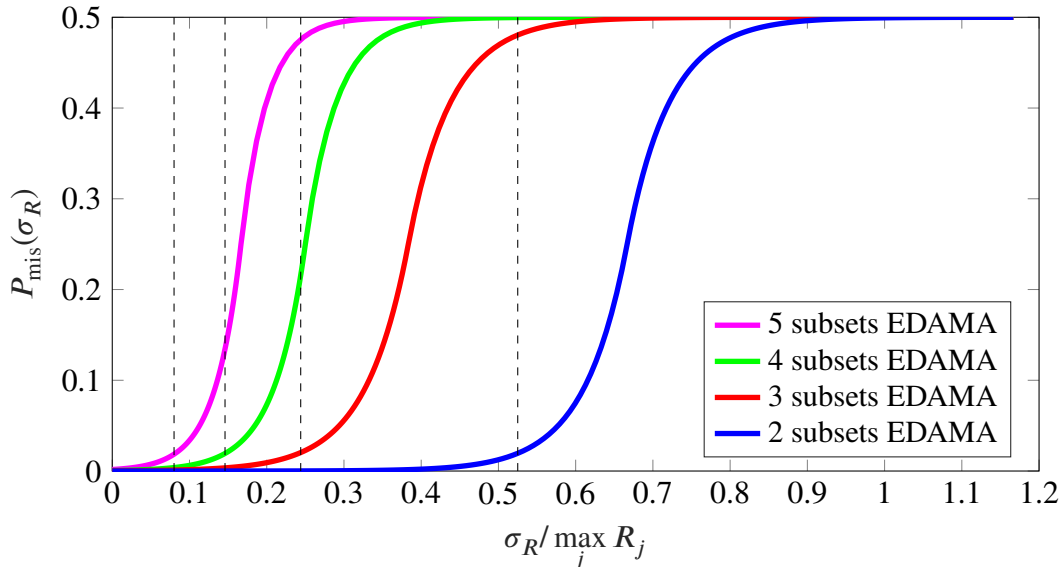
Fig. 4.1. Misadjustment probability $P_{\text{mis}}(\sigma_R)$ dependence on the standard deviation σ_R of noise-like signal

4.2 Simulation Results

Simulations verified the performance and convergence properties of the proposed algorithm. The signal forming at the equalizer input corresponds to the communication system model described in Section 1.2. The transmitting signal was generated using standard 32-QAM constellations. According to the previously described communication system model, the signal forming block incorporated the transmitter's pulse-shaping and the receiver's matched filters. The multipath phenomenon emulation was performed using a two-ray propagation model described in Section 1.3. The depth of the notch utilized as the channel was equal to 10 dB and 15 dB.

The results of the simulations are illustrated with convergence curves, which show the dependence of the residual error on the iteration, or clock cycle, number. The residual error, in this case, is calculated as the difference between the output radius and the radius of the estimated symbol. For each parameter set, 200 Monte Carlo runs of the simulations were performed.

Fig. 4.2 shows the simulation results for the 10 dB deep notch blind equalization in the case of 32-QAM signal. The switching threshold is chosen to ensure the misadjustment probability $P_{\text{mis}}(\sigma_R) = 2\%$.

The experiments show that the switching approach ensures low residual error, as at the final
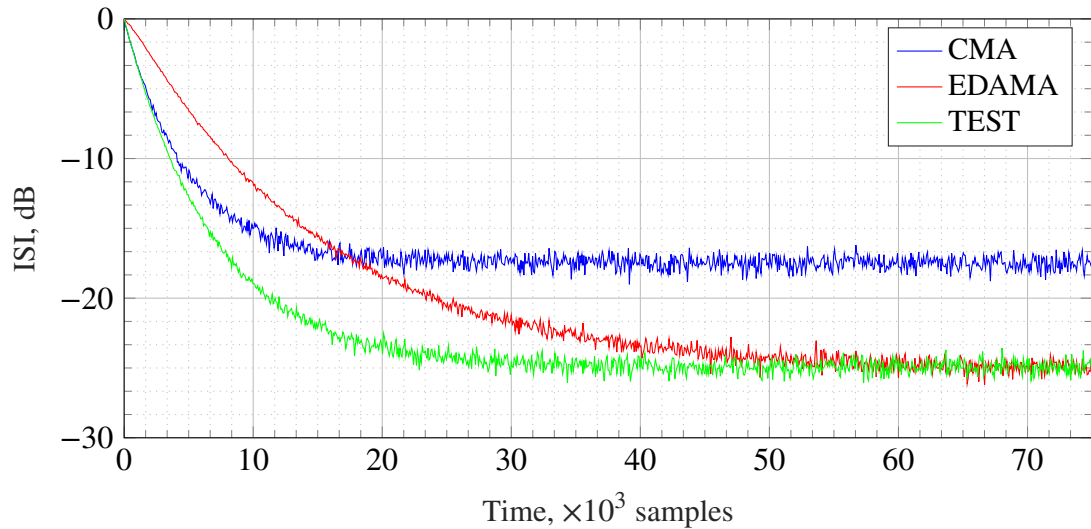
Fig. 4.2. Equalizer convergence plots for CMA, EDAMA, and the switching approach for the 10 dB deep notch channel

stage of this algorithm it uses the EDAMA cost function. On the other hand, it converges much faster because of the lower number of misadjustments at the initial stages.

In the second experiment, the same signal has been passed through the channel represented by a 20 dB deep notch. The convergence curves for this simulation are given in Fig. 4.3. The misadjustment probability is kept $P_{\text{mis}}(\sigma_R) = 2\,\%$.
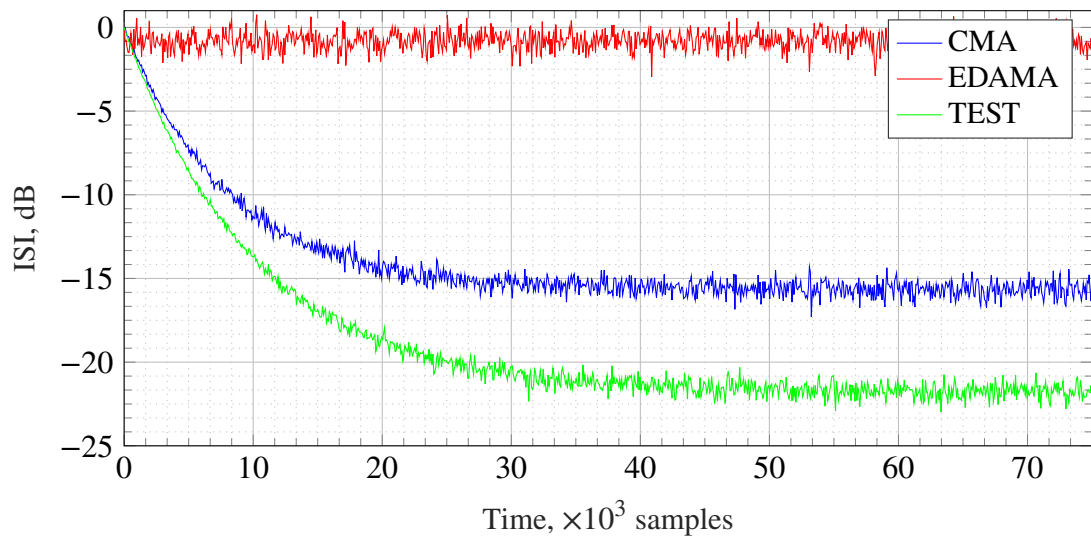
Fig. 4.3. Equalizer convergence plots for CMA, EDAMA, and the switching approach for the 15 dB deep notch channel

As previously, the switching approach converged with lower residual ISI comparing to the CMA. Notably, the EDAMA algorithm failed to converge because of high misadjustment probability. On the other hand, as the proposed approach's final stage, EDAMA ensured low residual error.

4.3 Conclusions

This chapter is devoted to the possibility of using blind equalization algorithms that are best suited to the current channel parameters and the degree of equalizer adjustment. In summary, the following considerations should be noted.

- It has been shown that for each unique union of adjacent constellation circles, the dependence of the probability of misadjustment of the equalizer is a monotonic growing function of the standard deviation.

- It has been demonstrated that the set of unique unions of adjacent constellation circles can be ordered so that the probability of misadjustment of the equalizer for each successive algorithm is greater for the same value of standard deviation.

- It has been demonstrated that the standard deviation estimate is independent of the transmitted symbol and can be obtained from the signal variance estimate.

- An approach in which, in the process of adjusting the equalizer and reducing the dispersion of the output signal, the cost function switches to an algorithm with a large number of detection zones was proposed.

- It was proposed to use a stop-and-go approach to adjust the equalizer in the case of the unidirectional equalization of two algorithms.

- The simulation results showed that the proposed approach provides the adjustment speed of CMA and the residual error level of EDAMA.

5 FPGA IMPLEMENTATION AND FIELD MEASUREMENTS

The theoretical foundations of blind equalization schemes have been discussed in the previous chapters. The simulations of the proposed algorithms showed their consistency for the multipath propagation effects mitigation. The current chapter is devoted to the VHDL implementation of a complex blind equalizer as an intellectual property (IP) core and its connection to a QAM modem. At the end of the chapter, the results of the field measurements of the designed equalization system are given.

The IP core of the equalizer is a half-baud-spaced finite impulse response filter with complex time-varying coefficients. The parallel design was compiled in the Xilinx Vivado environment to be verified on the Xilinx Zynq 7000 FPGA. The equalizer is configurable and capable of working with QAM modulation orders from 4-QAM to 128-QAM. Several debugging functions designed to evaluate the equalizer performance have also been implemented on the VHDL.

The chapter begins by setting the general goals of the implementation and describing the steps for its undertaking. The chapter does not describe the well-known VHDL programming approaches and focuses on equalizer-specific aspects. The general structure of the implemented device and the scheme for its verification are described. Attention is paid to the division of the mathematical operations performed into simple operations, ensuring pipeline and converting the device to fixed-point arithmetic. At the end of the chapter, a description of the setup for verifying the designed device on a notch emulator and a line of 25 analog repeaters is given.

5.1 Design Objectives

The IP core to be implemented is a linear complex half-baud-spaced blind equalizer. It is realized using the direct form complex equalizer structure, consisting of four real finite impulse response (FIR) filters. The IP core operates twice the symbol frequency and uses two clock-enable signals: one operates twice the symbol frequency, and the other operates at the symbol frequency. The equalizer output and tap coefficients are updated once per symbol period. The equalizer is configurable and capable of working with QAM modulation orders from 4-QAM to 256-QAM. Several debugging functions designed to evaluate the equalizer performance have also been implemented on the VHDL. There are two pipelining stages: the first stage is after the equalizer output is generated, while the second stage follows the error signal calculation. The primary goals of this implementation are:

- to implement an IP core of a dynamic complex equalizer for QAM signals in Matlab and implement this core in VHDL;
- to design the debug constructions that allow the construction of the equalizer's convergence curves in the FPGA and download them;
- to verify a possibility of the designed device to mitigate the multipath propagation effects for

QAM modulation of the order from 4-QAM to 128-QAM;

- to connect the blind equalizer IP core to the QAM receiver to test equalization capabilities using physical-world signals.

The design and analysis for CMA, EDAMA, and generic algorithms were performed in Matlab for radio relay-line channel models. These algorithms were converted to fixed-point algorithms using a script Matlab environment. The VHDL-like equalizer model was created by modifying the direct form complex equalizer architecture and using the fixed point models obtained for the target algorithms. The compilation process and initial timing analysis are performed using Xilinx Vivado. The following sections discuss these steps in detail and present the implementation results.

As mentioned above, the equalizer discussed in the Doctoral Thesis is an FIR filter with time-varying coefficients. The output of the equalizer can be expressed as a convolution of the input signal, $s_{\text{in}}[k]$, and its impulse response $c[k]$:

$$
s_{\text{ex}}[k] = \sum_{l=0}^{L-1} s_{\text{in}}[k-l]c[l] = \sum_{l=0}^{L-1} \mathfrak{Re}\{s_{\text{in}}[k-l]\}\mathfrak{Re}\{c[l]\} - \sum_{l=0}^{L-1} \mathfrak{Im}\{s_{\text{in}}[k-l]\}\mathfrak{Im}\{c[l]\}
$$
$$
+ j\left[\sum_{l=0}^{L-1} \mathfrak{Re}\{s_{\text{in}}[k-l]\}\mathfrak{Im}\{c[l]\} + \sum_{l=0}^{L-1} \mathfrak{Im}\{s_{\text{in}}[k-l]\}\mathfrak{Re}\{c[l]\}\right],
$$

$$(5.1)$$

where L is the length of equalizer. Thus, to implement the device that works following the algorithms presented in the Thesis, it is necessary to implement four filters with real coefficients, a coefficient update block, an estimator of the received symbol, a multiplexer of detection thresholds, and a variance estimator for the signal at the output of the equalizer. The following sections cover the prominent implementation details of these nodes.

5.2 Fixed-Point Arithmetic Implementation

The practical implementation of the algorithm in FPGA requires a transition to integer arithmetic. The equalizer input signal was digitized using a 12-bit ADC, then processed while maintaining the bit depth. Empirically, it was found that using 16 bits to represent the value of the coefficients is sufficient to ensure the convergence of the equalizer. Also, with this number of bits, the equalizer does not increase the dispersion of the output signal. In the previous chapters, the expression for updating the coefficients was presented as:

$$
c[l, k+1] = c[l, k] - \mu\left(\left|s_{\text{ex}}[k]\right|^2 - R_j^2\right) s_{\text{ex}}[k]s_{\text{in}}^*[k-l],
$$

$$(5.2)$$

where R_j is dispersion constant for current detection zone.

Expression (5.2) shows that updating the equalizer tap weight depends on the corresponding

input sample and common value for all coefficients on a given cycle. Getting this value requires the product of three variables, which increases the word length of the result. Preservation of the adjustment accuracy with a decrease in the bit width of this value is ensured by switching to floating-point arithmetic with a radix of 2. The value is converted to a fixed-point number using a multiplexer when updating the equalizer tap weight. Note that the step-size coefficient is applied as a power of two without a mantissa to simplify implementation. Updates of the equalizer taps weights are averaged using 32-bit accumulators. The 16 most significant bits of these accumulators are used as equalizer coefficients.

5.3   Blind Equalizer Implementation

It was noted that the practical implementation of the proposed algorithm consists of four real filters with variable dynamic tuning coefficients. Each contains a half-baud-spaced 35-tap delay line and is implemented in direct form using built-in multiply-and-accumulate blocks. The delay line also stores the input signal samples needed to generate the coefficient update. Calculating these values requires performing the steps described in Section 5.2. In practice, a stable implementation requires them to be divided into several clock cycles. Therefore, maintaining the correspondence of the input signal sample and the equalizer tap requires an increase in the length of the filter delay line.

The proposed algorithm offers a cost function that requires detecting the received signal. The boundaries of the detection zones and the dispersion constants of these detection zones are stored in a distributed random access memory. Their use in coefficient update calculation involves a number of multiplexers. Switching between algorithms with a different division of the constellation into detection zones requires an estimate of the output signal dispersion. Averaging, in this case, is performed by a first-order narrow-band low-pass filter with an infinite impulse response. A control node is also implemented that uses hysteresis decision-making to switch between algorithms.

The simulations of the implemented IP core was performed in Xilinx Vivado environment. The results are illustrated for CMA, EDAMA, and generalized algorithm for 10 dB and 15 dB notch channels in Figs 5.1 and 5.2, respectively.

The steady-state performance of the VHDL implemented algorithm is nearly identical to that of the floating-point algorithm for all simulations.

5.4   FPGA Test Environment Implementation

The evaluation of the performance of an equalizer is based on its ability to converge under given conditions. The convergence curves are necessary to draw conclusions about the adequacy of the proposed implementation. Since, in the case of FPGA implementation for 20–40 MHz bands, the equalizer convergence time is measured in tens of microseconds, the curve should be built automatically in FPGA.
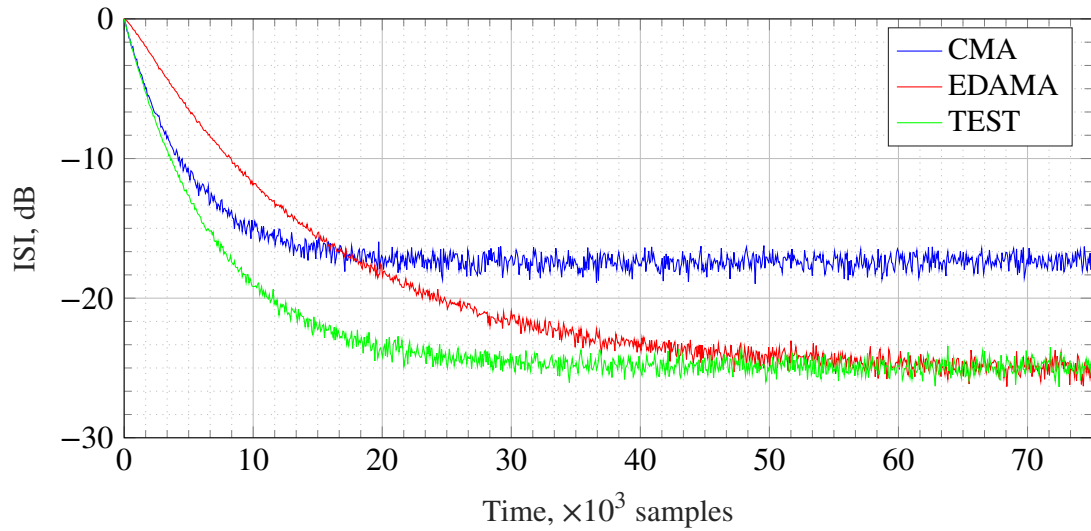
Fig. 5.1. Convergence curves for CMA, EDAMA, and the proposed algorithm in the case of the 10 dB notch channel
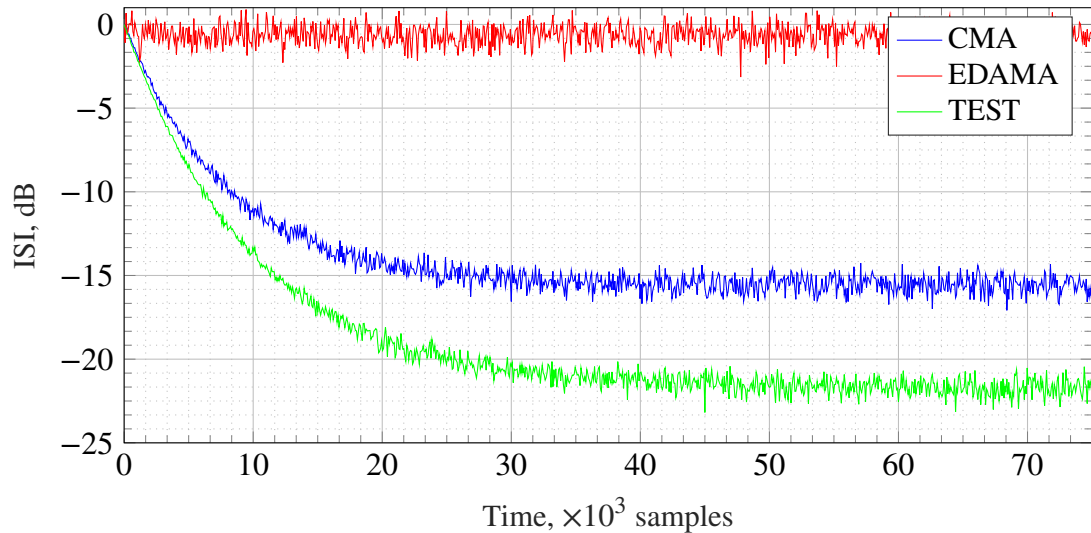
Fig. 5.2. Convergence curves for CMA, EDAMA, and the proposed algorithm in the case of 15 dB noth channel

To build a convergence curve, an estimate of the variance of the output signal, calculated in the equalizer, is used. After the equalizer exits the reset state, the saving of convergence curve values is controlled by a free-running counter. Once every certain number of cycles, the value of the variance estimate is sampled. The intersymbol interference value for the modulation used is estimated based on the dispersion value. The obtained value is afterward written into a memory block. After the equalizer converges, the stored values are read in from the FPGA.

5.5 Implementation Results

Verification of the implemented block took place at several stages of development. First, separating the math involved in updating the equalizer weights into a chain of simple actions and the pipeline

resulted in increased latency in the equalizer feedback loop. Secondly, the transition to fixed-point arithmetic can be interpreted as introducing an additional noise component into the values of the coefficients. Both of these operations were performed in the Matlab environment, after which the simulation was restarted. After that, the finished model was rewritten in the VHDL language. Several single launches were made in the Vivado Simulator with signals synthesized in Matlab fed to the equalizer input to check the bit-to-bit compatibility between the models. The goal, in this case, was to obtain a signal at the output of the equalizer identical to that in the Matlab environment.

After verification, the IP core was synthesized using Xilinx Vivado. The compiled core was incorporated into the QAM modem project. The final device, which is the receiving part of the data transmission system based on QAM, was tested in the field. The ability to converge at initial deep notches was demonstrated on a multipath emulator. Connecting the device to a line of multiple analog repeaters has shown improved performance in the event of band-limiting and system ripples. Inside the FPGA, the equalizer weights were repeatedly reset and the ISI was read at the equalizer output as a function of time. Thus, as a result of averaging, convergence curves were obtained for each of the equalizer algorithms. The resulting convergence curves are shown in Fig. 5.3.
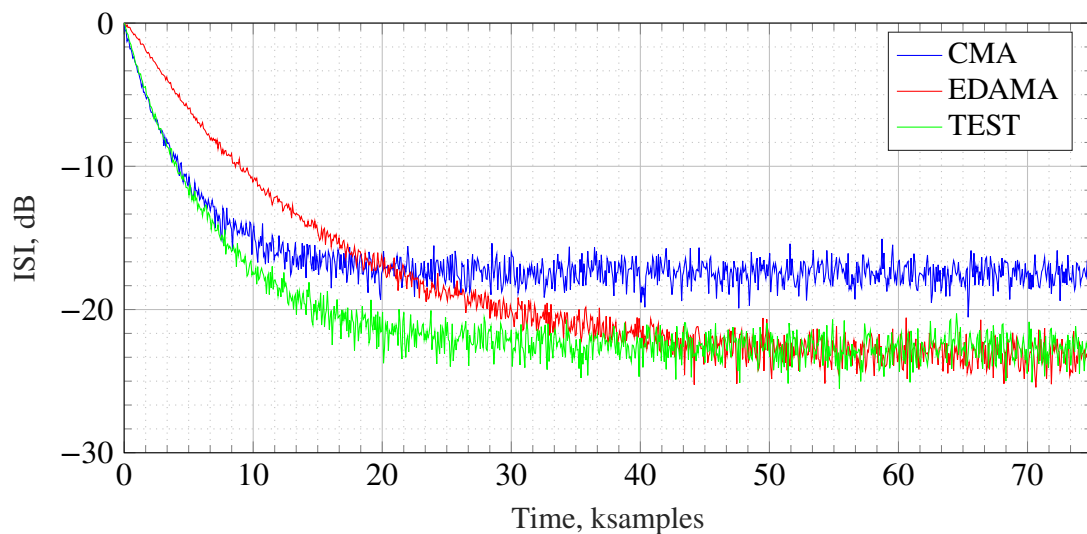
Fig. 5.3. FPGA read convergence curves for CMA, EDAMA and the proposed algorithm in the case of 15 dB notch channel

5.6 Conclusions

This chapter was devoted to the implementation of blind equalization algorithms on VHDL and subsequent verification of their performance in FPGA. In this regard, the following points should be noted.

- The problems of equalization and adjustment of the equalizer coefficients were decomposed into simple mathematical or logical operations to enable their description in VHDL.

- The decomposition of logically related operations into groups was carried out to ensure the possibility of their implementation in a parallel environment.

- The detection implementation was optimized in order to minimize the resources used by the FPGA.

- Rounding and implementation of blocks in integer arithmetic and with a limited word length was made.

- The created IP core was incorporated into the existing QAM modem project, and its performance was verified.

FINAL CONCLUSIONS

This Doctoral Thesis is devoted to the issues of blind equalization of QAM signals. The author has proposed several approaches to forming cost functions for blind equalization algorithms. Practical implementation and field tests of the final device showed the engineering viability of the proposed technique for blind equalization. In particular, the alignment algorithms presented in the Thesis simultaneously provide a high convergence capability under conditions of significant initial multipath distortion. At the same time, these algorithms show a low residual error level in the signal at the output of the equalizer after its adjustment. This feature eliminates the necessity of usual switching to decision-directed channel changes tracking algorithms after converging the equalizer. The practical applicability of the proposed solutions also justifies finding a commercial application of the developed device.

The most important results of the research carried out within the framework of this Doctoral Thesis are as follows.

- The work suggests the optimal calculation of detection thresholds for estimating the received symbol at the output of the equalizer. A combination of methods for calculating thresholds and a CMA-based equalizer adjustment cost function is proposed in [36]. This algorithm makes it possible to reduce the residual error level down to zero in the absence of noise at the equalizer input and its infinite length.

- A probability density was proposed as a metric for assessing the equalizer misadjustment probability at a certain radius of the output. As a solution to reduce misadjustment probability, in [37], it is proposed to merge constellation circles in regions of high misadjustment probability density.

- The Thesis proposes switching between algorithms with different combinations of constellation circles to consider the level of variance in the output signal. The approach was first described in [39] and showed a high convergence capability with a low residual error level.

- Practical implementation and verification showed the characteristics of the proposed algorithms corresponding to the simulations. Some implementation details were published in [35].

Thus, we can conclude that the proposed methodology of QAM signals equalization is practically applicable and that the objective set for this Thesis has been successfully achieved. Moreover, the results obtained can be easily extended to more sophisticated communication schemes that use the QAM concept.

BIBLIOGRAPHY

[1] Y. Sato. "A Method of Self-Recovering Equalization for Multilevel Amplitude-Modulation Systems." In: *IEEE Trans. Commun.* 23.6 (June 1975), pp. 679–682. ISSN: 0096-2244. DOI: 10.1109/TCOM.1975.1092854.

[2] D. N. Godard. "Self-Recovering Equalization and Carrier Tracking in Two-Dimensional Data Communication Systems." In: *IEEE Trans. Commun.* 28.11 (Nov. 1980), pp. 1867–1875. ISSN: 0096-2244. DOI: 10.1109/TCOM.1980.1094608.

[3] M. J. Ready and R. P. Gooch. "Blind Equalization Based on Radius Directed Adaptation." In: *International Conference on Acoustics, Speech, and Signal Processing*. Albuquerque, USA: IEEE, Apr. 1990, pp. 1699–1702. DOI: 10.1109/ICASSP.1990.115806.

[4] W. Sethares, G. Rey, and C. R. Johnson Jr. "Approaches to Blind Equalization of Signals with Multiple Modulus." In: *IEEE International Conference on Acoustics, Speech, and Signal Processing (ICASSP-89)*. Vol. 89. Glasgow, UK: IEEE, May 1989, pp. 972–975. DOI: 10.1109/ICASSP.1989.266592.

[5] K. N. Oh and Y. O. Chin. "Modified Constant Modulus Algorithm: Blind Equalization and Carrier Phase Recovery Algorithm." In: *Gateway to Globalization*. Vol. 1. Seattle, USA: IEEE, June 1995, pp. 498–502. ISBN: 978-0-7803-2486-2. DOI: 10.1109/ICC.1995.525219.

[6] J. Yang, J.-J. Werner, and G. A. Dumont. "The Multimodulus Blind Equalization and Its Generalized Algorithms." In: *IEEE J. Select. Areas Commun.* 20.5 (June 2002), pp. 997–1015.

[7] S. Abrar and R. A. Axford Jr. "Sliced Multi-Modulus Blind Equalization Algorithm." In: *ETRI Journal* 27.3 (June 2005), pp. 257–266. ISSN: 1225-6463. DOI: 10.4218/etrij.05.0104.0027.

[8] V. Weerackody and S. A. Kassam. "Dual-Mode Type Algorithms for Blind Equalization." In: *IEEE Trans. Commun.* 42.1 (Jan. 1994), pp. 22–28.

[9] G. Picchi and G. Prati. "Blind Equalization and Carrier Recovery Using a "Stop-and-Go" Decision-Directed Algorithm." In: *IEEE Trans. Commun.* 35.9 (Sept. 1987), pp. 877–887. ISSN: 0096-2244. DOI: 10.1109/TCOM.1987.1096877.

[10] S. Abrar. "Stop-and-Go Algorithms for Blind Channel Equalization in QAM Data Communication Systems." In: *National Conference on Emerging Technologies*. Pakistan, Dec. 2004.

[11]   R. A. Axford Jr., L. Milstein, and J. Zeidler. "A Dual-Mode Algorithm for Blind Equal-
       ization of QAM Signals: CADAMA." In: *Conference Record of the Twenty-Ninth Asilo-
       mar Conference on Signals, Systems and Computers*. Vol. 1. Pacific Grove, USA: IEEE
       Comput. Soc. Press, 1996, pp. 172–176. ISBN: 978-1-55937-533-7 978-0-8186-7370-2. DOI:
       10.1109/ACSSC.1995.540535.

[12]   L. Litwin et al. "Blended CMA: Smooth, Adaptive Transfer from CMA to DD-LMS." In:
       IEEE Wireless Communications and Networking Conference, 1999. New Orleans, USA:
       IEEE, 1999, pp. 797–800. ISBN: 978-0-7803-5668-9. DOI: 10.1109/WCNC.1999.796764.

[13]   M. Shahmohammadi and M. Kahaei. "A New Dual-Mode Approach to Blind Equalization of
       QAM Signals." In: *Eighth IEEE International Symposium on Computers and Communi-
       cation (ISCC 2003)*. Kemer, Turkey: IEEE, July 2003.

[14]   W. SiYuan. "Blind Equalization of QAM Signals Based On Dual-Mode Multi-modulus Al-
       gorithms." In: *Procedia Engineering* 15 (2011), pp. 2434–2438. ISSN: 18777058. DOI: 10.
       1016/j.proeng.2011.08.457.

[15]   C.-H. Tseng and C.-B. Lin. "A Stop-and-Go Dual-Mode Algorithm for Blind Equalization."
       In: *Communications: The Key to Global Prosperity*. Vol. 2. London, UK: IEEE, Nov. 1996,
       pp. 1427–1431. ISBN: 978-0-7803-3336-9. DOI: 10.1109/GLOCOM.1996.587681.

[16]   D. Ashmawy et al. "Joint MCMA and DD Blind Equalization Algorithm with Variable Step-
       Size." In: *IEEE International Conference on Electro/Information Technology* (June 2009),
       pp. 174–177.

[17]   Z. Jiang et al. "A Newly High-Speed MCMA Algorithm for QAM System." In: *4th Inter-
       national Conference on Wireless Communications, Networking and Mobile Computing*.
       Dalian, China: IEEE, Oct. 2008, pp. 1–4. ISBN: 978-1-4244-2107-7. DOI: 10.1109/WiCom.
       2008.443.

[18]   B. Yang, D. Wang, and Y. Wu. "Joint Batch Implementation of Blind Equalization and Timing
       Recovery." In: *Journal of Communications* 8.7 (2013), pp. 449–455. ISSN: 17962021. DOI:
       10.12720/jcm.8.7.449-455.

[19]   M. S. Faruk. "Low Complexity Carrier-Phase Estimation Based on Sign-Error Modified CMA
       for 16-QAM Coherent Optical Receivers." In: *3rd International Conference on Electrical
       Information and Communication Technology (EICT), 2017*. Khulna, Bangladesh: IEEE,
       Dec. 2017, pp. 1–3. ISBN: 978-1-5386-2305-3 978-1-5386-2307-7. DOI: 10.1109/EICT.
       2017.8275194.

[20] M. Kaur, P. Singh, and S. Singh. "CMA Technique: A Solution for Minimum PAPR in OFDM." In: *2nd International Conference on Recent Advances in Engineering & Proceedings of Computational Sciences (RAECS)*. Chandigarh, India: IEEE, Dec. 2015, pp. 1–4. ISBN: 978-1-4673-8253-3. DOI: 10.1109/RAECS.2015.7453323.

[21] R. Mahmoud et al. "A Calibration Method for Hybrid Technique Based on CMA with Clipping in MIMO-OFDM System." In: *2018 11th German Microwave Conference (GeMiC)*. Freiburg: IEEE, Mar. 2018, pp. 203–206. ISBN: 978-3-9812668-8-7. DOI: 10.23919/GEMIC.2018.8335065.

[22] T. Huang, K. Ren, and X. Li. "Full-Range Carrier Frequency Offset Estimation for CO-OFDM Based on CMA Equalizers." In: *16th International Conference on Optical Communications and Networks (ICOCN)*. Wuzhen, China: IEEE, Aug. 2017, pp. 1–3. ISBN: 978-1-5386-3271-0 978-1-5386-3273-4. DOI: 10.1109/ICOCN.2017.8121597.

[23] S. Kun and Z. Xudong. "A New CMA-based Blind Equalization for MIMO Systems." In: *International Conference on Communications, Circuits and Systems (ICCCAS)*. Vol. 1. Chengdu, China: IEEE, 2004, pp. 167–171. ISBN: 978-0-7803-8647-1. DOI: 10.1109/ICCCAS.2004.1345998.

[24] P. O. Taiwo and A. Cole-Rhodes. "MIMO Equalization of 16-QAM Signal Blocks Using an FFT-based Alphabet-Matched CMA." In: *51st Annual Conference on Information Sciences and Systems (CISS)*. Baltimore, USA: IEEE, Mar. 2017, pp. 1–6. ISBN: 978-1-5090-4780-2. DOI: 10.1109/CISS.2017.7926076.

[25] X. Xiang et al. "Performance Comparison of DA-TDE and CMA for MIMO Equalization in Multimode Multiplexing Systems." In: *14th International Conference on Optical Communications and Networks (ICOCN)*. Nanjing, China: IEEE, July 2015, pp. 1–3. ISBN: 978-1-4673-7373-9. DOI: 10.1109/ICOCN.2015.7203722.

[26] L. Cui et al. "Research on Cross-Polarization Interference Canceller with Blind Adaptive Algorithm." In: *International Conference on Computational Problem-Solving (ICCP)*. Leshan, China: IEEE, Oct. 2012, pp. 202–204. ISBN: 978-1-4673-1697-2 978-1-4673-1696-5 978-1-4673-1694-1 978-1-4673-1695-8. DOI: 10.1109/ICCPS.2012.6384214.

[27] M. S. Faruk. "Modified CMA Based Blind Equalization and Carrier-Phase Recovery in PDM-QPSK Coherent Optical Receivers." In: *16th International Conference on Computer and Information Technology (ICCIT)*. Khulna, Bangladesh: IEEE, Mar. 2014, pp. 469–472. ISBN: 978-1-4799-3497-3 978-1-4799-3496-6. DOI: 10.1109/ICCITechn.2014.6997333.

[28] W. Liu et al. "Two Modified Constant Modulus Methods Based on Independent Component Analysis for Polarization Demultiplexing." In: *16th International Conference on Optical*

Communications and Networks (ICOCN). Wuzhen, China: IEEE, Aug. 2017, pp. 1–3. ɪsʙɴ: 978-1-5386-3271-0 978-1-5386-3273-4. ᴅᴏɪ: 10.1109/ICOCN.2017.8121523.

[29]   M. Krairiksh. "Development of a Handset Adaptive Antenna Using Phased-Array of Switched-Beam Elements." In: *2008 International Workshop on Antenna Technology: Small Antennas and Novel Metamaterials*. Chiba, JApan: IEEE, Mar. 2008, pp. 87–90. ɪsʙɴ: 978-1-4244-1522-9. ᴅᴏɪ: 10.1109/IWAT.2008.4511297.

[30]   K. Sekiyama et al. "Blind Signal Separation Using Array Antenna with Modified Optimal-Stepsize CMA." In: *2020 International Symposium on Antennas and Propagation (ISAP)*. Osaka, Japan: IEEE, Jan. 2021, pp. 799–800. ɪsʙɴ: 978-4-88552-326-7. ᴅᴏɪ: 10.23919/ISAP47053.2021.9391234.

[31]   J. Tagapanij et al. "Phased Array of Switched-Beam Elements for Handset Adaptive Antenna." In: *2007 IEEE Radio and Wireless Symposium*. Long Beach, CA, USA: IEEE, 2007, pp. 137–140. ɪsʙɴ: 978-1-4244-0444-5. ᴅᴏɪ: 10.1109/RWS.2007.351786.

[32]   K. Maruta and C.-J. Ahn. "Uplink Interference Suppression by Semi-Blind Adaptive Array With Decision Feedback Channel Estimation on Multicell Massive MIMO Systems." In: *IEEE Trans. Commun.* 66.12 (Dec. 2018), pp. 6123–6134. ɪssɴ: 0090-6778, 1558-0857. ᴅᴏɪ: 10.1109/TCOMM.2018.2863679.

[33]   K. Maruta and C.-J. Ahn. "Enhanced Semi-Blind Uplink Interference Suppression on Multicell Massive MIMO Systems for Multi Modulus Signals." In: *2019 IEEE 90th Vehicular Technology Conference (VTC2019-Fall)*. Honolulu, HI, USA: IEEE, Sept. 2019, pp. 1–6. ɪsʙɴ: 978-1-72811-220-6. ᴅᴏɪ: 10.1109/VTCFall.2019.8891412.

[34]   D. Kolosovs and E. Bekeris. "Chaos Code Division Multiplexing Communication System." In: *7th International Conference on Computational Intelligence, Communication Systems and Networks (CICSyN)*. Riga, Latvia: IEEE, June 2015, pp. 65–69. ɪsʙɴ: 978-1-4673-7016-5. ᴅᴏɪ: 10.1109/CICSyN.2015.22.

[35]   S. Šarkovskis et al. "Encoder Improvement for Simple Amplitude Fully Parallel Classifiers Based on Grey Codes." In: *Procedia Engineering* 178 (2017), pp. 604–614. ɪssɴ: 18777058. ᴅᴏɪ: 10.1016/j.proeng.2017.01.119.

[36]   D. Kolosovs, A. Zelenkov, and A. Jersovs. "Enhanced Decision Adjusted Modulus Algorithm for Blind Equalization." In: *Procedia Computer Science* 104 (2017), pp. 429–436. ɪssɴ: 18770509. ᴅᴏɪ: 10.1016/j.procs.2017.01.156.

[37]   D. Kolosovs. "A Generalization of the Enhanced Decision Adjusted Modulus Algorithm for Blind Equalization of Constellations with Closely Positioned Circles." In: *2020 IEEE Microwave Theory and Techniques in Wireless Communications (MTTW) (MTTW'20)*.

Riga, Latvia: IEEE, Oct. 2020, pp. 195–200. ISBN: 978-1-72819-398-4. DOI: 10 . 1109 / MTTW51045.2020.9244924.

[38]   F. Capligins et al. "FPGA Implementation and Study of Synchronization of Modified Chua's Circuit-Based Chaotic Oscillator for High-Speed Secure Communications." In: *2020 IEEE 8th Workshop on Advances in Information, Electronic and Electrical Engineering (AIEEE)*. Vilnius, Lithuania: IEEE, Apr. 2021, pp. 1–6. ISBN: 978-1-66542-538-4. DOI: 10.1109/AIEEE51419.2021.9435783.

[39]   D. Kolosovs. "A Multi-Mode Approach for the Enhanced Decision Adjusted Modulus Algorithm Usage in Blind Equalization of QAM Signals." In: *2021 IEEE Microwave Theory and Techniques in Wireless Communications (MTTW)*. Riga, Latvia: IEEE, Oct. 2021, pp. 40–45. ISBN: 978-1-66542-469-1. DOI: 10.1109/MTTW53539.2021.9607265.

[40]   F. Capligins, A. Litvinenko, and D. Kolosovs. "FPGA Implementation and Study of Antipodal Chaos Shift Keying Communication System." In: *2021 IEEE Microwave Theory and Techniques in Wireless Communications (MTTW)*. Riga, Latvia: IEEE, Oct. 2021, pp. 1–6. ISBN: 978-1-66542-469-1. DOI: 10.1109/MTTW53539.2021.9607226.

[41]   J. G. Proakis and M. Salehi. *Digital Communications*. 5th ed. Boston: McGraw-Hill, 2008. ISBN: 978-0-07-295716-7.

[42]   P. Bello. "Characterization of Randomly Time-Variant Linear Channels." In: *IEEE Trans. Commun.* 11.4 (Dec. 1963), pp. 360–393. ISSN: 0096-2244. DOI: 10 . 1109 / TCOM . 1963 . 1088793.

[43]   B. Molnar et al. "The WSSUS Channel Model: Comments and a Generalisation." In: *Proceedings of GLOBECOM'96. 1996 IEEE Global Telecommunications Conference*. London, UK: IEEE, 1996, pp. 158–162. ISBN: 978-0-7803-3336-9. DOI: 10 . 1109 / GLOCOM . 1996 . 586800.

[44]   M. C. Jeruchim, P. Balaban, and K. S. Shanmugan, eds. *Simulation of Communication Systems: Modeling, Methodology, and Techniques*. 2nd ed. Information Technology–Transmission, Processing, and Storage. New York: Kluwer Academic/Plenum Publishers, 2000. ISBN: 978-0-306-46267-2.

[45]   A. Aboltins and P. Misans. "Initial Version of Real Time Model of Acoustic Transmission System with Parametric Multicarrier Modulation." In: *2014 14th Biennial Baltic Electronic Conference (BEC)*. Tallinn, Estonia: IEEE, Oct. 2014, pp. 121–124. ISBN: 978-1-4673-9539-7. DOI: 10.1109/BEC.2014.7320571.

[46]   S. Abrar and A. K. Nandi. "Blind Equalization of Square-QAM Signals: A Multimodulus Approach." In: *IEEE Trans. Commun.* 58.6 (June 2010), pp. 1674–1685.

[47] S. Abrar, A. Amin, and F. Siddiq. "Stop-and-Go Square-Contour Blind Equalization Algorithms: Design and Implementation." In: *IEEE Symposium on Emerging Technologies*. Islamabad, Pakistan: IEEE, 2005, pp. 157–162. ISBN: 978-0-7803-9247-2. DOI: 10.1109/ICET.2005.1558872.

[48] K. Banovic, E. Abdel-Raheem, and M. Khalid. "A Novel Radius-Adjusted Approach for Blind Adaptive Equalization." In: *IEEE Signal Processing Letters* 13.1 (Jan. 2006), pp. 37–40.

[49] S. Barbarossa and A. Scaglione. "Blind Equalization Using Cost Function Matched to the Signal Constellation." In: *Conference Record of the Thirty-First Asilomar Conference on Signals, Systems & Computers*. Vol. 1. Pacific Grove, USA: IEEE Comput. Soc, 2, pp. 550–554. ISBN: 978-0-8186-8316-9. DOI: 10.1109/ACSSC.1997.680438.

[50] S. Chen and E. Chng. "Concurrent Constant Modulus Algorithm and Soft Decision Directed Scheme for Fractionally-Spaced Blind Equalization." In: *IEEE International Conference on Communications*. Vol. 4. Paris, France: IEEE, 2004, pp. 2342–2346. ISBN: 978-0-7803-8533-7. DOI: 10.1109/ICC.2004.1312937.

[51] S. Chen. "Low Complexity Concurrent Constant Modulus Algorithm and Soft Decision Directed Scheme for Blind Equalisation." In: *IEEE Proceedings - Vision, Image and Signal Processing* 150.5 (Oct. 2003), p. 312. ISSN: 1350245X. DOI: 10.1049/ip-vis:20030619.

[52] F. C. De Castro, M. C. De Castro, and D. S. Arantes. "Concurrent Blind Deconvolution for Channel Equalization." In: *IEEE International Conference on Communications (ICC 2001)*. Vol. 2. Helsinki, Finland: IEEE, 11-14 June 20014, pp. 366–371. DOI: 10.1109/ICC.2001.936964.

[53] T. J. Endres et al. "Blind Adaptive Channel Equalization Using Fractionally-Spaced Receivers: A Comparison Study." In: *Conference on Information Sciences and Systems (CISS-96)*. 1996.

[54] E. Eweda. "Convergence Analysis and Design of an Adaptive Filter with Finite-Bit Power-of-Two Quantized Error." In: *IEEE Transactions on Circuits and Systems II: Analog and Digital Signal Processing* 39.2 (Feb. 1992), pp. 113–115. ISSN: 10577130. DOI: 10.1109/82.205815.

[55] I. Fijalkow, C. Manlove, and C. Johnson. "Adaptive Fractionally Spaced Blind CMA Equalization: Excess MSE." In: *IEEE Transactions on Signal Processing* 46.1 (Jan. 1998), pp. 227–231. ISSN: 1053587X. DOI: 10.1109/78.651224.

[56] M. Ghosh. "Blind Decision Feedback Equalization for Terrestrial Television Receivers." In: *Proceedings of the IEEE* 86.10 (Oct. 1998), pp. 2070–2081. ISSN: 00189219. DOI: 10.1109/5.720253.

[57] S. Gollamudi et al. "Set-Membership Adaptive Equalization and an Updator-Shared Implementation for Multiple Channel Communications Systems." In: *IEEE Transactions on Signal Processing* 46.9 (Sept. 1998), pp. 2372–2385. ISSN: 1053587X. DOI: 10.1109/78.709523.

[58] Y. Han, F. Cao, and T. Zheng. "The Study and Improvement on Constant Modulus Algorithm for MIMO System." In: *2010 First International Conference on Pervasive Computing, Signal Processing and Applications*. Harbin, China: IEEE, Sept. 2010, pp. 603–606. ISBN: 978-1-4244-8043-2. DOI: 10.1109/PCSPA.2010.151.

[59] L. He and M. Amin. "A Dual-Mode Technique for Improved Blind Equalization for QAM Signals." In: *IEEE Signal Processing Letters* 10.2 (Feb. 2003), pp. 29–31. ISSN: 1070-9908, 1558-2361. DOI: 10.1109/LSP.2002.806699.

[60] L. He, M. Amin, and C. Reed. "A Hybrid Adaptive Blind Equalization Algorithm for QAM Signals in Wireless Communications." In: *IEEE Transactions on Signal Processing* 52.7 (July 2004), pp. 2058–2069. ISSN: 1053-587X. DOI: 10.1109/TSP.2004.828913.

[61] G.-H. Im, C.-J. Park, and H.-C. Won. "A Blind Equalization with the Sign Algorithm for Broadband Access." In: *IEEE Communications Letters* 5.2 (Feb. 2001), pp. 70–72. ISSN: 1089-7798. DOI: 10.1109/4234.905939.

[62] N. K. Jablon. "Joint Blind Equalization, Carrier Recovery, and Timing Recovery for High-Order QAM Signal Constellations." In: *IEEE Trans. Signal Process.* 40.6 (June 1992), pp. 1383–1398. ISSN: 1053587X. DOI: 10.1109/78.139243.

[63] C. R. Johnson Jr. et al. "Blind Equalization Using the Constant Modulus Criterion: A Review." In: *Proceedings of the IEEE* 86.10 (Oct. 1998), pp. 1927–1950. ISSN: 00189219. DOI: 10.1109/5.720246.

[64] Y. Li and Z. Ding. "Global Convergence of Fractionally Spaced Godard Equalizers." In: *Proc. 28th Asilomar Conf. on Signals, Syst. and Computers* (Oct. 1994), pp. 617–621.

[65] A. Litvinenko et al. "The Impact of Waveform on the Efficiency of RF to DC Conversion Using Prefabricated Energy Harvesting Device." In: *2017 Advances in Wireless and Optical Communications (RTUWO)*. Riga: IEEE, Nov. 2017, pp. 61–66. ISBN: 978-1-5386-0585-1. DOI: 10.1109/RTUWO.2017.8228506.

[66] J. Liu and X. Lin. "Equalization in High-Speed Communication Systems." In: *IEEE Circuits and Systems Magazine* 4.2 (2004), pp. 4–17. ISSN: 1531-636X. DOI: 10.1109/MCAS.2004.1330746.

[67] R. Mahmoud et al. "A Calibration Method for Hybrid Technique Based on CMA with Clipping in MIMO-OFDM System." In: *11th German Microwave Conference (GeMiC)*. Freiburg, Germany: IEEE, Mar. 2018, pp. 203–206. ISBN: 978-3-9812668-8-7. DOI: 10 . 23919/GEMIC.2018.8335065.

[68] J. Mai and A. Sayed. "A Feedback Approach to the Steady-State Performance of Fractionally Spaced Blind Adaptive Equalizers." In: *IEEE Transactions on Signal Processing* 48.1 (Jan. 2000), pp. 80–91. ISSN: 1053587X. DOI: 10.1109/78.815481.

[69] J. Sadovskis, A. Aboltins, and J. Eidaks. "Modulation Recognition of Unmanned Aerial Vehicle Control Signals Using Software-Defined Radio." In: *2018 IEEE 6th Workshop on Advances in Information, Electronic and Electrical Engineering (AIEEE)*. Vilnius, Lithuania: IEEE, Nov. 2018, pp. 1–5. ISBN: 978-1-72811-999-1. DOI: 10 . 1109 / AIEEE . 2018 . 8592442.

[70] P. Schniter and C. R. Johnson Jr. "Dithered Signed-Error CMA: Robust, Computationally Efficient Blind Adaptive Equalization." In: *IEEE Transactions on Signal Processing* 47.6 (June 1999), pp. 1592–1603. ISSN: 1053587X. DOI: 10.1109/78.765129.

[71] K. Sekiyama et al. "Blind Signal Separation Using Array Antenna with Modified Optimal-Stepsize CMA." In: *2020 International Symposium on Antennas and Propagation (ISAP)*. Osaka, Japan: IEEE, Jan. 2021, pp. 799–800. ISBN: 978-4-88552-326-7. DOI: 10 . 23919 / ISAP47053.2021.9391234.

[72] J. Shynk, D. Witmer, and M. Ready. "Adaptive Equalization Using Multirate Filtering Techniques." In: *1991*. Pacific Grove, USA: IEEE Comput. Soc. Press, 4, pp. 756–762. ISBN: 978-0-8186-2470-4. DOI: 10.1109/ACSSC.1991.186549.

[73] S. Tjukovs, J. Eidaks, and D. Pikulins. "Experimental Verification of Wireless Power Transfer Ability to Sustain the Operation of LoRaWAN Based Wireless Sensor Node." In: *2018 Advances in Wireless and Optical Communications (RTUWO)*. Riga, Latvia: IEEE, Nov. 2018, pp. 83–88. ISBN: 978-1-5386-5558-0. DOI: 10.1109/RTUWO.2018.8587790.

[74] L. Tong, G. Xu, and T. Kailath. "Blind Identification and Equalization Based on Second-Order Statistics: A Time Domain Approach." In: *IEEE Transactions on Information Theory* 40.2 (Mar. 1994), pp. 340–349. ISSN: 00189448. DOI: 10.1109/18.312157.

[75] J. R. Treichler and B. G. Agee. "A New Approach to Multipath Correction of Constant Modulus Signals." In: *IEEE Trans. Acoust., Speech, Signal Processing* 31.2 (Apr. 1983), pp. 459–472.

[76] J. R. Treichler, I. Fijalkow, and C. R. Johnson Jr. "Fractionally Spaced Equalizers." In: *IEEE Signal Processing Magazine* 13.3 (May 1996), pp. 65–81. ISSN: 10535888. DOI: 10.1109/ 79.489269.

[77] R. N. Vanka, S. B. Murty, and B. C. Mouli. "Adaptive Blind Equalization of QAM Transmitted Constellations across Linear Band-Limited Channel." In: *IOSR Journal of VLSI and Signal Processing* 4.3 (June 2014), pp. 36–42.

[78] J. Werner, J. Yang, and D. Harman. "Blind Equalization for Broadband Access." In: *IEEE Communications Magazine* 37.4 (Apr. 1999), pp. 87–93. ISSN: 01636804. DOI: 10.1109/35.755455.

[79] B. Wu et al. "A Low-Complexity Blind Equalization Algorithm for 4096-QAM Systems." In: *24th Asia-Pacific Conference on Communications (APCC)*. Ningbo, China: IEEE, Nov. 2018, pp. 530–534. ISBN: 978-1-5386-6928-0. DOI: 10.1109/APCC.2018.8633561.

[80] F. Xiong. *Digital Modulation Techniques*. Artech House Telecommunications Library. Boston: Artech House, 2000. ISBN: 978-0-89006-970-7.

A STATIC SIGNAL PROCESSING

A.1 Transmitter Signal Forming

```matlab
N=1000; % number of symbols to transmit

ALPH=-3:2:3; ALPH=repmat(-3:2:3,4,1)+1j*repmat(ALPH.',1,4);

% Generate user data
usrDat=kron(ALPH(randi(numel(ALPH),1,N)),[1 0 0 0]);

% Pulse-sahping filter
firTx=firrcos(46,0.25,0.25,2,'rolloff', 'sqrt');

usrDatFlt=filter(firTx, 1, usrDat); usrDatFlt=usrDatFlt(46:end);
```

A.2 Clock Signal Frequency Difference Application

```matlab
function oupt=deSyncV1p0(initPh, ppm, datIn)
% deSyncV1p0(initPh, ppm, datIn) performs signal's desynchronization.
%   initPh - initial phase: fractional non-negative
%   ppm   - clock frequency difference: both positive and negative
%   datIn - input signal

    load('intrpCoe'); % loading coefficients
    tbLn=size(CfS,1); % interpolator coefficient table length
    tAddr=mod(fix(mod(initPh,4)*tbLn+(1:length(datIn))*(ppm*tbLn/1e6)),tbLn)+1;
        % forming address
    idExc=cumsum((diff(tAddr)>tbLn/2)-(diff(tAddr)<-tbLn/2))-fix(initPh); %
        index excess
    datOu=zeros(1,length(datIn)-idExc(end));
    for k=4-idExc(1):length(datIn)-abs(idExc(end))
        datOu(k-1)=datIn(k+idExc(k-1):-1:k+idExc(k-1)-3)*CfS(tAddr(k),:)';
    end

oupt=datOu;
```

A.3   Carrier Frequency Difference and Phase Noise Application

```matlab
% Rotation in the channel
RotVa=(2*pi*(0:Td:Td*(length(chNoise)-1))*dF+phi+...
    phNseGenV1p0(length(chNoise),phNdBc,Fd));
chRot=chNoise.*exp(1i*RotVa);

% Phase noise
function OutPt=phNseGenV1p0(Nin, phdBc, Fd)
% Phase noise generation. Spectrum mask is embedded
% Nin - realiation length
% phdBc - phase noise power in dBc

if Nin<1e5, N=1e5;
else      N=Nin;
end
fn=4;
f0=1e-5*fn; f1=7e-4*fn; f2=9e-3*fn;
f=(fix(-N/2):ceil(N/2-1))/(N/2);

A1=1*f0^1.5; A2=A1*f1^(-0.5); A3=A2*f2^(-0.8);
X=ones(1,length(f));
r1=abs(f)>f0;
r2=abs(f)>f1;
r3=abs(f)>f2;
X(r1)=A1./(abs(f(r1))).^1.5;
X(r2)=A2./(abs(f(r2)));
X(r3)=A3./(abs(f(r3))).^0.2;
X=fftshift(X);

Xen=1^2*f0+0.5*A1^2*(1/f0^2-1/f1^2)+A2^2*(log(f2)-log(f1));
X=X/sqrt(Xen)*sqrt(10^(-0.1*phdBc));

y=randn(1,N);
y=y/sqrt(mean(y.^2))*sqrt(Fd);
Y=2*real(ifft(fft(y).*X));

OutPt=Y(1:Nin);
```

B ADAPTIVE SIGNAL PROCESSING

B.1 Automatic Gain Control

```matlab
% Reference level calculations:
% E[(x^2-PW)*x^2]=E[x^4 -PWx^2]=E[x^4] -E[PWx^2]=E[x^4] -PW*E[x^2]=0 =>
    PW=E[x^4]/E[x^2]
% E[x^2-PW]=E[x^2]-PW=0 =>  PW=E[x^2]
% E[|x|-PW]=E[|x|]-PW=0 =>  PW=E[|x|]


% Jumping window averager
mu=5e-6;
% REF=mean(usrDatFlt.^4)/mean(usrDatFlt.^2);%4.6754;
% REF=mean(usrDatFlt.^2); % USE IN YOUR LABS
REF=mean(abs(usrDatFlt));
y1gain=zeros(size(usrRx));
y1data=zeros(size(usrRx));
gainAcc=1;
agcOut=0;
for k=1:length(usrRx)

    agcOut_tmp=agcOut;

    % Apply compensation
    agcOut=usrRx(k)*gainAcc;

    % Move parameter to the local minimum
    % gainAcc=gainAcc-8*mu*(agcOut_tmp^2-REF)*gainAcc*usrRx(k)^2;
    % gainAcc=gainAcc-8*mu*(agcOut_tmp^2-REF); % USE IN YOUR LABS
    gainAcc=gainAcc-8*mu*(abs(agcOut_tmp)-REF);

    % Output debug values
    y1gain(k)=gainAcc;
    y1data(k)=agcOut;

end
```

B.2 Timing Recovery Block

```matlab
smbCnt=0;
phCrnt=0;
nAddr=1;
yOut0=0;
yOut1=0;
yOut2=0;
yCst=0;
phAcc=0;


yOutDat=zeros(size(yDeSync));
yOutCst=zeros(size(yDeSync));
yOutPhs=zeros(size(yDeSync));


yDeSync=yDeSync(4:end);

for k=1:length(yOutDat)

    % Temporary variable
    phIncr_tmp=phIncr;


    % Form phase increment
    phAcc=phAcc+yCst;
    phIncr=1+0.01*yCst+0.0001*phAcc;

    % Estimate time error
    if smbCnt==1
        yCst=(yOut1-ALPH(find(min(abs(ALPH-yOut1))==abs(ALPH-yOut1),1)))...
            *(yOut2-yOut0);
    end


    % Interpolation output and delay line
    yOut2=yOut1;
    yOut1=yOut0;
```

```
38    %yOut0=yDeSync(nAddr:nAddr+3)*lpntrp(3,phInit).';
39    yOut0=yDeSync(nAddr:nAddr+3)*lpntrp(3,phCrnt).';
40
41
42    % Increment instantaneous phase delay
43    phCrnt=phCrnt+phIncr_tmp;
44    if    phCrnt>2
45        phCrnt=phCrnt-2;
46        nAddr=nAddr+2;
47    elseif phCrnt>1
48        phCrnt=phCrnt-1;
49        nAddr=nAddr+1;
50    else
51        phCrnt=phCrnt;
52        nAddr=nAddr;
53    end
54
55    % Counter to mark symbols
56    smbCnt=mod(smbCnt+1,4);
57
58    % The output signals
59    yOutDat(k)=yOut1;
60    yOutCst(k)=yCst;
61    yOutPhs(k)=phCrnt;
62
63    % Break if there is no inut data
64    if nAddr+3>length(yDeSync), break; end
65
66  end
```

B.3   Carrier Recovery Block

```
1  mu=1e-3;
2  y1phase=zeros(size(usrRx));
3  y1data=zeros(size(usrRx));
4  phaseAcc=1;
5  phseOut=0;
6  phseEst=0;
7  for k=1:length(usrRx)
```

```matlab
8
9      phseOut_tmp=phseOut;
10     phseEst_tmp=phseEst;
11
12     % Apply compensation
13     phseOut=usrRx(k)*exp(-j*phaseAcc);
14     phseEst=usrDatFlt(k);
15
16     % Move parameter to the local minimum
17     phaseAcc=phaseAcc+real(2j*mu*(phseOut_tmp-phseEst_tmp)*phseOut_tmp);
18
19
20     % Output debug values
21     y1phase(k)=phaseAcc;
22     y1data(k)=phseOut;
23
24 end
```

C   MULTIPATH CHANNELS

C.1   Diffuse multipath channel

```matlab
t=0:1:500;
Ft=5e-2;
T=3*round(1/Ft)
p=exp(-((t-T)*Ft).^2);

pr=resample(p,10,1);
tr=0:1:(length(pr)-1);

L=150;
R=zeros(L,L);

for n=0:size(R,1)-1
    for k=n:size(R,1)-1
        R(n+1,k+1)=sum(pr.*sinc(0.002*(tr-10*(n+0))).*...
                   sinc(0.002*(tr-10*(k+0))));
    end
end

% Copy upper triangle to the lower truangle
R=R+triu(R,1).'
R0=R


[S L]=eig(R)
L = diag(max(diag(L),1e-6));
R = S*L*S'

R=triu(R)+triu(R,1).'

% Check for the positive semi-definitiveness
if ~issymmetric(R), disp('Not symmetric!'); return; end

% Ensure positive semi-definitivity
M=real(eig(R)) % eigenvalues of the covariane matrix

```

```matlab
36  N=1e5;

37  L=chol(R)

38  x=sqrt(1/2)*randn(N,size(R,1))+sqrt(1/2)*j*randn(N,size(R,1));

39

40  hd=fir1(100,0.02);

41  x=filter2(hd.',x)/sqrt(sum(hd.^2));

42

43  c=x*L;
```

C.2   Two-ray multipath channel

```matlab
1   h=1/sqrt(1+(1-DP)^2)*[zeros(1,8) 1 zeros(1,9)]+...

2     (1-DP)/sqrt(1+(1-DP)^2)*lpntrp(17,0.5)*exp(-j*2*pi*f0*5.5e-9);

3

4   usrChan=filter(h,1,usrDatFlt); usrChan=usrChan(9:end);

5   usrChan=usrChan/sqrt(mean(abs(usrChan).^2))*sqrt(mean(abs(usrDatFlt).^2));

6

7   function output=lpntrp(N, dly)

8   %LPNTRP  Function to generate coefficients of the fractional delay
        interpolator.

9   %   B = LPNTRP(N, DELAY) designs interpolation filter of the order N > 2 which

10  %   delays input signal by DELAY of cycles cycles such as 0 < DELAY < 1.

11  %

12  %   Notice, vector B will have N+1 elements, but overall filter delay will be

13  %   FlOOR(N/2)+DELAY

14

15  % Overall delay

16  D=floor(N/2)+dly;

17

18  output=prod(D-flipud(reshape(repmat(0:N,N,1), N+1,N)).').'./...

19        prod(repmat(0:N,N+1,1)-repmat((0:N)',1,N+1)+diag(ones(1,N+1)));
```

D BLIND EQUALIZATION ALGORITHMS

D.1 Constant Modulus Algorithm

```matlab
% Dispersion constant for CMA
R=mean(abs(ALPH).^4)/mean(abs(ALPH).^2);

cntMain=0;
eqCoef=zeros(1,33); eqCoef(17)=1;
eqFltr=zeros(size(eqCoef));
yOut=0;
yCst=0;
yVrf=0;

% Debug signals
yOutDat=zeros(size(usrChan));
yOutCnv=zeros(size(usrChan));
yOutVrf=zeros(size(usrChan));


for k=1:length(usrChan)

    % Equalization
    yOut=eqFltr*eqCoef.';

    % Coefficient adjustment
    if cntMain==0
        yCst=yOut-ALPH(find(min(abs(yOut-ALPH(:).'))==abs(yOut-ALPH(:).'),1));
        % eqCoef=eqCoef-0.001*yCst*conj(eqFltr); % LMS
        eqCoef=eqCoef-0.00001*(abs(yOut)^2-R)*yOut*conj(eqFltr); % CMA
    end

    % Filter delay line
    eqFltr=[usrChan(k) eqFltr(1:end-1)];

    % Counter to indicate symbols positions
    cntMain=mod(cntMain+1,4);

    % Form output
```

```
36    yOutDat(k)=yOut;

37    yOutCnv(k)=yCst;

38    yOutVrf(k)=yVrf;

39

40  end
```

D.2 Enhanced Decision-Adjusted Modulus Algorithm

```
1   % Finding constellation radii

2   RadVa=sort(abs(Cnst)); RadPos=[find(diff(RadVa)>0) length(RadVa)]; % finding
        radii for all possible constelation points

3   RadVa=RadVa(RadPos); % unique radii

4   RadPos=[RadPos(1) diff(RadPos)]/RadPos(end); % possibility for the point to be
        at the current radius

5

6   % Evaluating comparators for absolute value

7   RadComp=(RadVa(1:end-1).*RadPos(2:end)+RadVa(2:end).*RadPos(1:end-1))./...

8   (RadPos(2:end)+RadPos(1:end-1));

9

10

11  % Equalization

12  eqLg=32; % equalizer length

13  eqC=zeros(eqLg,1); eqC(fix(eqLg/2))=1; % equalizer coefficient array

14  mu=0.00001/(sqrt(length(Cnst))-1); % equalizer convergence coefficient

15  muT=0.01; % timing synchronization adjustment coefficient

16  Cmp=RadComp.^2; % radii comparators (constellation parameters)

17  Rad=RadVa.^2; % radii (constellation parameters)

18  TauAd=1; % current intepolator's memory address

19

20  % Used variables

21  yp=zeros(1,n); % interpolated received signal samples

22  y0=zeros(1,n); % equalized input received signal -OUTPUT of the equalizer
        module

23  y1=zeros(1,n); % interpolated equalizer's output signal

24  err=zeros(1,n); % current radius deviation from ideal radius

25  tau=zeros(1,n); % timing synchronization current offset phase -tau/256 cock
        cycles

26

27
```

```matlab
28  DLY=mod(ntrpLg+fix(eqLg/2),4); % clock cycle to evaluate radius and adjust
        equalizer coefficients -symbol position
29
30  for k=eqLg+ntrpLg:n
31
32  % New positioning system -equalization + interpolation
33      yp(k)=dtChRxF(k:-1:k-ntrpLg+1)*ntrpCoe(fix(tau(k))+1,:)'; % input data
            samples interpolation (only fo inner use)
34      y0(k)=conj(dtChRxF(k:-1:k-eqLg+1))*eqC; % input signal equalization
35      y1(k)=y0(k:-1:k-ntrpLg+1)*ntrpCoe(fix(tau(k))+1,:)'; % equlized samples
            interpolation
36      curDt=yp(k:-1:k-eqLg+1).'; % forming sample vector currently kept in the
            equalizer registers
37
38      % Dynamical system adjustments -once per 4 clock cycles
39      if mod(k,4)==DLY,
40          R=Rad(logical(diff([0 abs(y1(k))^2<Cmp 1]))); % nearest radius
                determination
41          err(k)=abs(y1(k))^2-R; % error evaluation
42          if abs(err(k))>5, err(k)=5*sign(err(k)); end % error value limitation
43          eqC=eqC-2*mu*err(k)*curDt*(y1(k)); % equalizer coefficient adjustment
44          tau(k)=mod(tau(k-4)-muT*err(k-4)*(abs(y1(k-5))^2-abs(y1(k-3))^2),1023);
                % timing offset adjustment
45          eqC(fix(eqLg/2))=1; % equalizer coefficient normalization (preventing
                eqalizer to be AGC ot synchronizer)
46      end
47
48      % Processing progress indication
49      if mod(k,10000)==0, disp(['Symbols have been processed: ' num2str(k)]); end
50
51  end
```